Discovery of Minimalistic Biocatalysts *via* Biocatalytic Self-Assembly

A thesis submitted to the University of Strathclyde for the degree of Doctor of Philosophy in the Department of Pure and Applied Chemistry

2016

Krystyna Louise Duncan

Declaration

‘This thesis is the result of the author’s original research. It has been composed by the author and has not been previously submitted for examination which has led to the award of a degree.’

Signed:

Date:

Acknowledgements

First and foremost I would like to thank my supervisor, Prof. Rein Ulijn, for providing me with the opportunity to undertake this research project and for his guidance and encouragement throughout my time as a member of his group. I would also like to thank my second supervisor Dr. Roberto de la Rica for his invaluable discussions and direction with regards to my project. Thanks also go to Dr. Charles Knapp for allowing me to use his laboratory and providing instrumental knowledge on microbiological techniques.

I would also like to thank the Ulijn group, both past and present members, for their support and helpful discussions over the last 3 and a half years. In particular I would like to thank Nadeem Javid for his support and encouragement in the lab. I would also like to thank team TG425, Joy, Babis and Scott, without whom I would never have made it out the other side. You managed to pick me up when science brought me down and made the experience extremely fun and enjoyable. Finally my TIC team, Mari, Ines, Ana, Vini, Yousef, Jugal, Ivan (thanks to Ivan for the IR) and Gary, thank you for your friendship and encouragement over the last few years.

In terms of external collaborators I would like to thank Prof. Hiroshi Matsui and Dr. Yuka Kanetsuki for their contributions towards this project and also for hosting me in their lab during a collaborative visit. The experience and discussions were extremely useful. I would also like to thank Prof. Cecilia Rouque and Dr. Ana Pina for their collaboration and encouragement. Thanks to Ana for her company while on a collaborative trip to New York for 4 weeks, what a great experience we had together and thanks for a great new friendship.

Thanks go to my family, my parents, Caroline and Donald and my sisters, Eleanor and Hannah. You have been there for me throughout this experience and shared the highs and the lows. Without you I would not be where I am today so thank you. Finally, thanks go to my boyfriend David who has been there for me throughout this whole experience. Thank you for listening to my science based rants, helpful discussions about chemistry and just being there with a hug when I needed it most. I couldn't have done it without you.

The Author

Publications:

Spot light article - **K. Duncan**, Y. Maeda, N. Javid, L. Birchall, K.F. Gibson, D. Cannon, Y. Kanetsuki, C. Knapp, T. Tuttle, R. V. Ulijn, H. Matsui, Discovery of Catalytic Phages by Biocatalytic Self-Assembly, *J. Am. Chem. Soc.*, 2014, **136**, 15893-15896.

K. L. Duncan, R. V. Ulijn, Short Peptides in Minimalistic Biocatalyst Design. *Biocatalysis*, 2015, **1**, 67-81.

K. L. Duncan, R. de la Rica, R. V. Ulijn, A Dodecapeptide di-Cysteine Esterase - submitted to *Chem. Commun*.

K. L. Duncan, R. de la Rica, R. V. Ulijn, A Tripeptide for Ester Hydrolysis – manuscript in preparation.

J. K. Sahoo, S. Roy, N. Javid, **K. Duncan**, L. Aitken, R. V. Ulijn, Biocatalytic Self-Assembly for Pathway-Dependant Templating of Gold Nanoparticles – submitted to *Chem. Sci.*

Presentations:

Peptide Materials 2013 International Conference (Poster) – 'Discovery of Catalytic Peptides *via* Phage Display'.

Chemical Biology Forum 2014 UK conference (Poster) – 'Biocatalytic Self-Assembly Enables Discovery of Catalytic Peptides *via* Phage Display'.

Nanopeptide 2015 International Conference (Poster – top 5) – 'Discovery of Catalytic Phages by Biocatalytic Self-assembly'.

15th Iberian Peptide Meeting 2016 (Oral Communication) – 'Biocatalytic Self-Assembly Enables Discovery of Catalytic Peptides *via* Phage Display'.

Grants/Bursaries:

2013 - The Armourers and Brasiers Gauntlet Trust: Travel Grant for PhD Students for Industrial Placements. Awarded £1000.

2014 - Chemistry International Alumni Ambassadors (CIAA): Postgraduate CIAA Bursary. Awarded £500.

2014 – WestCHEM PEER and Postdoctoral and Early Career Researcher Exchanges Funding. Awarded £2000.

2015 - WestCHEM PEER and Postdoctoral and Early Career Researcher Exchanges Funding. Awarded £1000.

2016 – RSC Travel Grant. Awarded £400.

Public Engagement:

Member of Really Small Science, a public engagement group from the University of Strathclyde. Involved in workshops for the public at the Glasgow Science Center in 2013/14 as well as events such as Glasgow Science Festival 2013. Also, involved in workshops with school children to encourage interest in science from 2013 - 2015.

Abbreviations

Aib	2-Aminoisobutyric acid
Ala	Alanine
Arg	Arginine
Asp	Aspartic acid
ATP	Adenosine triphosphate
BSA	Bovine Serum Albumin
Cbz	Carboxybenzyl
Cys	Cysteine
CD	Circular Dichroism
DABCYL	4-((4-(dimethylamino)phenyl)azo)benzoic acid
DCM	Dichloromethane
DIPEA	N,N-Diisopropylethylamine
DMF	Dimethylformamide
DMSO	Dimethyl sulfoxide
DNA	Deoxyribonucleic acid
DNPA	2,4-dinitrophenylacetate
dNTPs	Deoxynucleotide
E. Coli	Escherichia coli
EDANS	5-((2-Aminoethyl)amino)naphthalene-1-sulfonic acid
FITC	Fluorescein isothiocyanate
Fmoc	Fluorenyl-9-methyloxycarbonyl
FRET	Forster resonance energy transfer
FTIR	Fourier transform infrared spectroscopy
Glu	Glutamic acid
Gln	Glutamine
Gly	Glycine
Gua	Artificial arginine analogue
HBTU	*N,N,N′,N′*-Tetramethyl-*O*-(1*H*-benzotriazol-1-yl)uronium hexafluorophosphate
His	Histidine
HPLC	High performance liquid chromatography
Ile	Isoleucine
IPTG	Isopropyl β-D-thiogalactopyranoside
IR	Infra-red
LB	Lysogeny Broth
LC-MS	Liquid chromatography – mass spectrometry
Leu	Leucine
Lys	Lysine
M	Molar

mM	Millimolar
MUA	4-Methylumbelliferone acetate
NaCl	Sodium chloride
nm	Nanometer
OD	Optical density
OMe	Methyl ester
PB	Phosphate buffer
PBS saline	Phosphate buffered
PCR reaction	Polymerase chain
PEG	Polyethylene Glycol
pfu	Plaque forming units
Phe	Phenylalanine
pmol	Picomole
*p*NPA acetate	para-nitrophenyl
*p*NPP	para-nitrophenyl phosphate
Pro	Proline
rpm	Revolutions per minute
Ser	Serine
TEM	Transmission Electron Microscopy
TFA	Trifluoroacetic acid
Thr	Threonine
Trp	Tryptophan
Tyr	Tyrosine
UV	Ultraviolet
Val	Valine
Vis	Visible
Xgal	5-bromo-4-chloro-3-indolyl-β-D-galactoside
µg	Microgram
µL	Microliters
µM	Micromolar

Abstract

Efficient and selective catalysis of chemical reactions and biological pathways by enzymes[1] has long inspired bio- and supramolecular chemists. Many have tried to mimic this enzymatic activity through the design of *de novo* catalysts however the proficient rate of an enzyme has not yet been matched by a synthetic mimic. Short peptide sequences have emerged as potentially useful molecules in the design and discovery of synthetic catalysts. Their side chains provide the same chemical functionality as found in proteins and can also manipulate the local environment to favor catalysis. They may also form self-assembled nanostructures which can be utilized to present ordered functionality[2-4] as well as demonstrating the ability to display catalytic and binding functionalities in a multivalent fashion.[5, 6] This has been shown to improve catalytic rates although they still do not match that of natural enzymes.[7] In contrast to designing catalysts, there are several approaches to screen libraries of peptide sequences for transition state binding with the advantage being that sequence can be directly linked to functionality.[8] Phage display in particular is a useful tool for the discovery of new peptide catalysts[9, 10] based on specific enzymatic activity.

By utilizing enzymatically triggered self-assembly of an aromatic peptide amphiphile, Fmoc-Thr-Leu-OMe,[11] formed *in situ* by condensation of the amino acid precursors, in combination with a phage display peptide library; a new methodology has been developed to identify peptide catalysts for specific enzymatic function based on a direct link between sequence and activity. The self-assembly of the precursors in the presence of the catalytic peptide results in a gel aggregate at the tip of the phage allowing this extra weight to be used to separate the phage from the bulk sample by centrifugation before being amplified and sequenced. It was possible to characterize the amidase and esterase activity of the phage identified in this manner by several techniques including TEM, HPLC, fluorescence as well as UV-Vis spectroscopy, demonstrating by several means that the sequences identified do possess (modest) amidase and esterase functionality. In addition to the full characterization of the catalytic phage which demonstrated the desired activity, the peptide sequences alone were also characterized for amidase and esterase enzymatic

functionality using ester hydrolysis assays based on fluorescence and UV-Vis spectroscopy.

Of the sequences identified by phage display, one cysteine containing peptide sequence demonstrated significant rate enhancement in comparison to the remaining histidine containing samples therefore it was studied further to gain an insight into the mechanism of catalysis utilizing CD and UV-Vis spectroscopy. Cysteine is a known catalytic amino acid and is the main source of nucleophilic attack in the presence of a basic amino acid.[12, 13] Terminal amino groups have also been found to enhance the rate at which ester bonds are broken and this is demonstrated by the tripeptide KYF. CD, TEM, fluorescence and UV-Vis spectroscopy were utilized to demonstrate the self-assembling propensity as well as catalytic activity of KYF and again show an understanding of the catalytic mechanism. This system self-assembles at low concentrations to form short fibrils, although in this case, the formation of nanostructures in the sample does not enhance the catalysis as seen in literature examples.[7]

Next, as combinatorial methodology was successfully developed for the identification of amidase and esterase active peptides, the same technology was taken advantage of to screen for phosphatase activity. Fmoc-Tyr$(PO_4)^{3-}$-Ala-OH and Fmoc-Phe-Tyr$(PO_4)^{3-}$-OH [14] form self-assembled hydrogel materials on the addition of alkaline phosphatase. Fibrous networks develop trapping water and result in a self-supporting gel. These gelators were used in the phage display panning experiment to identify phosphatase peptides, which were fully characterized by HPLC and UV-Vis spectroscopy.

Overall, this thesis contributes to the field by utilizing an alternative technological platform, phage display and biocatalytic self-assembly, to screen for enzymatic activity rather than *de novo* rational design. It demonstrates that random, unassembled dodecapeptides possess catalytic activity with respect to amides and esters, establishing that the rigid scaffold of an enzyme is not strictly necessary for catalysis. Traditional amino acids *i.e.* histidine, are also not always fundamental for catalysis and alternative amino acids can be used in its place *e.g.* cysteine. This thesis also contributes to new knowledge by identifying that peptides as short as tripeptides

possess the ability to hydrolyze ester bonds. This broadens the horizon for discovery and design of peptidic enzyme mimics.

Table of Contents

1.0 Introduction

1.1 Introduction

Enzymes are natural compounds which catalyze challenging chemical reactions and biological pathways which have half-lives of years. For example, amide and ester hydrolysis have half-lives of 400 and 4 years respectively.[1] Although enzymes are efficient and selective catalysts, their use in commercial processes, both industrial and biomedical, is limited due to their expense, their complex structure and their instability in some reaction conditions. It would be advantageous to design simpler, cost-effective catalysts that can be used for specific reaction conditions. In addition, systematic studies of simpler catalysts could provide insights into the fundamentals of biocatalysis.

As a result, chemists have been inspired to produce synthetic mimics of natural proteins, such as short peptides, however none of these mimics have reached the efficiency of natural enzymes. In the design of these mimics, several factors have been taken into consideration including primary sequence of the peptide which provides catalytic functionality as well as a local microenvironment based on the residues present. Histidine is typically present as a catalytic residue[15] and it is rare to find an example of a peptide catalyst without this key residue.[7] Also taken into consideration is whether the peptide can self-assemble and form a nanostructure. This provides the peptide with an organized internal structure which in turn allows the presentation of catalytic residues on the surface of the structure in a multivalent fashion.[2, 4-6] Binding pockets and the introduction of metal ions[3] are other aspects which have been studied for the design of enzyme mimics.

There is huge potential in peptide materials to design enzyme mimics. However, screening for function is also an option for the discovery of peptide catalysts based on a direct link between structure and function.[16] Making use of the well exploited technique of phage display[17] offers the opportunity to screen for catalytic dodecapeptides and in turn study the peptides identified to gain an insight into their mechanism of action. This can then provide further insight for the design of peptide catalysts. Screening phage display libraries, characterization of the identified peptides and mechanistic studies will be the focus of three of the following chapters. Minimalistic tripeptides will also be studied for breaking ester bonds.

1.2 Motivation of the Project

The motivation of this research was to develop methodology to help identify catalytic peptides by innovative library screening. In addition, the aim is to fully characterize the amidase and esterase activity of catalytic peptides identified using the combinatorial technology of catalytic gelation with phage display and, furthermore, to gain an understanding of the mechanism of action for CPN3 peptide catalyst. It is also to study a minimalistic tripeptide for ester cleavage after a serendipitous discovery and to achieve an insight into its mechanism of action. The final aim is to undertake phage display panning for identification of peptides with phosphatase activity.

1.3 Layout of the Thesis

This thesis is divided into nine chapters. The first of these chapters (2.0) is an extensive literature review of peptidic enzyme mimics which becomes increasingly focused on esterase activity in aqueous reaction conditions.[7] The remaining chapters contain experimental work presented separately, each with its own introduction, objectives, results and conclusions section to allow presentation of one area of the overall research project in an individual manner.

The first experimental chapter 3.0 investigates the enzymatic activity of catalytic peptides identified by phage display panning in combination with peptidic gel precursors Fmoc-Thr and Leu-OMe. This was in collaboration with the Matsui Group at Hunter College, CUNY, USA.[8] These gel precursors were chosen as they are well characterized in the literature and are known to form stable gels on incubation with thermolysin. Therefore, they can be used to screen for amidase activity.[11] Phage display panning has already been used for the identification of peptides for a specific function[16] and so the same methodology was utilized to identify catalytic peptides. These peptides were studied for amidase and esterase activity utilizing a variety of spectroscopic techniques as well as HPLC and TEM. Studies both on phage and separately synthesized peptides demonstrated that CPN3 was the best esterase peptide and this sequence was further investigated to gain an

insight into its mechanism of action in chapter 4.0, with cysteine playing a key role in catalysis.

In chapter 5.0, the first example of a tripeptide which does not contain traditional catalytic amino acids was reported. Self-assembly was observed at different peptide concentrations and aminolytic behavior was monitored by UV-Vis spectroscopy. Again a mechanistic insight into the catalytic mechanism was established using mutant sequences ascertaining that lysine and the terminal amino functionality are necessary for catalysis as seen in examples from nature.

Chapter 6.0 describes phage display panning for phosphatase activity with precursors Fmoc-Tyr(PO_4)$^{3-}$-Ala-OH and Fmoc-Phe-Tyr(PO_4)$^{3-}$-OH. The first gelator is a newly developed peptide based on the attributes required for the panning process and the second is an already characterized example from the literature.[14] Peptide sequences were identified and characterized on phage. This process was optimized for future use.

Key findings from the previous chapters are summarized in chapter 7.0, as well as directions for future research. Finally chapter 8.0 contains materials and methodology for all of the work contained herein.

2.0 Short Peptides in Minimalistic Biocatalyst Design*

***** This work was published in part as: **K. L. Duncan**, R. V. Ulijn, Short Peptides in Minimalistic Biocatalyst Design. *Biocatalysis*, 2015, **1**, 67-81.[7]

Declaration of contribution to published article: Any reproduced practical work from the aforementioned published article; I was solely responsible for, unless otherwise stated.

2.1 Introduction

Both chemists and biologists have long been inspired by the efficiency and selectivity of natural enzymes in catalyzing wide ranging reactions, some of which are extremely challenging to achieve using non-enzymatic means. This has been the basis for extensive research into elucidating the basic mechanisms of biochemical catalysis as well as the development of biologically inspired synthetic catalysts that may have biotechnological or biomedical uses. The ability of an enzyme to fold into a structure and organize functional groups for catalysis and binding is reliant on its amino acid sequence (and in some cases, the presence of cofactors such as metal ions, porphyrin or flavin adenine dinucleotide, amongst others).[18, 19] The majority of enzymes are greater than one hundred amino acid residues in length. Proteins of this size have a vast number of potential primary sequences capable of folding (thereby producing binding pockets) and function (presenting residues for catalysis).[20, 21] Remarkably, the process of evolution has selected for relatively few stable three-dimensional structures from the vast number of possibilities.

Today's enzymes emerged initially from simpler structures to more developed and complex levels of organisation.[22, 23] One common class of hydrolase enzymes contain conserved serine and histidine as active components in their catalytic triad, complemented by an acidic residue such as aspartic or glutamic acid, which directly contribute to peptide bond hydrolysis.[24] The fact that enzymes evolved suggests that simpler functional precursors to hydrolases may exist and these could inform the design of short peptide catalysts. Indeed, it has been observed that the dipeptide seryl-histidine (Ser-His) is able to catalyze a number of hydrolytic reactions in water,[25] albeit with low selectivity and modest rates.

The use of peptide self-assembly and nanoparticle functionalization approaches opens up new opportunities for catalyst design that are not found in natural enzymes. This is a review of recent developments in this area and assesses the relative importance in enhancing reaction rates of five features that have been explored in biocatalyst design.

2.2 Hydrolase Enzyme – the Catalytic Triad

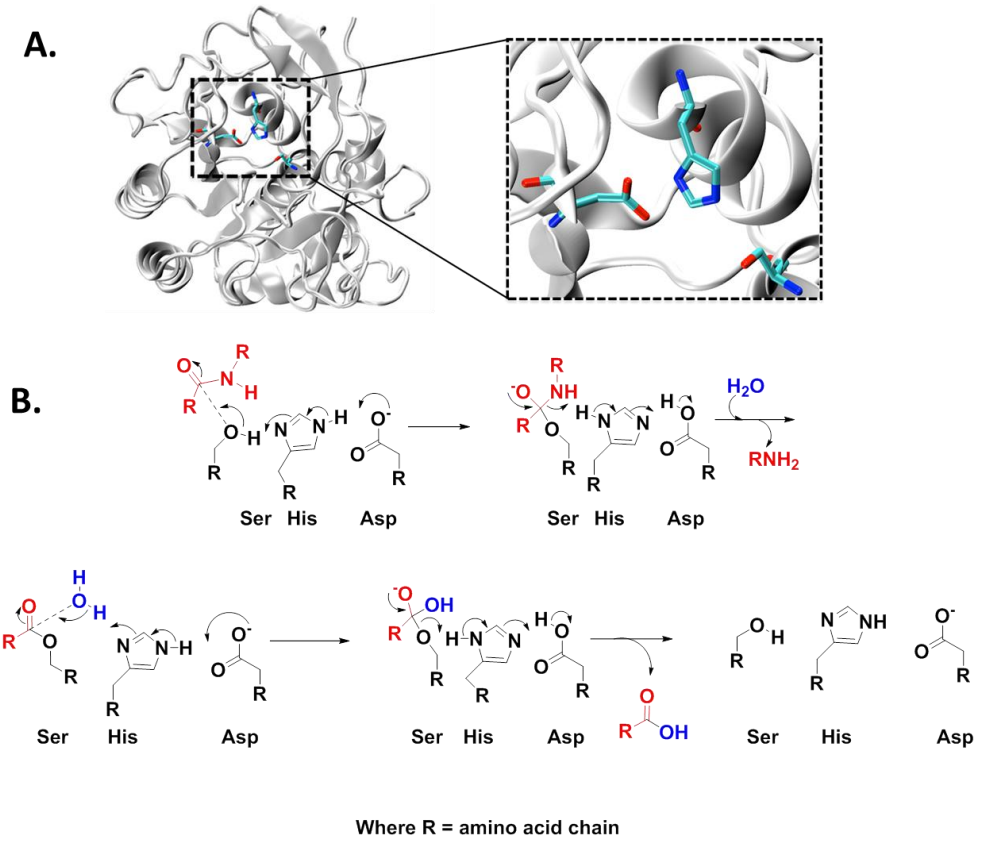

Figure 2.1. Example of a hydrolase with catalytic triad. A. Subtilisin with catalytic residues highlighted in molecular detail (PDB 1ST2). **B.** Mechanistic outline for the hydrolysis of a peptide bond by a serine protease enzyme.

As an example, one can consider a common class of biocatalysts, proteases, which possess the ability to hydrolyze amide (as well as ester) bonds. This amide hydrolysis reaction is extremely challenging with a half-life of 450 years.[1, 26] Protease enzymes make use of a catalytic triad (Figure 2.1A) in the following manner to facilitate this reaction. The serine side chain acts as a nucleophile attacking the carbonyl carbon of an amide or ester substrate whilst the imidazole ring in histidine acts as either a proton donor or acceptor.[27] The acidic residue is used to polarize and align the base which in turn activates the substrate to form the tetrahedral transition state (Figure 2.1B). The triad residues were identified as crucial components through mutagenesis studies, *i.e.* mutating the serine, histidine or acidic residues resulted in a reduction of activity.[24, 28] The most important residue with respect to catalysis is histidine as the

catalytic activity dropped most dramatically upon mutation. In addition to providing the chemical moieties required for chemical catalysis, the three-dimensional structure is fundamental for defining a microenvironment with the right physicochemical properties for catalysis to occur, defining selectivity of the catalyst (through hydrophobic binding pockets), active sites buried inside the protein structure and fixing the conformation of the catalytic site in a dynamic structure, which are all essential for enzymes to function effectively.[29]

Other classes of hydrolase enzymes, for example carbonic anhydrase, require the presence of a metal ion (Zn^{2+}) as a cofactor. The mechanism of catalytic activity for these enzymes does not utilize a catalytic triad but coordinates the metal ion in three places by histidine side chains. Water occupies the fourth coordination site causing polarization of the oxygen-hydrogen bond and weakening it. A fourth histidine residue is positioned close by and accepts a proton leaving a hydroxide attached to the metal. The active site contains a specific pocket for carbon dioxide which brings it close to the hydroxide allowing the hydroxide to attack the carbon dioxide and form bicarbonate.[30]

2.3 Design Approaches in the Pursuit of Synthetic Catalysts

As discussed, nature evolved impressive catalysts in the form of enzymes; but they may not always be ideally suited for applications or environments that are different from their natural ones. Enzyme (directed) evolution[31-33] has achieved much in improving catalysts but it is not a rational design approach and the proteins produced are still complex. It is intriguing to consider whether simpler yet efficient synthetic, low-molecular weight catalysts can be produced.

A number of approaches have emerged in the pursuit of a synthetic catalyst as an enzyme mimetic (Figure 2.2). These approaches seek to mimic multiple aspects of biocatalysis, including (a) use of the properties of primary peptide sequences to control the immediate chemical environment and functionality.[25] To further enhance activity the peptides may be engineered into a designed environment, for example: (b) presentation of reactive sites for catalysis on scaffolds and particles, [34, 35] (c)

design of binding pockets for substrates or transition states. Furthermore, (d) factors not normally associated with natural enzymes, such as multivalency may be considered and finally, (e) introduction of metal co-factors to enhance activity.

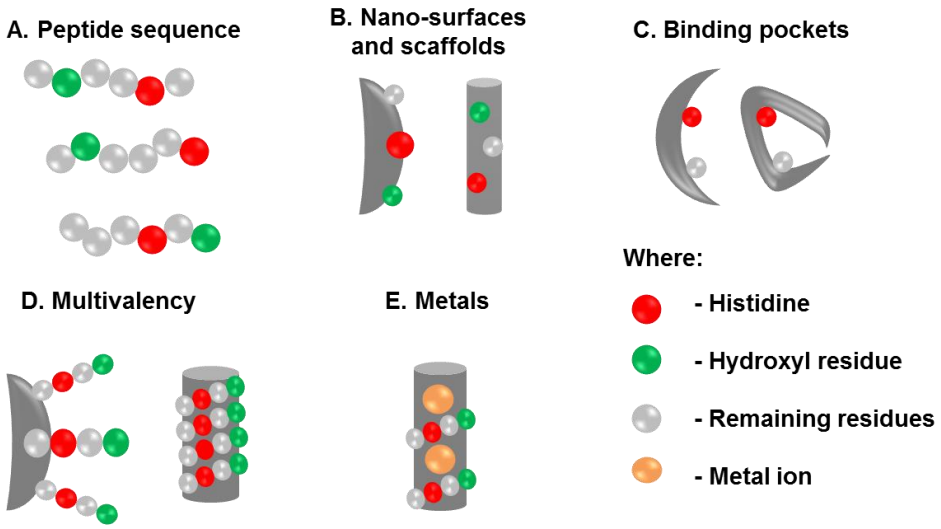

Figure 2.2. Approaches used in the mimicry of natural esterase enzymes.

The first approach (a) is focused on the inclusion of catalytic residues found in the active site of the natural enzyme. This approach takes into consideration primary sequence *i.e.* the relative positioning of chemical residues. This may have direct or indirect effects. Literature examples of designed esterases invariably include histidine that has a direct role in catalysis.[2, 5, 6, 15] Other residues involved in catalytic triads may also be included. It is clear that the amino acids directly surrounding this residue can further influence the catalytic activity by modulating the microenvironmental conditions, such as local pH or polarity to facilitate interactions with substrate molecules or transition states. The second approach (b) is focused on utilizing nano-surfaces and scaffolds for the presentation of catalytic and binding groups on the surface of a structure. This can be achieved using surfaces produced by self-assembly of peptide derivatives, or by using non-peptidic scaffolds, for example (inorganic) nanoparticles. These approaches may improve the catalytic activity due to the ordered presentation of catalytic moieties and the reduced dynamics of the system. Binding pockets (c) can be incorporated into synthetic structures to bind the transition state of the substrate and aid in catalysis. Commonly, these are hydrophobic surfaces or patches achieved by molecular self-assembly of amphiphilic

peptides. Approach (d) focusses on multivalency. Although not normally found in naturally occurring proteins, designed systems offer the possibility of introducing multivalency in very large numbers, *i.e.* presentation of multiple catalytic residues and binding sites by using *e.g.* dendritic architectures. The final approach (e) focusses on the introduction of metal co-factors. These features have all been taken into account in our assessment of recent examples of synthetic, peptide based catalysts.

This chapter endeavors to summarise some of the more recent examples of the use of short peptides in biocatalysis with an emphasis on hydrolase (and mainly esterase) activity, as this is the most abundantly studied reaction where the natural enzyme it is intended to mimic is also well understood. Specifically, this will investigate which of the above approaches gives rise to efficient catalytic activity and whether combinations can give rise to cooperative effects. If successful, synthetic mimics may provide an insight into the fundamental understanding of enzyme catalysis and pave the way towards rational design. This has the potential to result in robust catalysts for industrial applications but also designer catalysts for biotechnologies and potential therapeutic applications that can interfere with biological pathways and facilitate the prevention and treatment of disease.

2.4 Primary Sequence in Catalysis

Chen and co-workers were first to explore the simplest mimic of a catalytic triad enzyme – by just considering minimal sequences of the His, Asp, and Ser residues. What they discovered is surprising, in that the dipeptide Ser-His has the capability to cleave amide and ester bonds. The group reported that on incubation with Ser-His, cleavage was observed with linear and circular DNAs, proteins (BSA) and carboxyl ester substrate *p*-nitrophenyl acetate (*p*NPA).[25] These processes occur over a wide range of physical and chemical conditions. These authors also studied related oligopeptides, flanking the Ser-His motif with glycine and aspartic acid in different sequences or replacing serine or histidine (Figure 2.3).

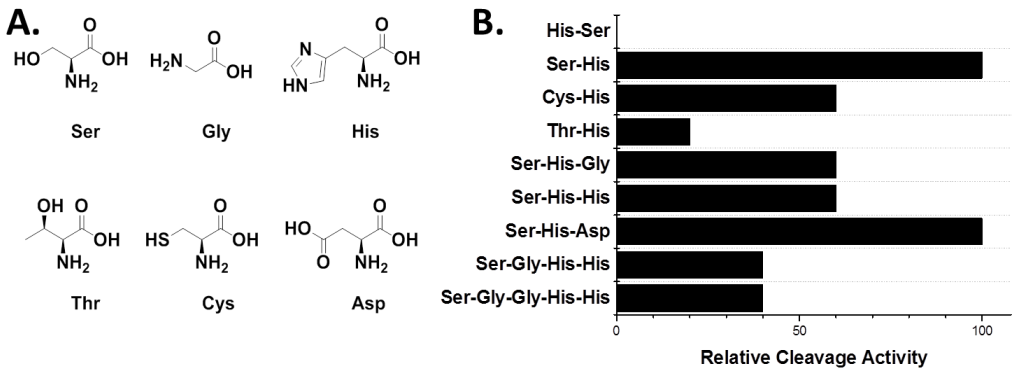

Figure 2.3. Chemical structures of the peptides studied. (b) DNA and protein cleavage of Ser-His and related oligopeptides.[25]

It has been demonstrated that the single amino acid components of the triad, including histidine, in isolation do not exhibit cleavage activity, suggesting that they have to be covalently linked for cleavage to occur. The reverse sequence, His-Ser, is also inactive, suggesting a possible role for the terminal amine and acid groups in proximity to the imidazole and nucleophilic OH. Mutating these short sequences by replacing either histidine or serine with an alternative amino acid, results in the loss of cleavage activity. There are two exceptions; when serine is replaced with cysteine or threonine, however the activity is still lower than the Ser-His dyad. The former has a sulfhydryl side chain that has the potential to mirror the nucleophilic nature of the hydroxyl group on serine. Histidine was found to be essential for catalysis as all activity is lost upon the mutation of this residue. Residues can be added to the C terminus of the peptide or *in situ* while maintaining 40-60% of the original activity. Finally, with aspartic acid (Asp) attached to form the Ser-His-Asp tripeptide, the catalytic activity is at least as efficient as that of the dyad. The work demonstrates the peptide's requirement of a terminal acid or a neighboring acidic side chain to assist in the catalysis mechanism. Strong evidence has been presented that it is the dipeptide itself that is responsible for the esterase activities, implicating that the serine hydroxyl side chain and the histidine imidazole side chain have key mechanistic roles.

In addition to protein and DNA cleavage activity, it has also been reported that short peptides have the ability to catalyze peptide bond formation through trans-acylation.

Luisi and co-workers described how Ser-His can catalyze the synthesis of a peptide bond from activated amino acid precursors, with comparable yields to chymotrypsin however on a time-scale which was approximately 6 times longer compared to the enzyme.[36] Upon incubation with the single amino acids and the isomer His-Ser, no peptide product was observed over the same time-frame and under the same conditions. The reaction is pH dependent with hydrolytic activity increasing in basic conditions, > pH 7. This study was considered to be of relevance to the chemical origin-of-life in that it seems reasonable that today's enzymes were preceded by simpler peptidic precursors.

Overall, these studies clearly demonstrate that even minimal primary sequences of relevant residues alone can influence the catalytic activity of that peptide. This includes the residues that make up the sequence but also the order in which they appear as demonstrated in the above examples. A core sequence, Ser-His, can be modified by adding residues to the termini of the sequence with minimal loss of catalytic activity however no additional amino acids had been found to enhance the observed activity. Unfortunately no rates were reported for these examples so it is currently not possible to directly compare their catalytic activity with those of other design approaches.

2.5 Self-Assembling Peptides in Catalysis

The ability of certain peptide-based molecules to self-assemble into ordered nanostructures is now well established.[37-42] These often highly ordered structures can be chemically modified through choice of amino acids and may therefore be ideally suited for the design of catalysts. Due to the nature of the interactions within these structures; hydrogen bonding, hydrophobic interactions, π-π stacking *etc.*, the resulting materials may possess features that are similar to those of natural enzymes (*e.g.* amphiphilicity of architectures as well as substrate recognition and specific microenvironments for catalysis to take place,) however they would be simpler and tunable. In addition, they may add additional features that are not normally found in naturally occurring catalysts, including multivalency and multiple, cooperative active sites situated along the length of the self-assembling fibers. Therefore,

supramolecular self-assemblies based on peptides have become of great interest to biochemists and bionanotechnologists to produce new biologically inspired catalysts.

Stupp and co-workers reported a nanostructured peptide-based catalyst obtained by molecular self-assembly. They demonstrated ester hydrolysis catalyzed by histidine residues positioned on the surface of these cylindrical nanostructures (Figure 2.4A).[2] The core peptide segment of the structures is Lys-Leu-Leu-Leu-Ala-Ala-Ala with histidine incorporated on the lysine amine side chain and N-terminus whilst an aliphatic tail is present to encourage formation of cylindrical structures. Four variations of this structure were synthesized in order to study esterase activity alongside control peptides (1 – 4) (Figure 2.4B).

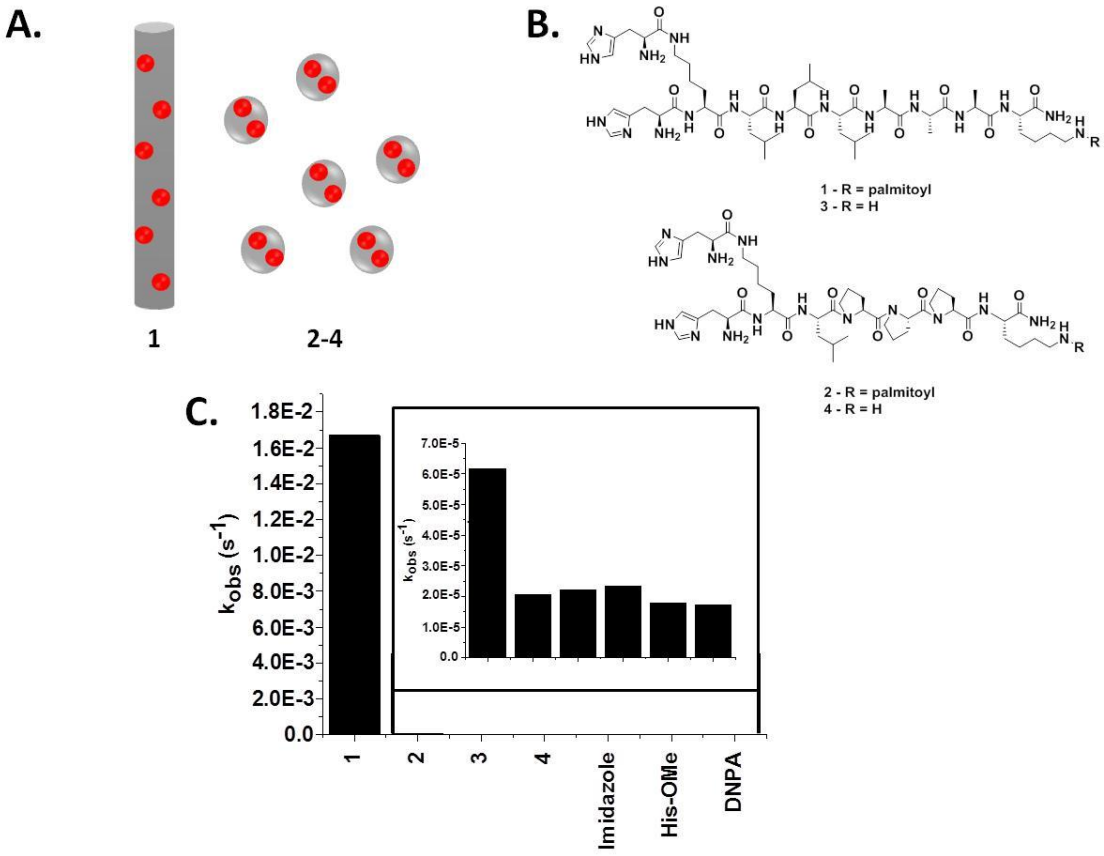

Figure 2.4. A. Schematic of self-assembled peptide nanofiber with histidine residues present (peptide 1) and a spherical aggregate with histidine residues present (peptides 2-4) **B.** Chemical structures of peptide amphiphiles used to build nanostructures. **C.** k_{obs} data of all peptides and controls.

Peptide 1 was the amphiphile used to create self-assembled nanofibers. Peptide 2 lacks the amphiphilic tail to favor the formation of spherical aggregates whilst peptides 3 and 4 contain proline mutations preventing the formation of β-sheet structures and again resulting in spherical aggregate formation. On incubation with the esterase substrate (2,4-dinitrophenyl acetate), peptide 1 was found to have a k_{cat} of $1.67 \pm 0.13 \ \ 10^{-2}\ s^{-1}$, three orders of magnitude greater than for peptides 2-4 (Figure 2.4C). The nanostructure formed by peptide amphiphile 1 is a highly ordered architecture which presents numerous reactive sites on the surface of this structure, utilizing multivalency, and it is thought that this highly-ordered structure is key for efficient catalysis.

As an alternative to aliphatic peptide amphiphiles, aromatic peptide amphiphiles are made up of a short peptide sequence capped by an aromatic moiety.[41] For these molecules, self-assembly is based upon aromatic stacking interactions between the aromatic moieties and the β-sheet-like hydrogen bonding arrangement between the peptides.[43] Liu and co-workers reported functionalized nanotubes based on aromatic peptide amphiphiles as a hydrolase model.[5]

Fmoc-Phe-Phe-His (Figure 2.5B), based on the well-known Fmoc-Phe-Phe molecule,[41, 44] self-assembles to form uniform nanotubes with the capability to hydrolyze the esterase substrate *p*-nitrophenyl acetate (*p*NPA) through catalytic centers present as a part of the molecule. These structures also feature highly ordered β-sheet morphologies, determined by circular dichroism (CD) and Fourier transform infrared spectroscopy (FTIR). To investigate the role of chemical environment/primary structure in the mechanism of catalytic nanostructures, Fmoc-Phe-Phe-Arg (Figure 2.5B) was also incorporated into the nanotubes in an effort to provide stable transition state binding sites in the form of guanidyl groups through the method of co-assembly. A co-assembled nanotube structure obtained *via* this method gave rise to a β-sheet structure which was uninterrupted by the incorporation of Fmoc-Phe-Phe-Arg (confirmed by CD).[5] The function of these structures can be controlled through co-assembly of two peptides, so that a single catalytic system can integrate various combinations of catalytic and binding sites.[41]

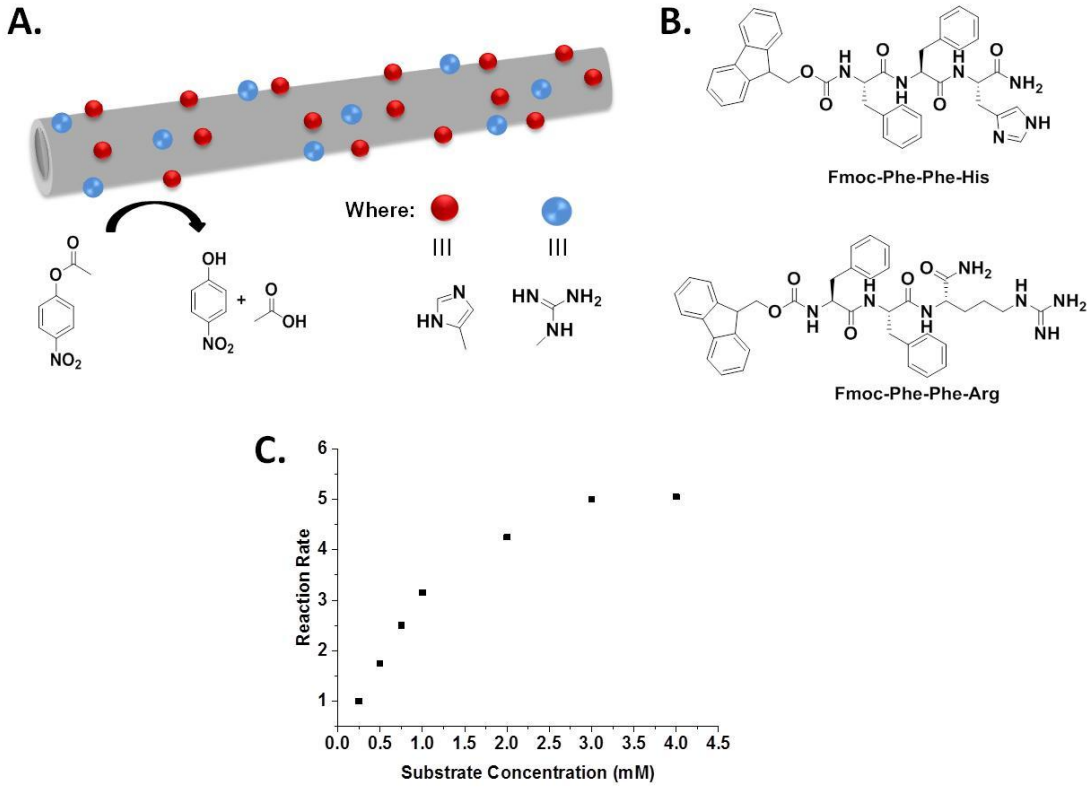

Figure 2.5. A. Schematic of a co-assembled nanotube. *Adapted from reference 5 with permission of The Royal Society of Chemistry.* **B.** Fmoc-Phe-Phe-His and Fmoc-Phe-Phe-Arg used to form co-assembly peptide nanotubes for a hydrolase model. **C.** Schematic of Michaelis-Menten plot of initial catalytic reaction rate vs. concentration of substrate as seen in reported data.

Initial investigation into the Fmoc-Phe-Phe-His nanotubes reported a distinct increase in hydrolysis of the esterase substrate, *p*NPA, with both the Arg and His present. Upon co-assembly of the two molecules the rate of hydrolysis increases confirming that the co-assembled system is a more efficient catalyst, suggesting a role for transition state stabilization (see table 2.1). Typical enzyme kinetics resulted in a k_{cat} of 1.38 x 10^{-3} s^{-1} for the co-assembled system.

A further example that utilizes peptide self-assembly to organize catalytic residues was published by Liang and co-workers.[6] Like the previous example, they make use of a self-assembling peptide to present catalytic centers (His) and binding sites (Arg) on the surface of a nanofiber. The self-assembling peptide (Q11) is salt-responsive and possesses the ability to self-assemble into a β-sheet nanostructure under mild conditions.[45, 46] The self-assembling segment of the Q11 peptide is Gln-Gln-Lys-Phe-

Gln-Phe-Gln-Phe-Glu-Gln-Gln,[46, 47] the N-terminus of the peptide is known to be presented on the surface of the fiber as shown by N-terminally biotinylated peptides, avidin-conjugated colloidal gold, and TEM – *i.e.* they should be available for catalysis.[47] Using co-assembly, functional residues can be arranged to gain the desired functionality (Figure 2.5A, histidine and arginine side chains are present on the surface of a nanostructure). [47] Peptides were synthesized with a terminal histidine residue (peptide Q11His) and with a terminal arginine residue as an electrostatic binding site (peptide Q11Arg). These peptides were then co-assembled to facilitate catalysis and substrate binding in the same sample.

Upon incubation of *p*NPA with Q11His an enhancement in hydrolytic rate was observed. This increase in activity was proportional to catalyst concentration and catalytic activity is believed to be due to the high density of catalytic residues presented on the surface of the fiber. The co-assembled system demonstrated a further enhancement in hydrolysis. Q11His had a value of 1.96×10^{-3} s^{-1} in comparison to 2.64×10^{-3} s^{-1} for Q11Arg/His (both of which are a marginal increase on the rate observed by Liu's co-assembled system at 1.38×10^{-3} s^{-1}). This suggests that the incorporation of an Arg residue is key to the increase in catalytic rate observed in the comparison of Q11His and Q11Arg/His.

As in the Fmoc-Phe-Phe-His/Arg system discussed above (Table 2.1 entry 3), the guanidyl group may act as an electrostatic binding site on the surface of the fiber which may be involved in stabilization of the transition state. It is thought that the imidazole group of histidine activates a water molecule to produce a hydroxide ion which in turn attacks the carbonyl group of the substrate to generate a transition state, *i.e.* water acts as the nucleophile and assumes the role that serine OH plays in the enzyme. The transition state is stabilized by the guanidyl group, binding the oxide ions and activating the ester bond for cleavage before finally releasing the product. This proposed mechanism is based on kinetics parameters calculated from the Michaelis-Menten equation. The binding constant for Q11Arg/His (K_M) demonstrated a stronger binding affinity for the substrate for Q11Arg/His in comparison to Q11His. The incorporation of arginine results in an enhanced catalytic rate for Q11Arg/His.

Korendovych *et al*. reported that heptapeptides formed from amyloid structures have efficient ester hydrolysis activity in the presence of metal cofactors.[3] The sequence Leu-Lys-Leu-Lys-Leu-Lys-Leu was used as a template before design modifications were introduced to develop rational mutants due to the alternating hydrophobic residues within the sequence and the ability of these to interact further by hydrophobic interactions with other β-sheets (Figure 2.6A). Sequence mutation took place, retaining the apolar residues to drive the self-assembly process whilst the side chains of lysine were mutated to different polar functionalities. This gave the molecule the potential to support transition metal binding and catalysis.

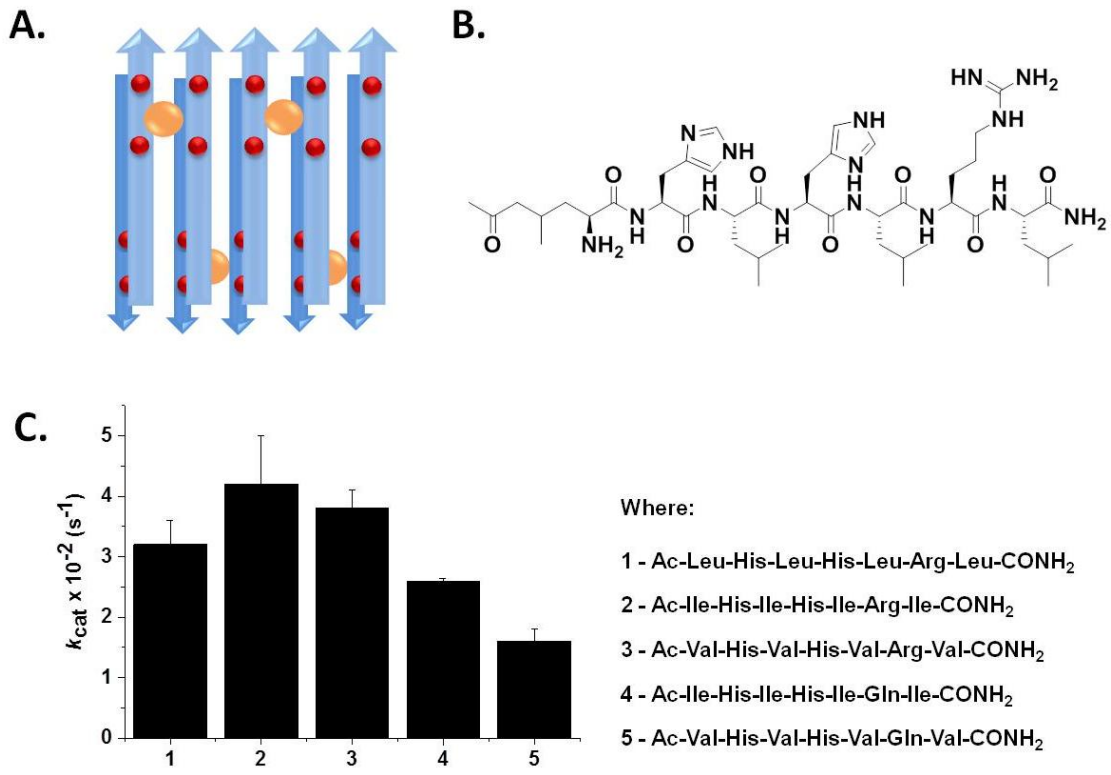

Figure 2.6. A. Schematic of amyloid fibrils containing histidine residues and co-ordinating metal ions. **B.** Structure of Ac-Leu-His-Leu-His-Leu-Arg-Leu-$CONH_2$. **C.** Esterase activity for designed peptides in the presence of 1 mM Zn^{2+}.

Ac-Leu-His-Leu-His-Leu-Arg-Leu-$CONH_2$ (Figure 2.6B) has an esterase activity of k_{cat} 3.2 $\pm$ 0.4 x 10^{-2} s^{-1} which was dependent on Zn^{2+} ions being present in the role of a cofactor (Figure 2.6C). Histidine residues within the sequence support a tetrahedral zinc coordination sphere. This catalytic activity is also dependent on the nature of the

residue at position 6, in this case arginine. The arginine residue plays a significant role in catalysis, related to the earlier described examples. Remarkably, upon replacement of the arginine residue with glutamine, the catalytic activity was reported to increase with regard to k_{cat}/K_M. This was the most active combination of residues. On mutation with aspartic acid, glutamic acid or histidine at position 6, the peptide had little or no activity.

The mutation of arginine with glutamine was intriguing due to an increase in observed catalytic activity. This new sequence was further mutated replacing the leucine residue with isoleucine or valine which is more susceptible to forming β-sheet structures. This resulted in the catalytic efficiency doubling in comparison to the original sequence Ac-Leu-His-Leu-His-Leu-Arg-Leu-$CONH_2$. On replacement of the leucine with alanine, a residue less likely to form the β-sheet structure, the catalytic activity decreased dramatically. The terminal acetyl and carboxamide groups were also reported to be important for catalysis to occur as on the removal of these groups, the peptide is inactive for esterase activity. These changes in activity are not always expected and the combination of rational design and mutagenesis is a good way to improve catalytic activity. Co-ordination of the zinc ions is also crucial for catalysis to occur and also increases the catalytic activity compared to non-metal based esterase peptides that Hecht previously identified using combinatorial libraries[48, 49] and as designed by Baltzer[50] and Mayo.[51]

Finally, a recent article from Escuder *et al.* highlights a low molecular weight bola-amphiphile hydrogelator composed of an alkyl functionalized at both ends with a valine residue which is covalently linked to an imidazole moiety.[15] This gelator has proven to be an efficient catalyst once self-assembled and can hydrolyze *p*NPA with k_{cat} calculated to range from $2.1 – 2.6 \times 10^2$ s^{-1} at pH 6-8. In this case, binding and catalysis takes place in reaction sites which are formed through non-covalent interactions. Further results hint at a role for binding and proposed contribution of both protonated (normally inactive) and non-protonated imidazole in a cooperative fashion, given the limited effect of pH on catalytic activity. This cooperativity may be a result of the unique self-assembly architecture used here and it is remarkable

that catalytic activity (k_{cat}) is enhanced by several orders of magnitude compared to other examples (Table 2.1).

In summary, (Table 2.1), the co-assembled Fmoc-Phe-Phe-His/Fmoc-Phe-Phe-Arg structure presents the lowest activity in comparison to the peptide amphiphile and the amyloid structures. It is possible that there are fewer catalytic reactive sites exposed on the surface of this nanostructure in comparison to the other examples and as a result the catalytic activity is slightly reduced. The importance of internal order of a structure is highlighted by the three orders of magnitude difference between Stupp's peptide amphiphile and his spherical aggregate samples. An insight into the importance of the co-ordination of metal ions in Korendovych's study of amyloid structures is obtained. In the presence of Zn^{2+} there is a significant rate enhancement over background activity resulting in the most efficient example of an enzyme mimic reported in this section. However, in the absence of the zinc ions, activity is reported as barely higher than that of background hydrolysis. These examples highlight some of the mimicry approaches which slightly enhance catalytic activity however the examples reported here are all within an order of magnitude of each other. Remarkably, the most significant rate enhancement is observed in a comparatively system composed of a bolaamphiphile functionalized with Val-imidazole residues at both termini. It is proposed that protonated and non-protonated imidazole operate in a cooperative fashion to enhance activity. Overall, it can be concluded so far it that a combination of design approaches can beneficial in the development of synthetic enzyme mimics.

Table 2.1. k_{cat} values for self-assembling peptide structures.[1]

Entry		Substrate	Peptide Catalyst	k_{cat} (s^{-1})	Mimicry Approaches
1	Guler *et al.* [2]	DNPA	Peptide amphiphile	$1.67 \pm 0.13 \times 10^{-2}$	a, b, d
2	Guler *et al.* [2]	DNPA	Peptide amphiphile (non-assembling)	$2.21 – 6.17 \times 10^{-5}$	a
3	Huang *et al.* [5]	*p*NPA	Co-assembly system	1.38×10^{-3}	a, b, c, d
4	Zhang *et al.* [6]	*p*NPA	Q11Arg/His	2.64×10^{-3}	a, b, c, d
5	Rufo *et al.* [3]	*p*NPA	Amyloid structures (with Zn^{2+})	$1.6 – 4.2 \pm 0.8 \times 10^{-2}$	a, b, e
6	Rufo *et al.* [3]	*p*NPA	Amyloid structures (without Zn^{2+})	-	a, b
7	Singh *et al.* [15]	*p*NPA	Low Molecular Weight Gelator	$2.1 – 2.6 \times 10^{2}$	a, c
8	Zaramella *et al.* [4]	CBZ-Phe-ONP	$H_{(n)}$WDDD/Au MPC complex	$5.2 – 9.74 \times 10^{-3}$	a, b, d
10	Albada *et al.*[52]	*p*NPA	TAC-scaffolded tripeptide arms	$1.9 - 7.7 \times 10^{-3}$	a, b, c

[1] The reaction conditions vary between study therefore they are summarized here for comparison. Guler - hydrolysis of DNPA (varying concentrations) by 1×10^{-5} M imidazole functionalized molecules at 25°C in pH 7.4 50 mM HEPES buffer monitored by UV-Vis at 400 nm. Huang - hydrolysis of *p*NPA (0.5 mM) by 0.1 mM peptide nanotube catalyst at 25°C in pH 7.4 10 mM HEPES buffer monitored by UV-Vis at 400 nm. Zhang – hydrolysis of *p*NPA (varying μM) by 200 μM of Q11His or Q11Arg/His in 1X PBS monitored by UV-Vis at 400 nm. Rufo - hydrolysis of *p*NPA (0.195 - 0.75 mM) by 24 μM peptide at 22°C in pH 8.0 25 mM Tris buffer monitored by UV-Vis at 405 nm. Singh – hydrolysis of *p*NPA (0-0.006 M) by 17×10^{-5} M low molecular weight gelator in 0.1 M Tris-HCl monitored by UV-Vis at 400 nm. Zaramella – hydrolysis of *N*-Cbz-D-Phe-ONP (10 μM) by peptides $H_0 – H_3$ (11 μM for H_0 and H_1; 8.5 μM for H_2 and H_3) in the presence of Au MPC 1 (60 μM) and HEPES (10 mM, pH 7.0) in H_2O:CH_3CN = 9:1 at 37 °C, monitored UV-Vis at 400 nm for 50 minutes. Albada – hydrolysis of *p*NPA (25 mM) by 0.1 mM tripeptide in 20 mM Bis-Tris (pH 6.0 and 7.0) buffer monitored by UV-Vis for 120 minutes.

2.6 Peptide Functionalized Particle Scaffolds in Catalysis

As discussed in the previous section, peptides have the ability to form nanoscale structures and can provide chemical functionality resulting in designed systems with desired properties. The combination of peptide assembly and inorganic nanoparticles enables another route to produce nanomaterials which may possess catalytic activity as they fulfil the requirements of order, presentation of chemical moieties plus multivalency.[2, 3, 5, 53, 54] Nanoparticles decorated with functional ligands are particularly interesting in the development of catalysts based on multivalency. As with structures described in the previous section, self-assembly may be relied on for the formation of multivalent structures and is a pre-requisite for catalysis for many peptides that are not active on their own in solution. These self-assembled monolayers are of a relatively low-complexity in comparison to enzymes. The surface not only brings the catalyst and the substrate into close proximity, it also generates a micro-environment with an increased local pH which activates the catalysis.

Prins and co-workers reported on histidine containing peptides which self-assemble on the surface of gold nanoparticles to give gold mono-layer protected clusters which possess esterase activity.[4] They previously reported that histidine residues within parts of a self-assembled mono-layer on the surface of a gold nanoparticle can act as a catalyst for transesterification reactions in a methanol-water solution.[55] In a more recent paper, they bring catalytic units together through co-assembly (Figure 2.7).

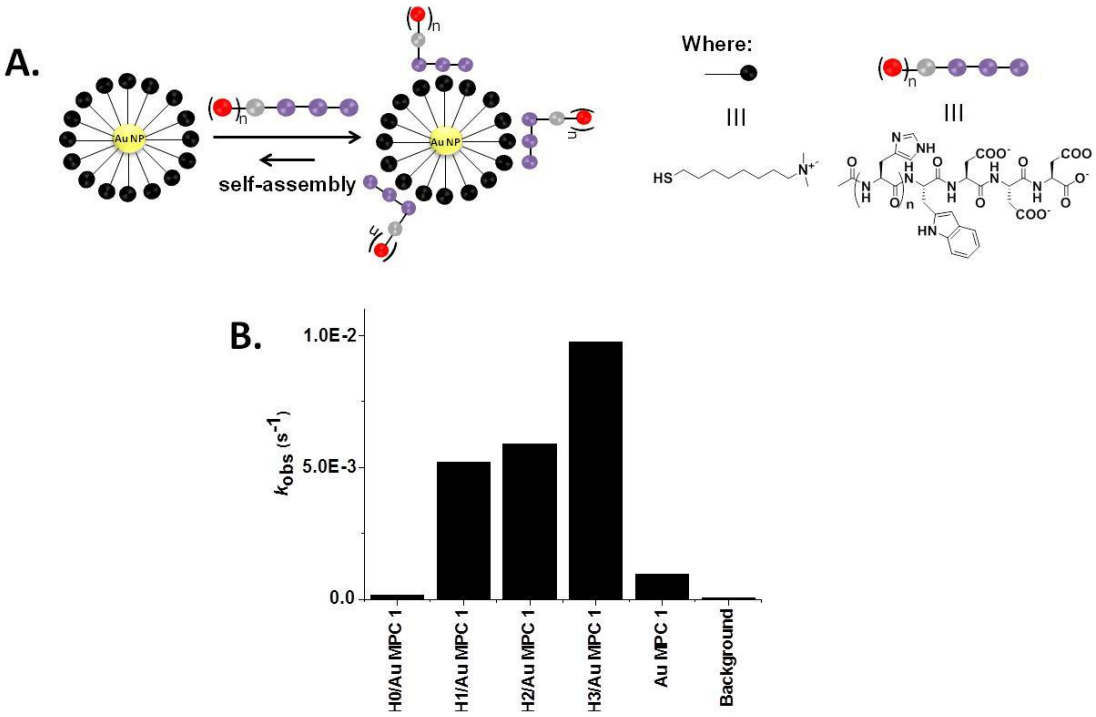

Figure 2.7. A. Self-assembling peptides on the surface of gold monolayer-protected clusters which catalyze transesterification. *Adapted with permission from reference J. Am. Chem. Soc., 2012, 134, 8396-8399. Copyright 2012 American Chemical Society*. **B.** k_{obs} rates for the gold mono-layer protected clusters.

The peptides were designed around having three aspartic residues as anchors to attach the peptide to the cationic functionalized nanoparticle *via* electrostatic interactions, the presence of tryptophan as a fluorescent label to confirm peptide binding (Figure 2.7) and the presence of catalytic histidine residues. On incubation with the substrate benzyloxycarbonyl-phenylalanine-4-nitrophenyl ester (Cbz-Phe-ONP) all complexes, His-$_1$ – His-$_3$/gold mono-layer protected clusters, demonstrated an increase in activity of two orders of magnitude relative to the background control sample. k_{obs} values were calculated to be 5.2 – 9.74 x 10^{-3} s^{-1} (Figure 2.7B). The peptides free from the complex state showed no activity; confirming that the gold mono-layered peptide complexes are necessary to trigger catalytic activity.

Kinetic profiles were obtained and, upon fitting of experimental data to the appropriate model, provided pseudo-first order rate constants with regards to catalytic activity. In order to make a direct comparison between peptides, the pseudo-first order rates were divided by the peptide concentration to yield second order rate

constants. A plot of the second order rate constants as a function of the number of histidines in the peptide sequence gave a straight line confirming that histidine residues are the origin of catalysis. It was reported that local pH of the monolayer/complex surface was higher than that of the bulk solution, indicating that catalysis through multivalent interactions across probes was unlikely to occur. Maximum catalytic activity per histidine residue was obtained when the peptide was on the surface of the cluster. As the peptide covers the surface of the nanoparticle, the carboxylates act as counter ions to the ammonium head groups decreasing the pH. The concentration of protonated imidazole residues therefore increases, thereby facilitating catalysis.

Further investigation into this system by Prins and co-workers yielded insights into the structural parameters that are necessary for catalysis to take place.[56] Once again, it has been demonstrated that the catalytic activity can be influenced by small structural changes in the primary peptide sequence of the supramolecular system. Mutation of the residues flanking histidine, from apolar to serine residues, results in an increase in catalysis rate. An investigation into substrate scope brought to light the finding that substrates that possess a hydrophobic component show increased levels of hydrolysis when incubated with the catalyst. This confirms that hydrophobic interactions with the hydrophobic section of the catalytic monolayer can play a key role in substrate binding. After four catalytic cycles while sequentially adding substrate, a decrease in catalytic rate is observed. It is hypothesized that this was due to competition between the carboxylate and the substrate.

The k_{cat} value for the $His_{(n)}$WDDD/Au MPC complex is in the same region as the self-assembled peptides discussed in the previous section albeit using a different substrate (the *p*-nitrophenol product is observed as before and the absorbance at 400 nm measured over time). Again, histidine residues were present in the peptide monolayer as catalytic residues and there was order in the assembled structure. The sequence of the peptide is significant to its activity. In contrast to the self-assembling catalytic peptides mentioned previously, nanoparticles possess the advantage of mobility due to Brownian motion. Therefore, the active sites for catalysis can move with the nanoparticle and are not restricted as they are in self-assembled (gel) fibers.

Albada *et al.* reported scaffolded peptides towards artificial receptor molecules which have the ability to bind their substrate as well as possess esterase activity[52] on the back of work demonstrating scaffolds containing tripeptides for serine protease mimics.[57] Triazacyclophane (TAC)-scaffold (Figure 2.8) based peptides were explored with respect to hydrolytic activity. It was anticipated that the system, with three different tripeptide arms, would rely on cooperative action and the presence of multiple catalytic amino acid residues which would lead to receptors capable of hydrolysis.

The TAC-scaffolds were decorated with different sets of tripeptides which enables post-screening characterization of each of the scaffold arms. The tripeptides were designed based on the nucleophilic, basic or acidic part of the catalytic triad in each of the strands. As well as this, non-functional amino acids were introduced to provide a hydrophobic environment which can play a role in substrate binding. The nucleophilic peptide was made up of Cys/Ser/Phe, the basic set was His/Leu/Lys and the acidic arm was Asp/Glu/Ile. The scaffolds were prepared by the split-mix synthesis approach. Methodology described in the literature was used to assess hydrolytic activity of the scaffold bound peptides which involved the incubation of the beads with a fluorescent esterase substrate.[58] The beads were soaked in an aqueous, buffered solution of 8-butyryloxypyrene-1,3,6-trisulfonate and then decanted into a Petri dish. Solvent evaporation on the surface was quick however evaporation inside the beads was slow and therefore each acts as a microreactor. If the tripeptide has esterase activity, they demonstrate an intense, green fluorescence.

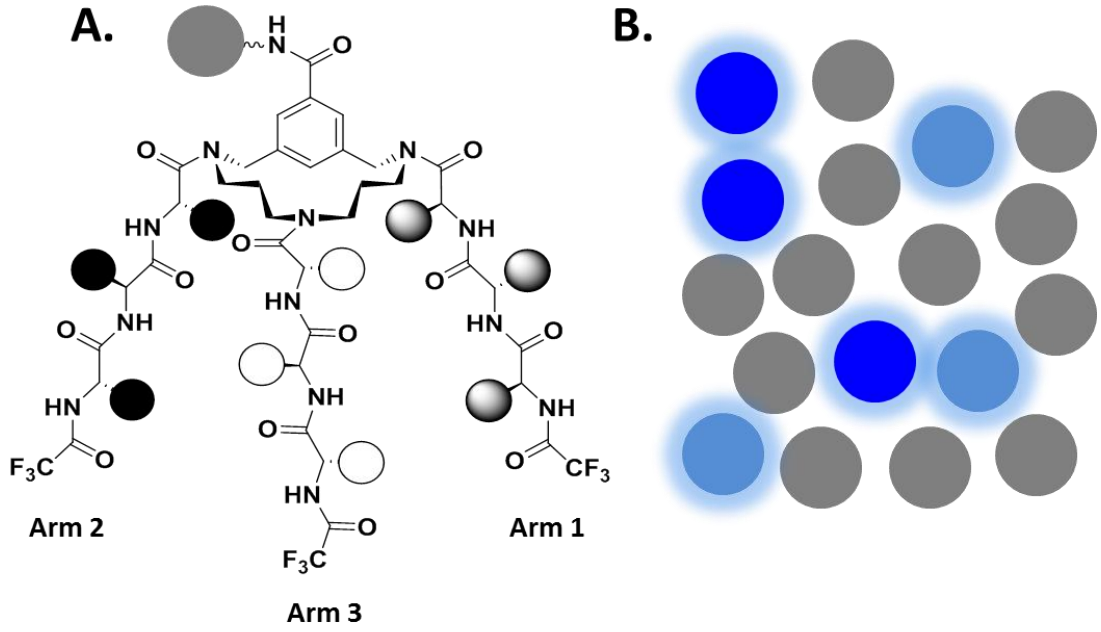

Figure 2.8. A. TAC-scaffold tripeptide with one nucleophilic, one basic and one acidic arm prepared by the split-mix method. **B.** Blue fluorescent beads indicating hydrolysis by the tripeptide arms visualized under a fluorescence microscope.

It was observed that although acid residues are the least important for hydrolysis, the acidic residue-containing tripeptide was most highly conserved with the identified receptors favoring aspartate over glutamate. It was also observed that histidine was more important for hydrolysis than serine. Two sequences were selected for characterization of catalytic activity, the first contained tripeptide arms Cys-Cys-Phe, Asp-Asp-Glu and His-His-His (1) whilst the second was Phe-Phe-Phe, Ile-Asp-Asp and His-Leu-Leu (2). Catalytic analysis was carried out at pH 7.4 using *p*PNA as the substrate and the catalytic rates obtained were 7.7×10^{-3} s^{-1} (1) and 1.88×10^{-3} s^{-1} (2) respectively. With regards to the constructs 1 and 2, there was a correlation between the number of histidine residues present and the hydrolytic activity, as histidine number increases hydrolysis also increases. It can also be said that the activity of the receptors is rather low, with activity being only a factor of 4.4 more active than 4-methylimidazole (4-MeIm). Finally, there is a difference in catalytic activity between the two most active receptors which each contain three histidine residues in the basic arm. Variations in the amino acid sequence in the other two arms of the peptide can affect the kinetic parameter of hydrolysis. These variations may result in more active

nucleophiles or a hydrophobic substrate binding site however, these receptors do not display a high affinity for binding. Catalytic activity is most likely to be a result of the nucleophilicity of the histidine imidazole rings and is assisted by very weak substrate binding. Regardless of the low rates of activity in this case, it demonstrates that there are a number of diverse catalytic receptor molecule combinations which can be synthesized and used for catalysis. The subtle changes in amino acid arms and the effect on catalysis should promote the need for further research in the area of scaffolded peptides as enzyme mimics.

2.7 Alternative Catalytic Systems

Whilst it is beneficial to design minimalistic biocatalysts that are suited to specific reactions and reaction conditions, the use of a discovery technique *e.g.* phage display, can identify potential catalysts from a vast library of potential sequences. Discovery techniques also directly relate sequence/structure to a particular, desirable function *i.e.* amide/ester hydrolysis. M13 phage display libraries are made up of viruses which display 5 copies of a single, short peptide (12 amino acids) on the tip of their protein coat. This technique can then be utilized to identify peptides of interest, the DNA can be sequenced to identify the peptide on display which in turn is synthesized for characterization and mechanistic studies.

A recent example that utilizes phage in the mimicry of enzymes comes from Belcher and co-workers.[59] They developed a robust catalyst for targeted reactions in unique environments that are not standard assay conditions. M13 bacteriophages were selected as a template for their design as they possess multivalency, thermostability, scalability and can be genetically modified. They sought to display catalytic motifs from the enzyme carbonic anhydrase on the major protein coat, the P8 protein, which is repeated 2,700 times to encase the phage DNA. This provides the virus with thousands of copies of the catalytic motif across the entire coat protein therefore providing multiple opportunities for the catalysis of hydrolysis reactions to occur. The binding pocket of this structure is open therefore it possesses a wide substrate scope. The catalytic efficiency of this protein structure was studied in aqueous

conditions (2% DMSO, 98% PBS), organic solvents (98% DMSO and 2% PBS) and at elevated temperatures, conditions which the natural enzyme could not withstand.

The active site of carbonic anhydrase, an efficient zinc-based metalloenzyme, possesses two histidine residues in its active site which are separated by a phenylalanine in an α-helical structure. A third histidine residue is situated in a β-sheet close by and the three histidines together bind the $zinc^{2+}$ ion. A hydroxyl ion or substrate occupies the 4^{th} coordination site of the metal ion. The natural geometry of the enzyme was replicated throughout the protein coat of the bacteriophage. A pair of histidine residues was encoded at fixed positions and surrounded by a random combination of other amino acids in 8 amino acids inserts at the N terminus of the coat protein which is displayed on the surface the phage. Deeper into the protein, a third histidine residue was inserted so that the N-terminal histidine residues would be in close proximity to the third residue on an adjacent P8 protein. Clones from the generated libraries were observed for sequence similarity to the natural enzyme and from a sub-population of 10 sequences, clone Asp-Asp-Ala-His-Val-His-Trp-Glu was selected for further study. Hydrolysis studies were carried out in the presence of zinc sulfate.

There was a significant increase in hydrolysis of *p*NPA in the presence of the clone. This suggests a degree of coordination between the catalytic residues, however the activity is still lower than that of the natural enzyme. Kinetics studies were carried out to obtain a k_{cat} value of 0.002 s^{-1} for the clone in comparison to the natural enzyme, 1.2 s^{-1}, implying that the rate of turnover is a far more important factor in this case when compared to substrate binding. This is in good agreement with chapter 4.3.2 which concludes that substrate binding does not play a role in ester hydrolysis with the catalytic phage and peptide. Finally, the surrounding amino acids that make up the insert and their interactions have not been designed for their purpose and in natural examples, they are known to play a role in catalytic activity. Their consideration would likely increase the catalytic behavior of the phage. These bacteriophages are also robust in non-aqueous solvents, including DMSO, and exhibit a 30 fold increase in catalytic efficiency in this solvent. They can also catalyze a range of substrates including *p*-nitrophenyl acetate (*p*NPA), *p*-nitrophenyl

propionate (*p*NPP), *p*-nitrophenyl butyrate (*p*-NPB) and *p*-nitrophenyl palmitate (*p*NPPa).The clone hydrolyzed *p*-NPB at half of the efficiency of *p*NPA and again the non-aqueous reactions had a higher efficiency than the aqueous systems. This capability to react with substrates of varying size makes the clone an interesting alternative to established biocatalysts. The catalytic efficiency was found to increase with higher temperatures, up to 65 ^{o}C, the bacteriophage was twice more active at higher temperatures in comparison to room temperature. The M13 capsid is a robust structure which provides a catalytic site which has the ability to catalyze reactions at high temperatures. This could prove useful in industrial reactions.

As a (more challenging) alternative to esterase activity, peptide mimics for phosphatase enzymes have also been studied. Gulseren *et al.* demonstrate peptide nanofibers which mimic alkaline phosphatase activity for osteogenic differentiation.[60] They take advantage of self-assembling peptide amphiphile Lauryl-Val-Val-Ala-Gly-His-NH_2 (pPA) as well as two controls, Lauryl-Val-Val-Ala-Gly-Glu (E-PA) and Lauryl-Val-Val-Ala-Gly-Lys-NH_2 (K-PA), which were mixed to produce non-active nanofibers for further study. The nanofiber that forms is a bioactive nanofiber, similar to the cylindrical supramolecular structure that Hartgerink *et al.* reports forms on the self-assembly of peptide amphiphiles[39] however in this case it is functionalized with imidazole as reported by Guler *et al*.[2] These fibers possess catalytic and biomineralization-enhancing properties which mimic the enzyme alkaline phosphatase. The fibrous network that forms is similar to that of the extra cellular matrix and is decorated with catalytic centers that are used to produce bioactive, catalytic and calcifiable bone matrix constructs.

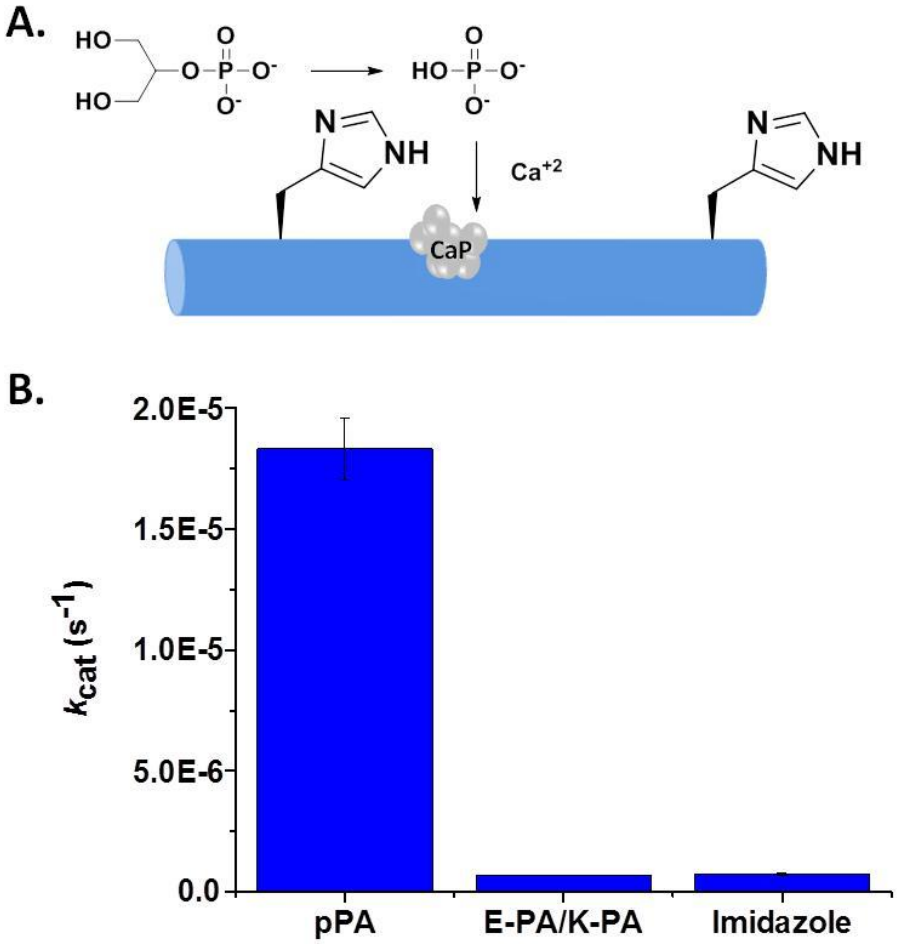

Figure 2.9. A. Phosphate hydrolysis by basic histidine and the mineralization of CaP on the catalytic nanofiber. **B.** k_{cat} rates for the bioactive nanofibers.

The peptide nanofibers which form have a β-sheet conformation as confirmed by CD. TEM demonstrates that that the peptide amphiphiles self-assemble into fibers with a diameter of 5 – 10 nm. A modified colorimetric assay, utilizing *p*-nitrophenyl phosphate, was used to assess the hydrolytic capability of the nanofibers for phosphate groups. The catalytic nanofibers which display histidine in a multivalent fashion were shown to have an enzymatic rate of 1.83×10^{-5} s^{-1} as a result of the reaction initiation by histidine. The combined control fibers demonstrated a lower activity of only 6.87×10^{-7} s^{-1}. It is clear that histidine enhances catalysis. There are two mechanisms through which this can occur, the first by increasing the nucleophilic character of water through proton deprotonation converting it to a

nucleophile to cleave the phosphate group of the substrate. The second is through the hydroxyl groups of the β-glycerolphosphate. The imidazole moiety can deprotonate the hydroxyl groups which in turn generates nucleophiles which attack the substrate and cleave the phosphate group. The organized presentation of the histidine residues through means of self-assembly, results in the enhancement of catalysis in comparison to free histidine which has a rate of 7.54×10^{-3} s^{-1}. It is clear that the specific presentation of imidazole functionality by self-assembled peptide amphiphiles is necessary in order to achieve catalysis.

The phosphatase activity of these catalytic nanofibers is favorable for several reasons. The first is that the activity presented is effective for the mineralization of CaP in the process of bone formation. Calcium was found to be present on the nanofibers which present histidine with no mineralization occurring on the control fibers. In this case, the accumulation of calcium phosphate (CaP) on the surface of the fibers begins to limit the catalytic activity which is similar to that of the natural enzyme, reducing towards the end of the mineralization process. These fibers can be used for controlled mineralization in a two dimensional environment. As well as this, the fibrous networks have been shown to induce osteogenic differentiation as well as enable maturation of osteoblast-like cells and mesenchymal stem cells into osteoblasts which is a huge step forward in the area of bone grafts. This is a new, biocompatible platform technology to develop functional biomaterials for numerous applications.

2.8 Conclusions

Efficient and effective catalysis of natural enzymes has long been an inspiration to chemists working to overcome the expense, complexity and reaction media limitations of these proteins and develop new simple, synthetic catalysts that can be modified to suit desired substrates/reaction conditions. The examples above illustrate that some headway has been made in this field and rules are beginning to come to light for the design of these synthetic catalysts. It has been shown that histidine is a crucial residue for catalysis in the majority of systems regardless of which activity is

being mimicked. It has also been demonstrated that design of the peptides can be used to alter catalytic activity, enhance stability and provide insights into the mechanisms of reactions. The most effective approaches seem to be based on primary peptide sequence, nano-surfaces/scaffolds and multivalency with an especially impressive rate enhancement observed in a system were cooperative interactions between imidazoles were facilitated.[15] The presence of metal ions has also been shown to improve activity.[3]

Self-assembly of nanostructures allows for the presentation of reactive sites on the surface of a highly ordered nanofiber scaffold. In comparison to spherical aggregate species the rate of hydrolysis of the catalytic nanostructures is significantly higher. The function of these structures can be taken advantage of, possibly through co-assembly, so that a single catalytic system can integrate various molecular recognition events.

Multivalent surfaces play a critical role in tuning the catalytic activity. New methodology for the design of efficient catalysis of ester hydrolysis displaying multiple functional residues on the surface of the fiber provides opportunities to design artificial enzyme mimics through the incorporation of residues with catalytic activity. The surface not only brings the catalyst and the substrate into close proximity, it also generates a micro-environment which may have a local pH which activates the peptide. The activity of the peptide can be influenced by the flanking residues of catalytic histidine residues. Therefore, the properties of a complex catalytic system can be controlled by small structural changes. Reduced efficiency of these systems after multiple turnovers could be due to the competition between carboxylates and the substrates. It can also be seen that metal ions have the potential to increase potential activity in some cases by interacting with metal ion binding sites.

It has been demonstrated that it is not only peptides that are being utilized as biocatalysts incorporating short peptides. M13 bacteriophages provide a new template to explore and work with in this field. Bacteriophages with catalytic capability have been designed and engineered for enzymatic activity by genetic modification. This system demonstrates multivalency by displaying catalytic

moieties in multiple positions and again histidine is present. These viruses are a great platform from which to spring into a new direction of enzyme mimicry and they have the potential to overcome severe drawbacks of natural enzymes including complexity and stability.

In summary, all reported methods that have been utilized in short peptide biocatalysis, both screening and design, result in very similar rates of hydrolysis which are still orders of magnitude lower than that of natural enzymes. However, it is clear that significant advancements are being made in the field of short peptides in biocatalysis. The designs featured here are promising and inspiring for future work into this area and for the development of future *de novo* peptide biocatalysts. In particular, supramolecular chemistry approaches offer opportunities to combine several design criteria, including those not found in natural enzymes. Identification of short peptide biocatalysts that rival enzymes may be only a matter of time.

3.0 Discovery of Catalytic Phages for Amidase/Esterase Activity by Biocatalytic Self-Assembly*

***** This work was published in part as: **K. Duncan**, Y. Maeda, N. Javid, L. Birchall, K.F. Gibson, D. Cannon, Y. Kanetsuki, C. Knapp, T. Tuttle, R. V. Ulijn, H. Matsui, Discovery of Catalytic Phages by Biocatalytic Self-Assembly. *J. Am. Chem. Soc.*, 2014, **136**, 15893-15896.[8]

Declaration of contribution to published article: Any reproduced practical work from the aforementioned published article; I was solely responsible for, unless otherwise stated. Prof. Hiroshi Matsui, Dr. Yoshiaki Maeda and Dr. Yuka Kanetsuki provided the phage display panning and TEM results. Dr. Mhairi Towler provided the phage cartoons.

3.1 Introduction

Enzymes and biocatalysts offer a wide range of different activities which have inspired biochemists in the field of design and discovery of minimalistic biocatalysts for demanding chemical reactions in aqueous media. This includes hydrolysis of an amide bond which is an extremely challenging reaction with a half-life of 400-600 years depending on whether the bond is internal or external.[1, 61] Advances have been made in design and discovery approaches for enzyme mimics[62] however; no example can match the catalytic efficiency and selectivity of natural enzymes. Screening of large combinatorial libraries has become one of the favored methods for the identification of potentially catalytic peptide sequences. This fairly straightforward set of techniques involves the exposure of a library of antibodies,[63] phages[64] or proteins[33] to immobilized transition state analogues in order to exploit favorable binding. As well as screening, design approaches have also been utilized to develop new biocatalysts. Many of these take advantage of the surface of a nanostructure, whether it is a self-assembled peptide structure[2, 3, 5, 6, 15] or a nanoparticle surface,[4, 56] to display catalytic residues which enhance catalysis *e.g.* histidine. Interestingly, the simple dipeptide Ser-His has been reported to hydrolyze ester and amide bonds,[25, 65] suggesting that it may not be necessary for the catalyst to possess a binding pocket or be exposed on a surface (chapter 2.0).

This chapter focusses on the development of methodology to discover minimalistic biocatalysts for challenging aqueous reactions by utilizing the well-known technique of phage display. A screening approach for selection of catalysts through a direct relationship with functionality, instead of the typical transition state binding methodology is described. In this case, a physical link is created between the catalyst and aggregate of reaction product at the catalytic site. This co-localization of product and catalyst allows library screening to identify catalysts with the required functionality.[66-68] The concept has been demonstrated previously whereby a potential catalyst can be identified by coimmobilization in a one-bead-one-pot library. One reaction partner (A) is attached to a bead which also possesses the potential catalyst. If the reaction partner (B) is labelled with, for example, a dye molecule then reaction between A and B leads to coimmobilization and identification of the bead with the

active catalyst.[66] Another example demonstrates that hydrogel immobilized enzyme catalysts can be used as a delivery model for hydrophobic drugs.[68] Phage display has been utilized to identify catalysts[16] however biocatalytic self-assembly has not yet been exploited for screening and has the potential to offer catalyst selection for a wider range of reactions.[46, 69, 70]

In particular, amidase activity is of interest however; in some cases enzymes that possess amidase activity can also possess esterase activity so this was also investigated (not all enzymes behave in this manner, for example, thermolysin does not act as an esterase). The catalytic activity of the phage extracted from the bulk library was assessed using high performance liquid chromatography (HPLC), transmission electron microscopy (TEM), ultraviolet-visible spectroscopy (UV-Vis) and fluorescence spectroscopy. Overall, this study demonstrates that this new combined methodology can identify phage with amidase and esterase activity.

The work builds on preliminary data obtained in collaboration between our laboratory and Matsui's laboratory prior to the start of this project, the objective was to use a combination of biocatalytic self-assembly with phage display to identify peptide sequences with amidase activity.

3.2 Preliminary Work carried out by Prof. Hiroshi Matsui at City University New York

*Methodology for the selection of catalytic phages**

* In collaboration with Prof. Hiroshi Matsui, Dr. Yoshiaki Maeda and Dr. Yuka Kanetsuki.

Catalytic phages were identified from a 10^9 library of unique M13 filamentous phage viruses which displayed five copies of a single dodecapeptide at their tip (Figure 3.1). The peptide sequence was encoded by DNA contained within the cavity created by the phage protein coat.

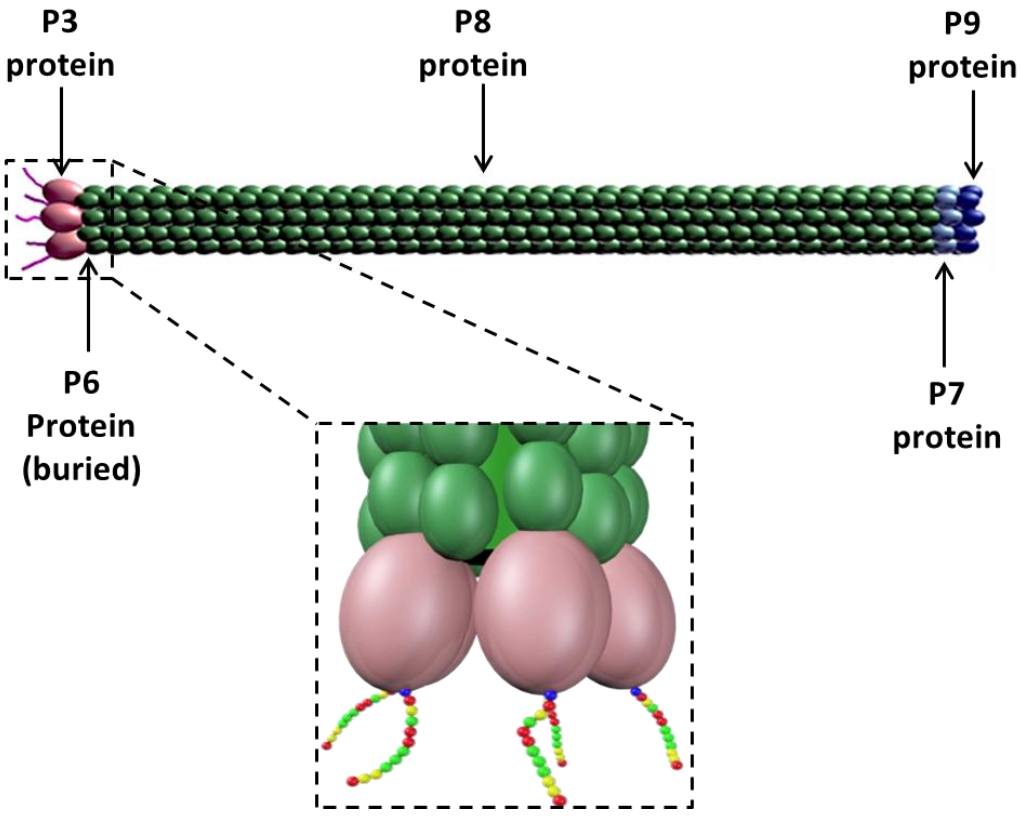

Figure 3.1. M13 phage virus displaying 5 identical dodecapeptides at the tip of the P3 protein.

The phage library was incubated with amino acid derivatives that are known to be precursors to catalytic self-assembly and hydrogel formation,[11] with co-localization of the catalyst and the reaction product expected. As a result, catalytic phages remain with the formed product creating a bulky, heavier virus which can be separated from the unreacted library compounds by centrifugation. In this case, screening focused on mimicking amidase and esterase activity in an aqueous environment.[71]

Hughes *et al.* previously reported the thermodynamically controlled, enzyme-assisted self-assembly of aromatic dipeptide hydrogels from the amino acid precursors Fmoc-Thr and Leu-OMe.[11] The condensation reaction catalyzed by thermolysin (Figure 3.2) was followed by HPLC and showed 75% conversion after 24 hours, resulting in a self-supporting gel. This hydrogel was further characterized by rheology to confirm the gel state.

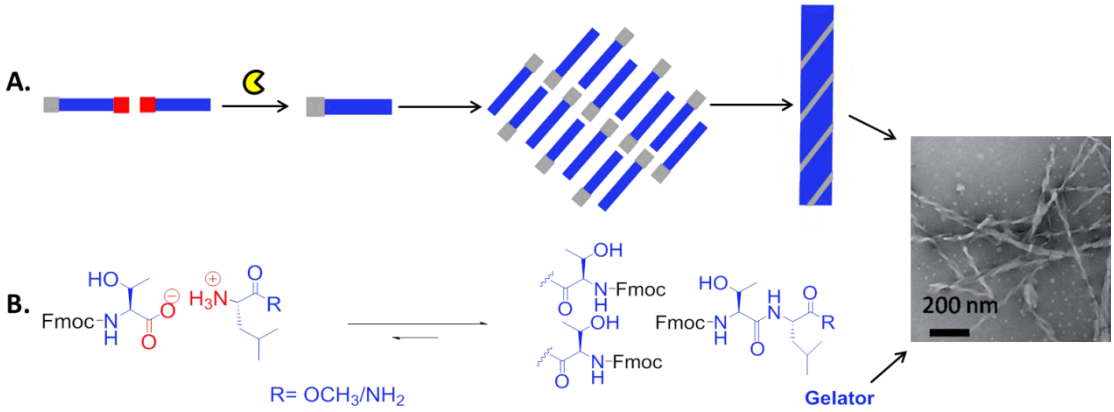

Figure 3.2. Enzymatic assisted self-assembly of aromatic peptide hydrogels. A. Self-assembly process catalyzed by the presence of an enzyme e.g. thermolysin. The addition of the enzyme results in a condensation reaction between two compounds to form a gelator. **B.** Self-assembly of Fmoc-Thr-OH and Leu-OMe/NH_2 to form the self-supporting gel Fmoc-Thr-Leu-OMe.[11]

Based on this earlier work, the self-assembling Fmoc-The-Leu-OMe dipeptide was selected for combination with a phage display library to screen for phage viruses which have the ability to catalyze the condensation reaction between the peptidic precursors.

3.2.1 Phage Display Panning Combined with Catalytic Gelation of Peptides

The library of phage viruses was incubated with the soluble, peptidic gel precursors Fmoc-Thr-OH and Leu-OMe; this will be referred to as the first generation experiment (Figure 3.2). Upon catalysis of the condensation reaction by selected peptides at the tip of the phage, an aggregate of the dipeptide Fmoc-Thr-Leu-OMe formed (Figure 3.3). Due to poor solubility in aqueous media, the resulting catalyst/product aggregate remains localized at the site of catalysis *i.e.* at the tip of the phage (Figure 3.3). This localized aggregation facilitates the elution of the phage virus of interest from the extensive library being screened. Centrifugation is employed to ensure separation and isolation of these specific phage viruses, a technique that has previously been used successfully.[16] Subsequently, the aggregate is removed from the tip of the phage by incubation with subtilisin which hydrolyzes the terminal methyl ester bond resulting in dissolution of the aggregate material. Amplification of the phage viruses was carried out in *Escherichia coli*, the viruses

were titrated and twenty colonies were selected for sequencing before the next round of panning took place. As the panning process continues, the diversity of the peptide sequences in the phage library is reduced and the library is enriched with the sequences which have activity. Two rounds of panning were carried out.

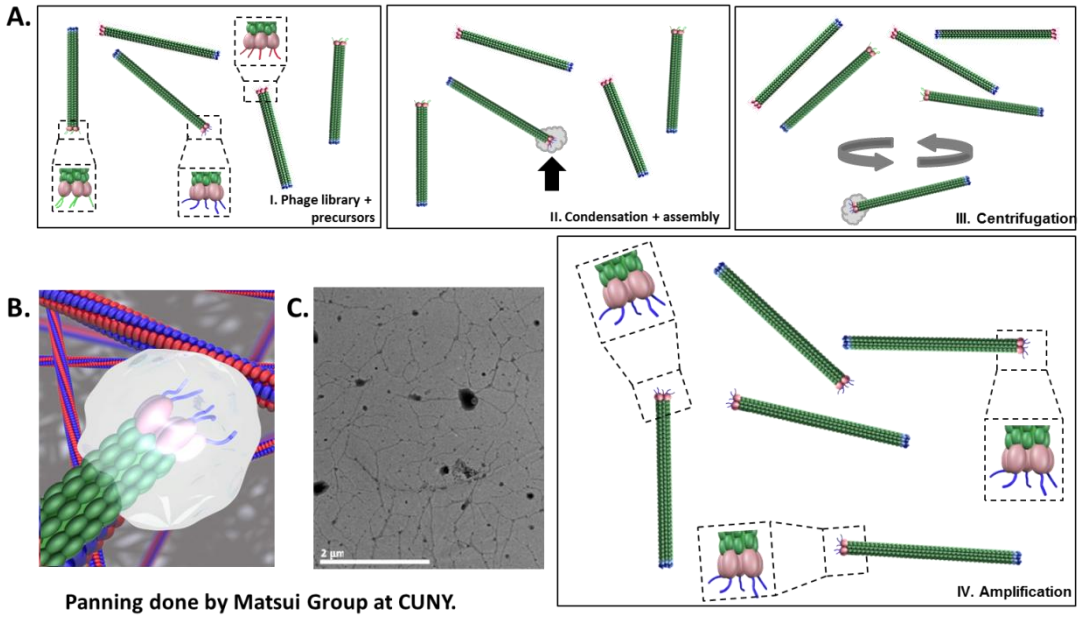

Figure 3.3. Phage display panning process combined with self-assembling gel precursor compounds. A. M13 phage library where I, precursor peptides are added to solution and left to incubate; II, resulting dipeptide product aggregates at the tip of the catalytic phage; III, catalytic phage and resulting aggregate are separated from the bulk library by gentle centrifugation; IV, catalytic phage are amplified in an *E. Coli* host. **B.** Cartoon representation of the aggregate at the tip of the catalytic phage. **C.** TEM analysis of the phage library plus gel precursors after 30 minutes incubation.

The TEM image (Figure 3.3C) illustrates phage particles with the gelation product attached at the tip of the phage after a 30 minute incubation period. This proves that the new combined technique does indeed progress by the formation of product aggregates which can be utilized for phage isolation.

This panning process was repeated using Fmoc-Thr-OH and Leu-NH_2 as the peptide precursors due to the concern that catalysts which possess the ability to hydrolyze amide bonds can also hydrolyze the more labile ester bonds *i.e.* the methyl ester bond of the peptide precursor.[72] This will be referred to as the second generation experiment. The selection process was identical except that the product aggregates

were removed using a 1:1 acetonitrile/water mixture. Once again selected virus plaques were amplified and sequenced.

Alongside the eighteen plaques from the first generation panning experiments, a further eighteen were sequenced from the second generation experiment and a selection of seven between both experiments were chosen for further investigations into their catalytic activity (Table 3.1). These were chosen on the basis that they possessed residues known to be involved in catalysis e.g. Ser, Thr, His, Cys, Asp, Glu. The CPN peptides were also chosen based on the factor that all of these sequences appeared repeatedly in the sequencing of only eighteen plaques.

Table 3.1. Peptide sequences selected by the catalytic self-assembly screening process. CP1-4 were selected using first generation methods while CPN1-3 were selected from the second generation experiments. The random sequences were selected by titrating the phage library and picking 5 sequences at random as controls. Histidine is highlighted in red and cysteine in blue and duplicate sequences in bold italics.

Name	Sequence	Number of Occurrences
CP1	T D H T H N K G Y A N K	1
CP2	T S H P S Y Y L T G S N	1
CP3	S H Q A L Q E M K L P M	1
CP4	S M E S L S K T H H Y R	1
	K L H I S K D H I Y P T	1
	N R P D S A Q F W L H H	1
	D P Q N H N W T N K P A	1
	Y L P H M L V H G S R H	1
	T Y P V V G H Q Q N V M	1
	D I M P K L R D D V H N	1
	N A H T S N N V V A F P	1
	Y G T S M T Q S N W R H	1
	S Y G S L Q T R F G H I	1
	K F F N N T E A T T R P	1
	N Y A L R D P V G Q R Y	1
	L P S V T E I L G S N F	1
	T S A V T L T S D P T L	1
	Q N F S Q M M S I P R K	1
CPN1	***A M H S L V G P A F N R***	**7**
CPN2	***H D T S E Q L L V A P S***	**2**
CPN3	***D L R S C T A C A V N A***	**2**
	A T T W T V A H G V S R	1
	S T D D D H L L A A T T	1
	H P T G S K S T T S T Y	1
	H T D S D P L L A A P S	1
	P T S E V Y L F S G N F	1
Random 1	N Y A D L L E L T G R D	1
Random 2	K Y E L N Q S V Y H P V	1
Random 3	R L H Q A E I N V Q F A	1
Random 4	S A C S A A N H Y L L N	1
Random 5	E G S T G A L R H S A N	1

From the sequences selected, it is clear that there is no obvious sequence similarity. Amino acids which are associated with nucleophilic catalysis (His, Ser, Asp, Glu and Cys) are prevalent within these dodecapeptides; this is however not unexpected based on random selection. If the sequence is twelve amino acids long then there is

0.6 chance of an amino acid featuring (number of amino acids in the sequence/number of available amino acids). The chance of two amino acids featuring, for example Ser and His, is 0.36 (0.6 x 0.6). Therefore, the combination of amino acids featured in these 'hits' was not surprising. The four CP peptides contain the Ser-His combination, although not necessarily directly adjacent to one another, and were specifically selected for further investigation. This was done because an in depth analysis of all sequences was deemed unfeasible and more so because it had been demonstrated that the Ser-His dipeptide possesses catalytic activity.[25] CPN1 and CPN2 also possess these amino acids however CPN3 lacks the catalytic histidine residue and instead possess two cysteine residues. These were taken forward alongside five random sequences as controls.

To confirm that the screening process does proceed through the proposed catalytic self-assembly model, amplified phages resulting from the screening process were incubated with Fmoc-Thr-OH and Leu-OMe and imaged at selected time intervals by TEM (Figure 3.4). The resulting images illustrate aggregates forming at the tip of CP4 phage, which possess catalytic peptides, within 30 minutes of being incubated indicating that the screening process does proceed *via* the catalytic self-assembly model. It is possible that any unreacted Fmoc-Thr-OH can result in non-selective binding to the phage tip which contributes to catalysis through enhanced localization of Fmoc-Thr-OH. Further work is required to investigate the importance of substrate aggregation at the tip of the phage. CP4 was the only peptide tested by TEM as it had the highest propensity for catalytic activity.

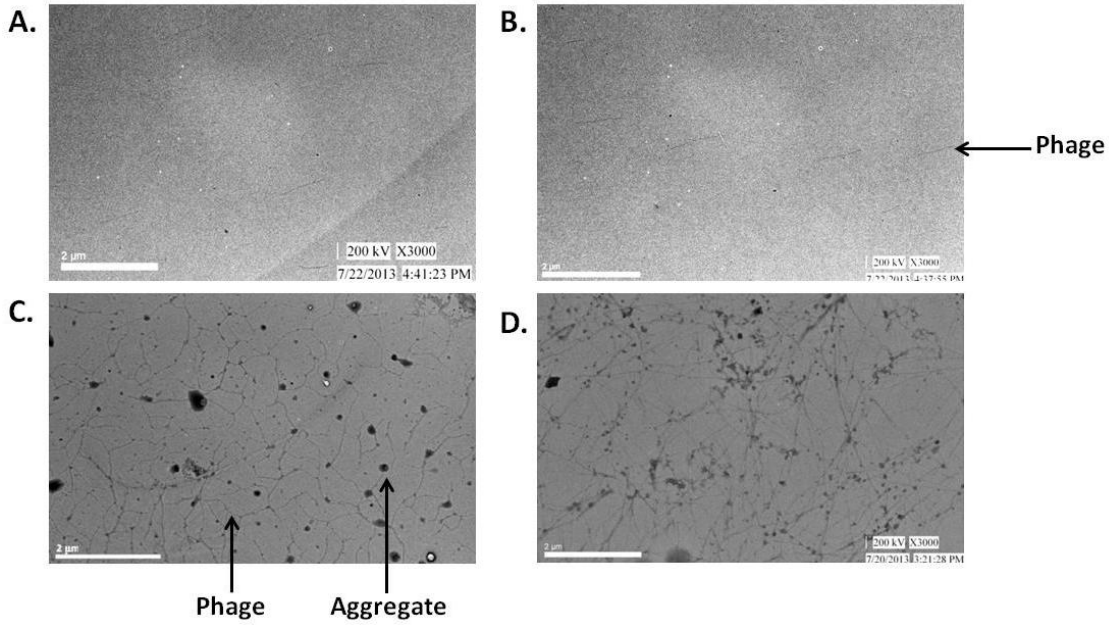

Figure 3.4. TEM of CP4 phage. A. CP4 phage incubation time 30 minutes with no peptidic precursors. **B.** CP4 phage incubation time 60 minutes with no peptidic precursors. **C.** CP4 phage incubation time 30 minutes in the presence of Fmoc-Thr-OH and Leu-OMe. **D.** CP4 phage incubation time 60 minutes in the presence of Fmoc-Thr-OH and Leu-OMe.

3.3 Objectives

Based on these initial studies, the aims of this chapter were to:

- Develop suitable HPLC and spectroscopic assays to determine the enzymatic activity of catalytic phage identified by biocatalytic self-assembly combined with phage display panning.
- Fully characterize the phage identified by the panning process for amidase and esterase activity.

3.4 Results and Discussion

3.4.1 Amidase Activity – Condensation Reaction

Before studying the catalytic activity of the selected phages from the screening process, they were amplified and transferred into buffer from LB media.

As a proof of concept, the first study looked to show the ability of the CP phage to catalyze the condensation reaction used in the second generation panning process. An initial study using Leu-OMe gave irreproducible results that could be due to the aforementioned competing ester hydrolysis reaction. This would lead to gel disassembly, enabling dissolution back into the bulk library and making the condensation reaction undetectable. HPLC was used to follow the condensation reaction and quantify the percentage conversion of starting material to product on catalysis by the catalytic phage (Figure 3.5).

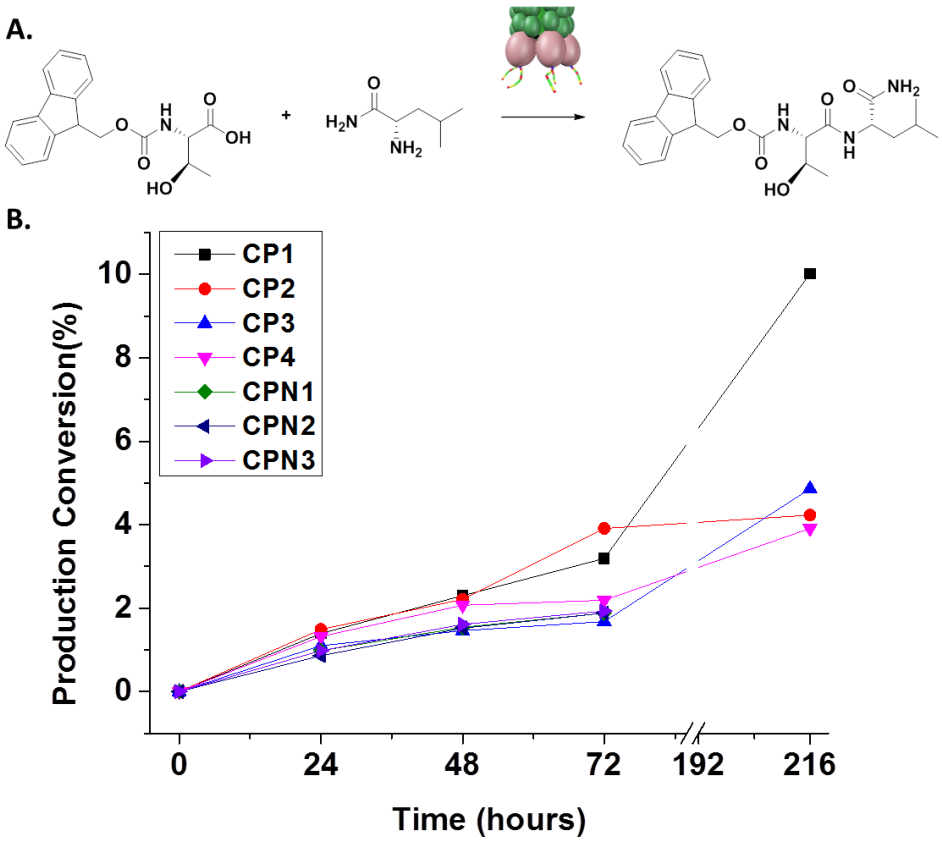

Figure 3.5. Amide condensation by HPLC. A. Schematic of condensation reaction of Fmoc-Thr-OH and Leu-NH_2. **B.** The graph shows % conversion to the reaction product Fmoc-Thr-Leu-NH_2 over time.

After 72 hours amide condensation was observed with CP1 3.2 %, CP2 3.9 %, CP3 1.7 % and CP4 2.2% conversion to the reaction product. The conversion further increased over 216 hours up to 10% for CP1 phage. The rate of conversion up to 72 hours is in line with the 3 day incubation time used in the phage display panning process. Condensation rates of the CPN phage were observed to be marginally over

the background rate with CPN1/CPN2 1.88 % and CPN3 1.93% conversion after 72 hours. It is hypothesized that the conversion to the product and therefore aggregation at the tip of the phage is self-limiting. The aggregates which form around the tip of the catalytic phage do not dissolve back into solution but remain localized at the catalytic site. This localization prevents the phage from diffusing through the solution and catalyzing further condensation reactions which in turn prevents conversion to the product and bulk gelation. Unexpectedly, the random phage also facilitated the condensation reaction, with up to 1 % conversion to product after 72 hours. This could be due to an autocatalytic process or residues incorporated into the phage protein coat and/or displayed on the surface of the virus which facilitate catalysis (Figure 3.6).

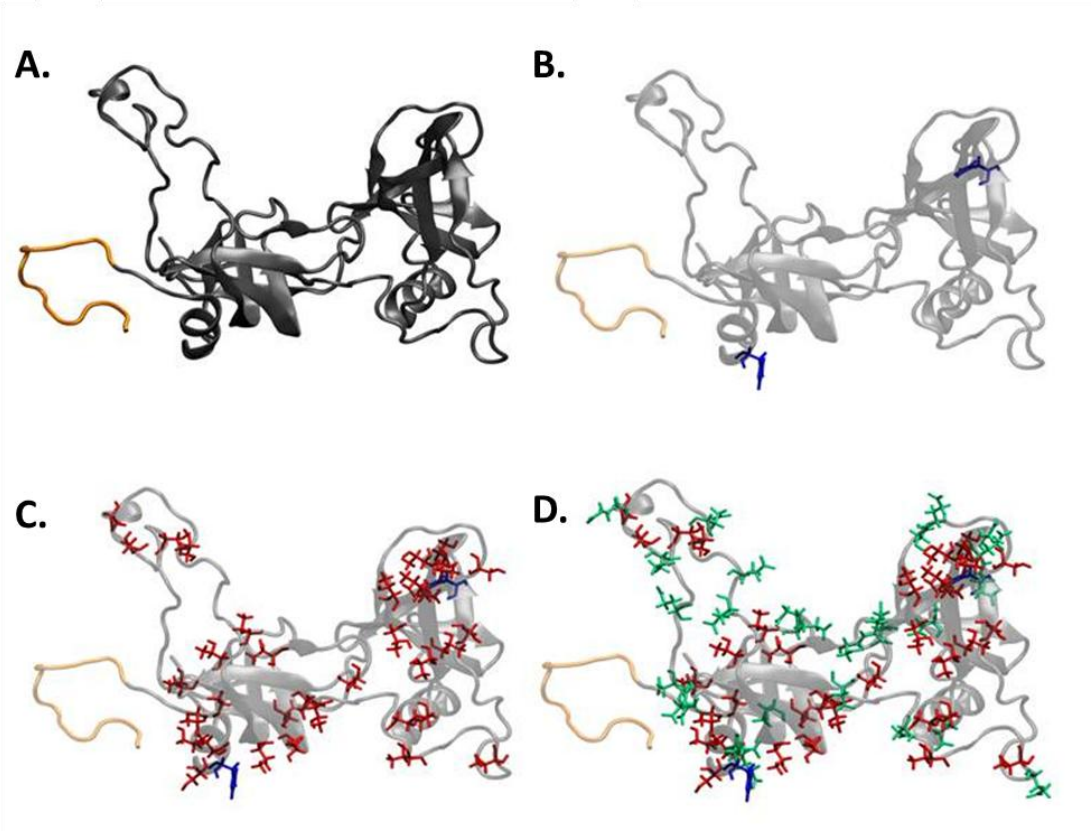

Figure 3.6. P3 protein, PDB 1G3P, A. P3 coat protein. **B.** P3 protein with histidine residues highlighted. **C.** P3 protein with histidine and hydroxyl amino acids highlighted. **D.** P3 protein with histidine, hydroxyl and acidic residues highlighted.

3.4.2 Amidase Activity – FRET Amide Hydrolysis

The direct reversal of amide condensation, amide hydrolysis, was also investigated using the catalytic phage from the screening selection. For this study, a Forster resonance energy transfer (FRET) peptide was utilized. A specifically designed peptide, which included the Thr-Leu sequence found in the gelation, was purchased with a donor 5-((2-aminoethyl)amino)naphthalene-1-sulfonic acid (EDANS) at one end of the peptide and an acceptor 4-((4-(dimethylamino)phenyl)azo)benzoic acid (DABCYL) at the other (Figure 3.7). The final sequence was Glu(EDANS)-Gly-Thr-Leu-Gly-Lys(DABCYL). Upon degradation of the Thr-Leu peptide bond, the resulting peptide fragments move apart from each other. When this occurs, the energy of the donor is no longer quenched by the acceptor. Therefore, the fluorescence of the separated donor compound can be measured and linked back to the rate of peptide bond hydrolysis.

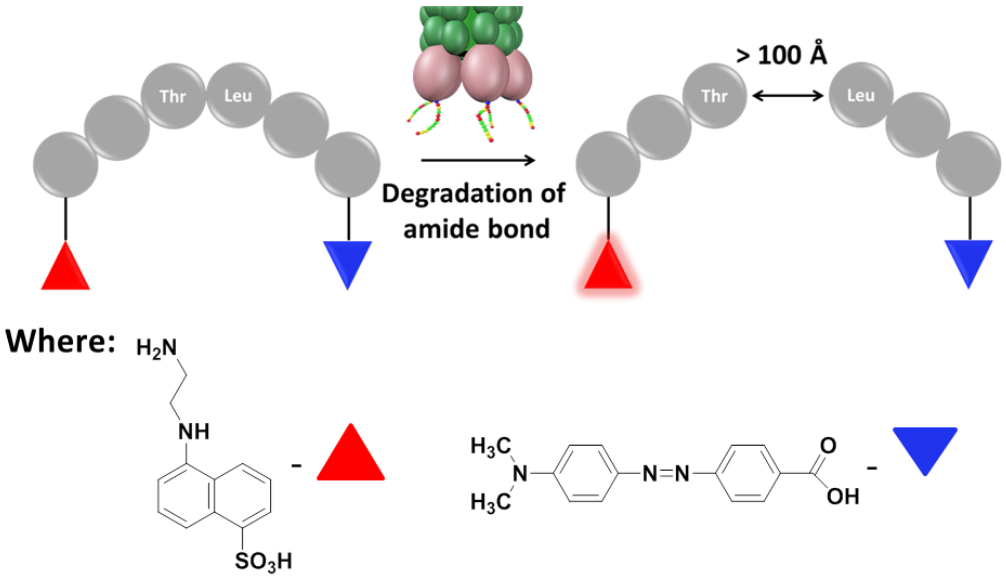

Figure 3.7. Amide hydrolysis by fluorescence. Cartoon representation of Förster resonance energy transfer.

Typical time courses were observed for hydrolysis of the FRET peptide in the presence of the catalytic phages (Figure 3.8). The fluorescence signal for these samples increases over time which can be observed in these plots. It should be noted

that the rates were slow and appreciable rates could only be observed when comparing 24, 48 and 72 hour time points.

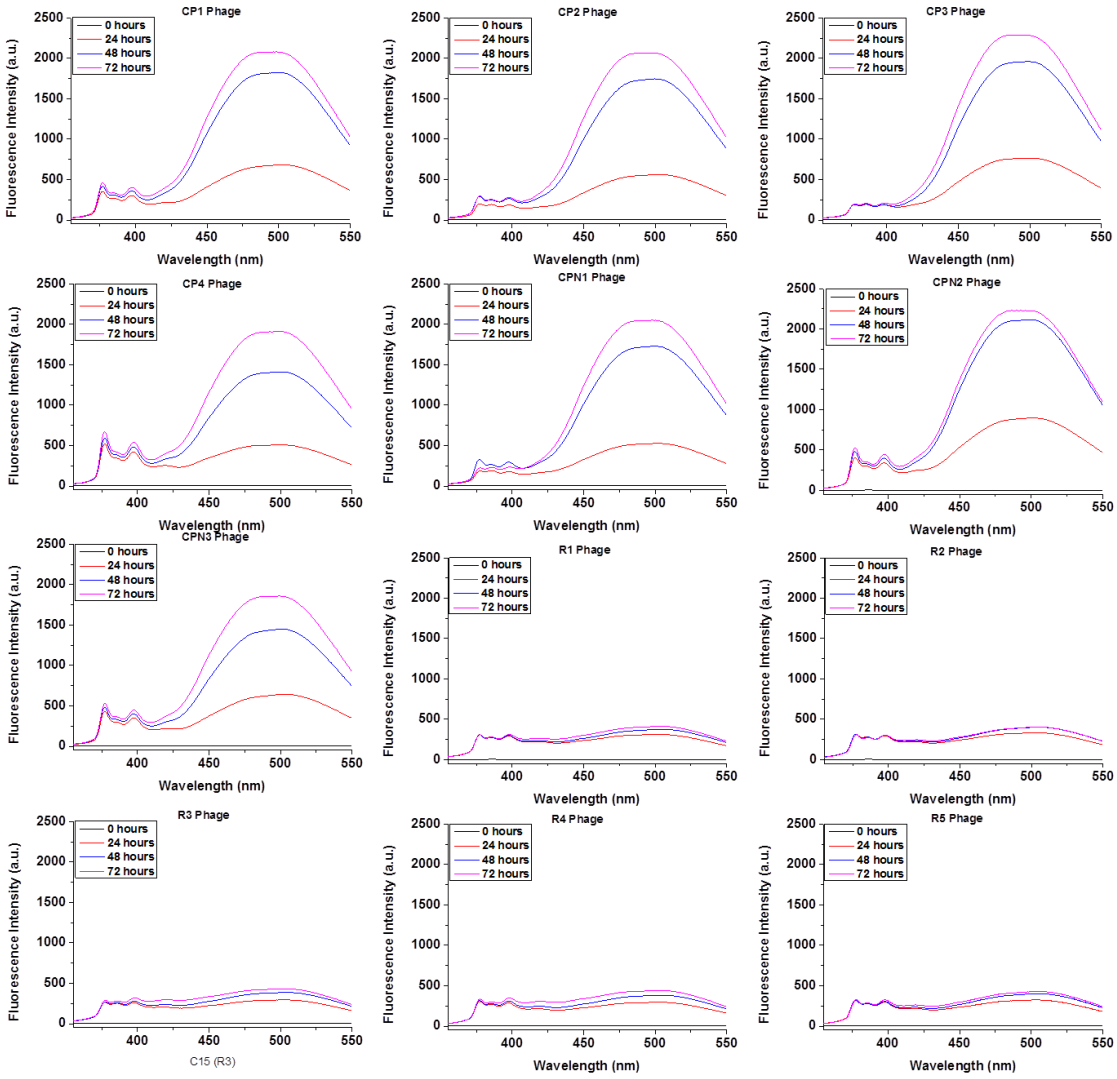

Figure 3.8. Amide hydrolysis by fluorescence. Raw data for the hydrolysis of FRET peptide using 0.0167 μM phage and 2 μM FRET peptide. Each time point is based on three repeats.

The increase in fluorescence was observed over time at 493 nm to deduce the kinetic profile of the hydrolysis of the Thr-Leu peptide bond (Figure 3.9).

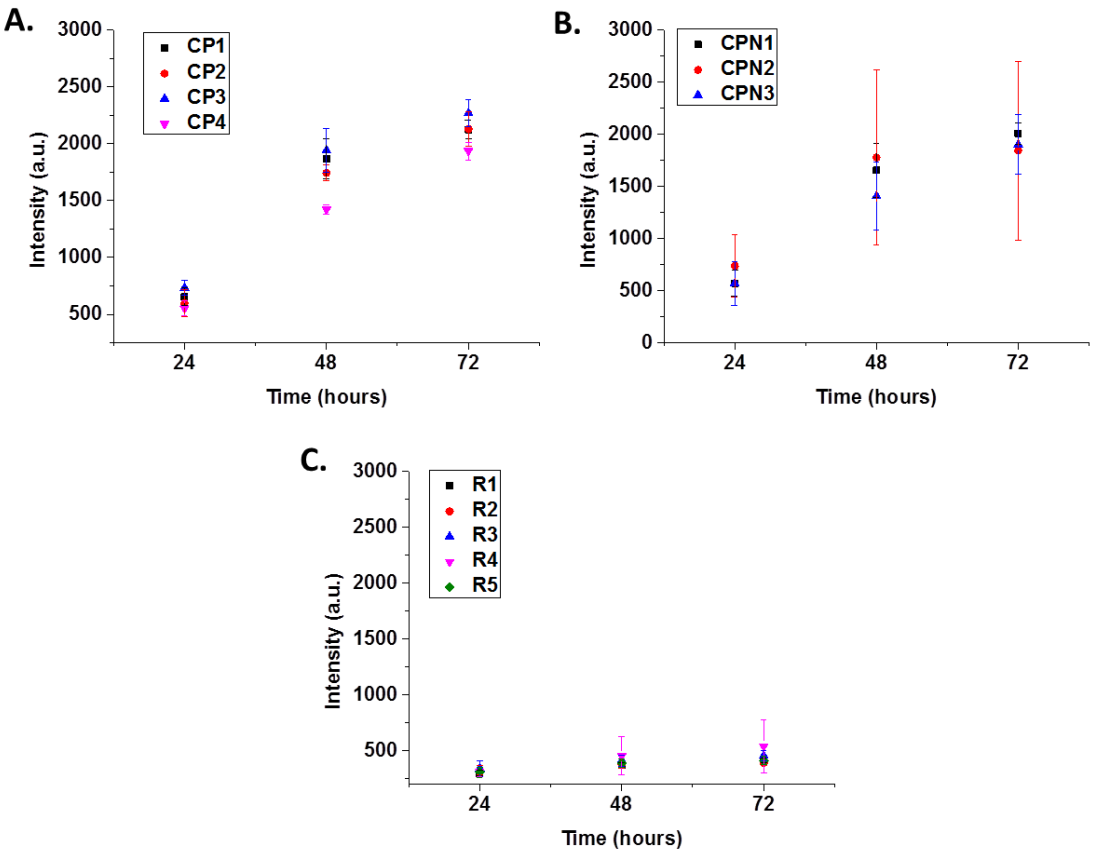

Figure 3.9. Amide hydrolysis by fluorescence. Time courses observed for the hydrolysis of FRET peptide using 0.0167 μM phage and 2 μM FRET peptide. Error bars are based on three repeats.

A rate constant was determined by using a calibration graph and equation 1 below. The reaction product was not available and as a result, the calibration curve was achieved by incubation of the FRET peptide with chymotrypsin. Fluorescence was measured over time and this plot was used to obtain the gradient of the calibration sample as seen in equation 1. The rate is further divided by 3600 to convert the rate from hr^{-1} to s^{-1}. All of the observed rates are based on the concentration of the catalytic peptides (five peptides per phage).

$$k_{obs} = \left(\frac{\left(Gradient\ of\ sample\ (hr^{-1})\right)}{(Gradient\ of\ calibration\ sample\ (nM^{-1})\ x\ Concentration\ of\ phage\ (nM)} \right) \qquad \textbf{(1)}$$

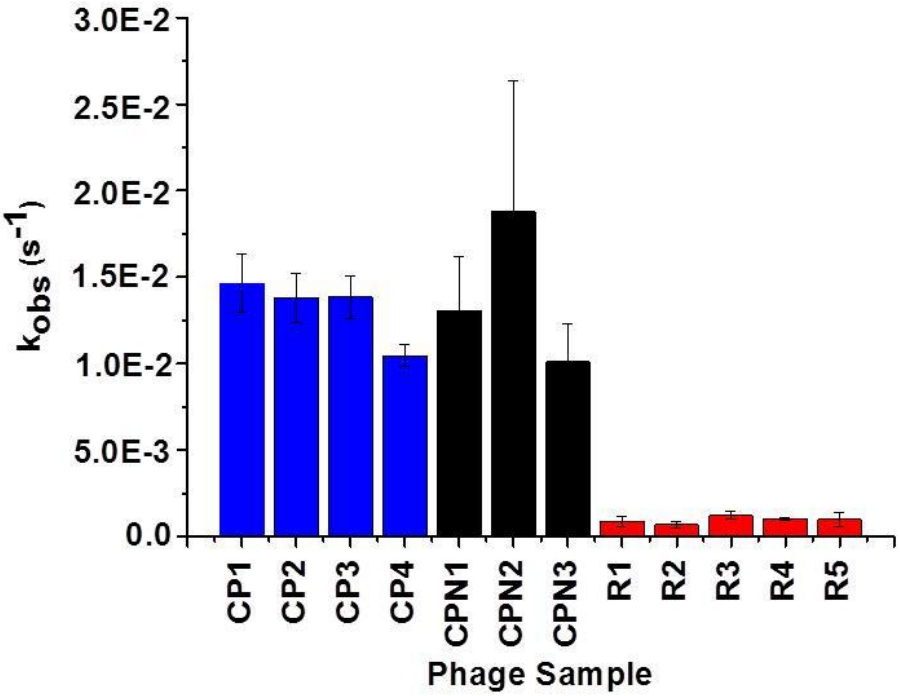

Figure 3.10. Amide hydrolysis by fluorescence. Rate data for the hydrolysis of FRET peptide using 0.0167 μM phage and 2 μM FRET peptide. The rate data is based on a 72 hour time course. Error bars are based on three repeats.

The CPN2 data does have a significant error associated with it. This is due to the triplicate data being significantly different from one another. Although CPN2 appears to be the best amidase sequence, on repetition of this assay it may come back in line with the other samples. All of the CP and CPN phage demonstrated hydrolytic activity whilst the random phage showed low levels of background hydrolysis (Figure 3.10). The observed rate constants for the catalytic phage (1-2 x 10^{-2} s^{-1}) are an order of magnitude higher than those observed for the randomly selected control phages (1 x 10^{-3} s^{-1}). CPN2 was the best amidase phage, demonstrating a 20-fold rate enhancement over the control phages. On further inspection of the individual peptide sequences, it was found that despite CPN2 having the fastest hydrolysis rate out of all of the catalytic phages, it does not contain a Ser residue directly adjacent to a His residue; contrasting expectations based on previous work by Li and co-workers to suggest that the Ser-His dyad is essential.[25] Another consideration is that while it is not the most effective at hydrolyzing amide bonds, CPN3 does have some hydrolytic

activity even though it does not contain the catalytic residue His at all. Instead, it contains two Cys residues. This obvious contrast in peptide sequence for catalytically active phages strongly suggests that there are different mechanisms of action at play and investigations are on-going in order to deduce how these work. This peptide turned out to have dramatically better esterase activity, as will be discussed in chapter 4.3.

3.4.3 Amidase Activity – FITC-casein Amide Hydrolysis

An assay that exploited fluorescein isothiocyanate (FITC) labelled casein was utilized to further explore amide bond hydrolysis (Figure 3.11). Phages were incubated with the FITC labelled casein. The intact casein substrate is labelled with FITC resulting in quenching of the fluorescence of the conjugates. Upon hydrolysis, peptide fragments containing the self-quenching conjugates are released yielding a green fluorescent dye attached to the peptide fragments. The increase in fluorescence is directly related to hydrolysis of the protein. The sample was acidified using trichloroacetic acid and any substrate that remains undigested precipitates from solution and is removed from the sample by centrifugation.

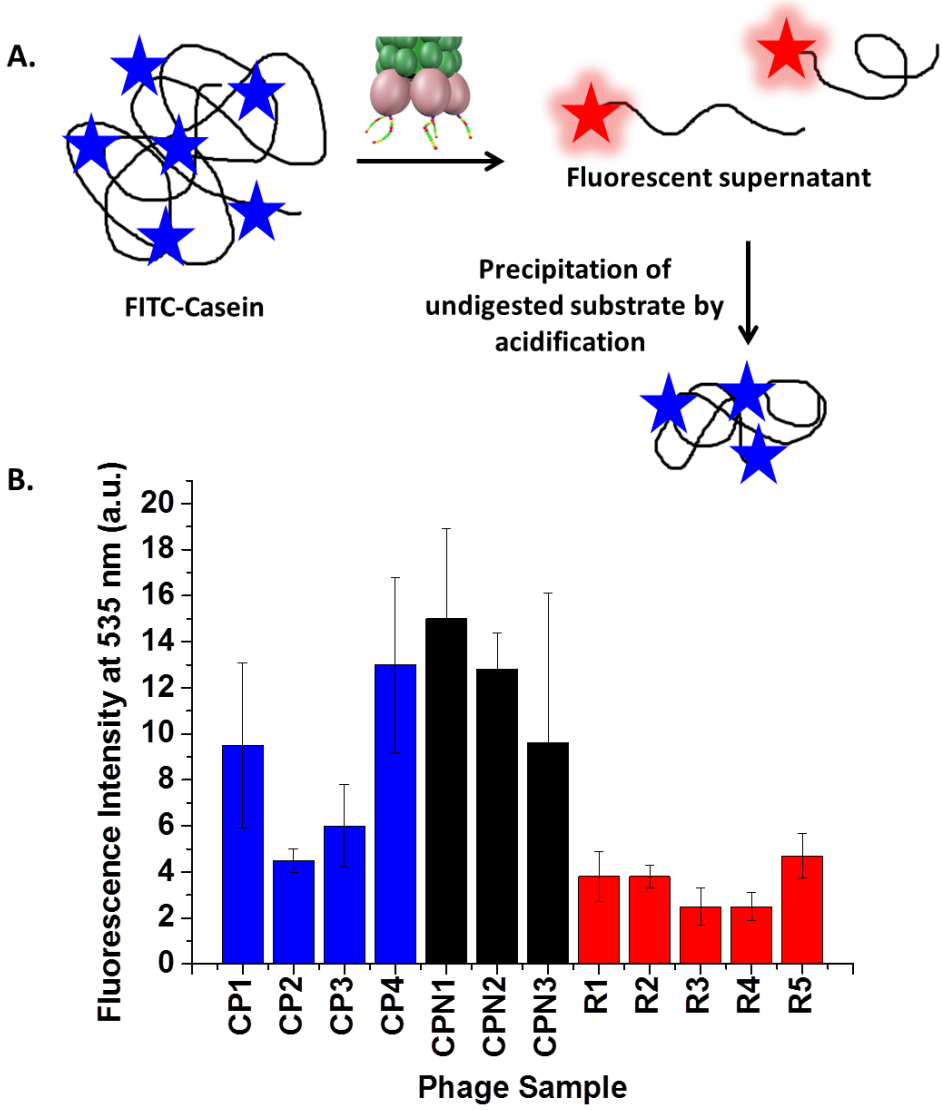

Figure 3.11. FITC-Casein hydrolysis assay A. Cartoon representation of the FITC-Casein reaction. **B.** Rate data for the hydrolysis of FITC-Casein using fluorescence. Error bars are based on three repeats.

CP1, CP4 and the CPN catalytic phages showed some increased levels of activity over the background rate of hydrolysis however CP2, CP3 and the random control phages illustrated very little difference between each other and also the background rate.

3.4.4 Esterase Activity – UV-Vis Assay

Most biocatalysts which have the ability to hydrolyze amide bonds also exhibit esterase activity *e.g.* serine proteases. Typically, the ester hydrolysis rates are much faster which will lead to rates that are more easily quantified and compared. *p*-Nitrophenyl acetate was used in a UV-Vis assay to investigate ester hydrolysis catalyzed by phages; allowing an insight into how the hydrolysis rates compare with literature examples of peptide-based catalysts.[3, 4, 25] This assay works on the basis that the hydrolysis product is yellow in color and can be measured by UV-Vis spectrometry (Figure 3.12).

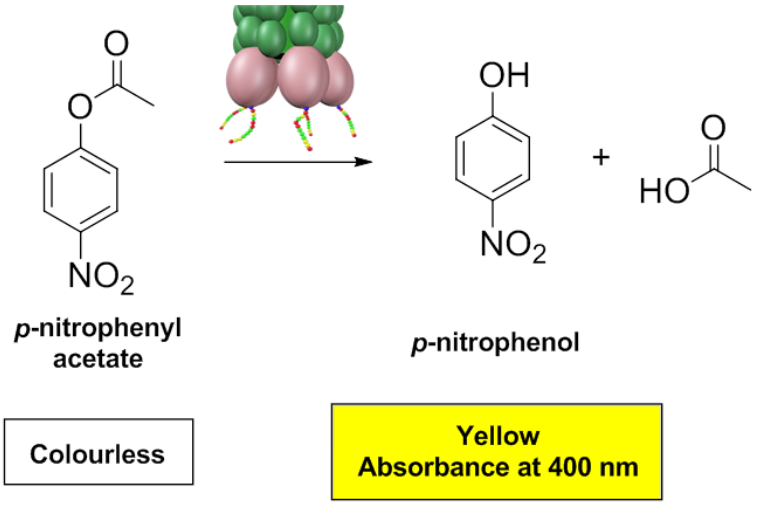

Figure 3.12. UV-Vis *p*NPA ester hydrolysis assay. Schematic of *p*NPA hydrolysis reaction.

Typical time courses were observed for hydrolysis of the ester bond in *p*NPA in the presence of the catalytic phages (Figure 3.13). The absorbance for these samples increases over time which can be observed in these plots.

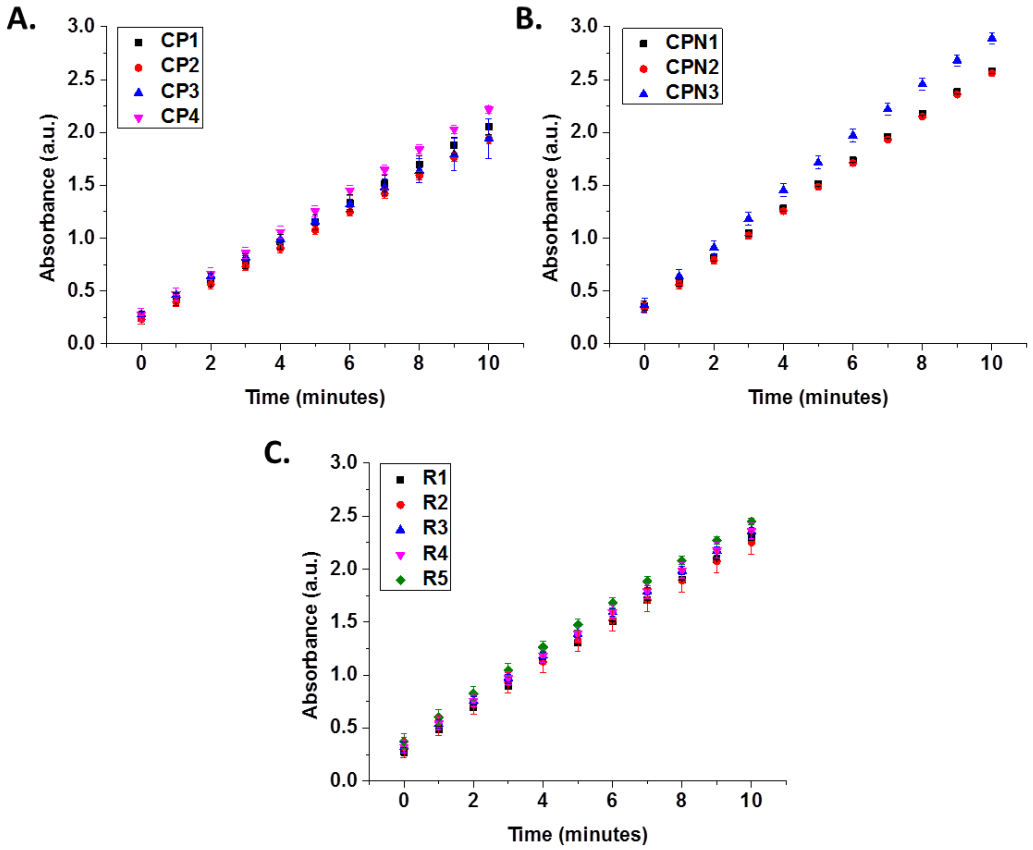

Figure 3.13. UV-Vis *p*NPA ester hydrolysis assay. Time courses observed for the hydrolysis of *p*-nitrophenyl acetate (*p*NPA) using 0.0249 μM phage and 6 mM *p*NPA. Error bars are based on three repeats.

The absorbance recorded at 400 nm can be correlated to the rate of hydrolysis. At first glance there does not appear to be an appreciable difference between the rates observed, due to substantial background hydrolysis (general acid/base catalyzed). The rate constant (k_{obs} in s^{-1}) for each phage (Figure 3.14) was determined from a UV-Vis calibration graph of *p*-nitrophenol and Equation 2. Once again the rates are based on the concentration of the catalytic peptides (five peptides per phage).

$$k_{obs} = \frac{(Gradient\ of\ sample\ (s^{-1}) - Gradient\ of\ background\ hydrolysis\ sample\ (s^{-1}))}{(Extinction\ coefficient\ (M^{-1}cm^{-1}) x\ Catalyst\ concentration\ (M) x\ Path\ length\ (cm))} \quad \textbf{(2)}$$

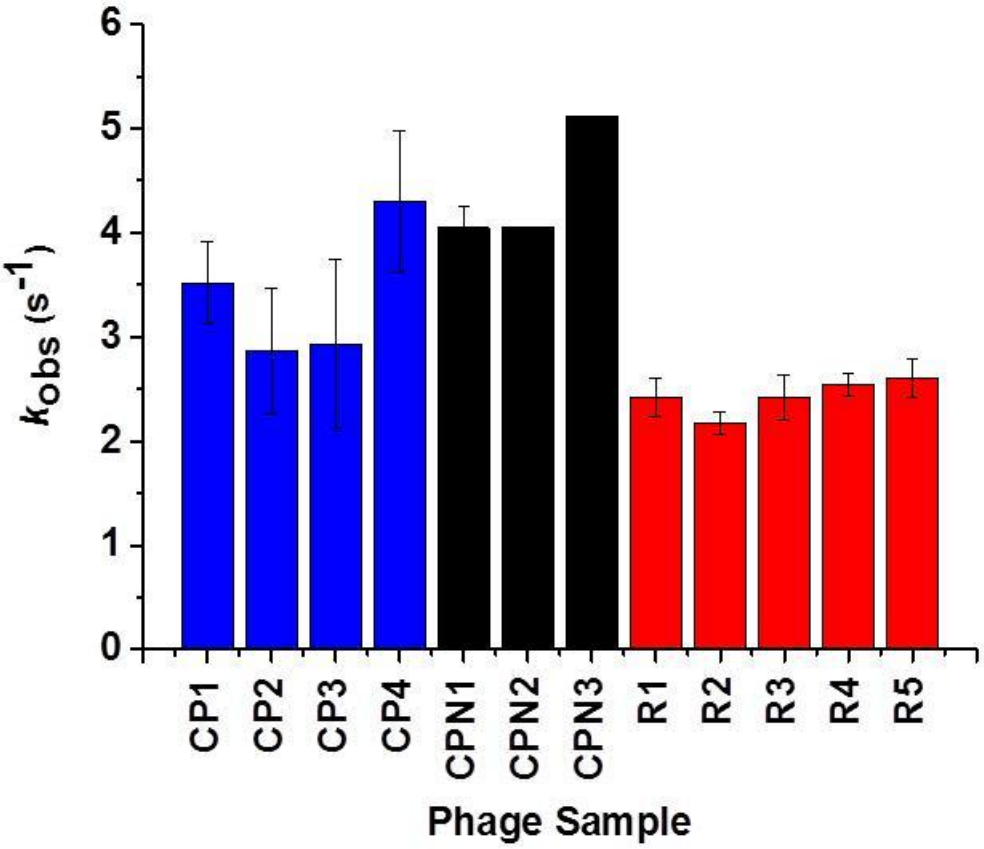

Figure 3.14. UV-Vis *p*NPA ester hydrolysis assay. Rate data for the hydrolysis of *p*-nitrophenyl acetate (*p*NPA) using 0.0249 μM phage and 6 mM *p*NPA. The rate data is based on a 10 minute time course. Error bars are based on three repeats. Samples are corrected for background hydrolysis to give a true rate based on the catalyst alone.

CPN3 phage showed the highest activity of the catalytic phage followed by CP4 = CPN1 = CPN2 and slightly lower again, CP1 phage. CP2 and CP3 phage demonstrated activity in line with that of the control phage. Again it is possible that the residues present on the phage protein coat itself are contributing to catalysis, resulting in an increased activity for the control samples. There are imidazole residues present on the P3 protein of the phage, where the peptides are displayed, which are known to possess catalytic properties as previously described.[51] Again, CPN3 suggests that histidine is not crucial for catalysis of ester hydrolysis to take place; CPN3 does not contain histidine but does contain two cysteine residues, a residue that is known to be a key component of cysteine protease enzymes.[12, 13] In cysteine protease enzymes, the reaction mechanism is initiated by deprotonation of

the thiol by a basic amino acid, usually histidine. However, other basic amino acids have the potential to initiate the deprotonation and induce catalysis; in this case arginine has this potential. The remarkable catalytic activity of CPN3 is discussed in more detail in chapter 4.3.3.

3.4.5 Esterase Activity – Fluorescence Assay

A fluorescence assay was also used to investigate the rate of hydrolysis of esters using 4-methylumbelliferyl acetate and independently verify the order of catalytic activity (Figure 3.15). This fluorescence assay works on the basis that on hydrolysis of the ester bond of the non-fluorescing substrate, electron density is maintained within the conjugated ring system resulting in a fluorescent product.[73]

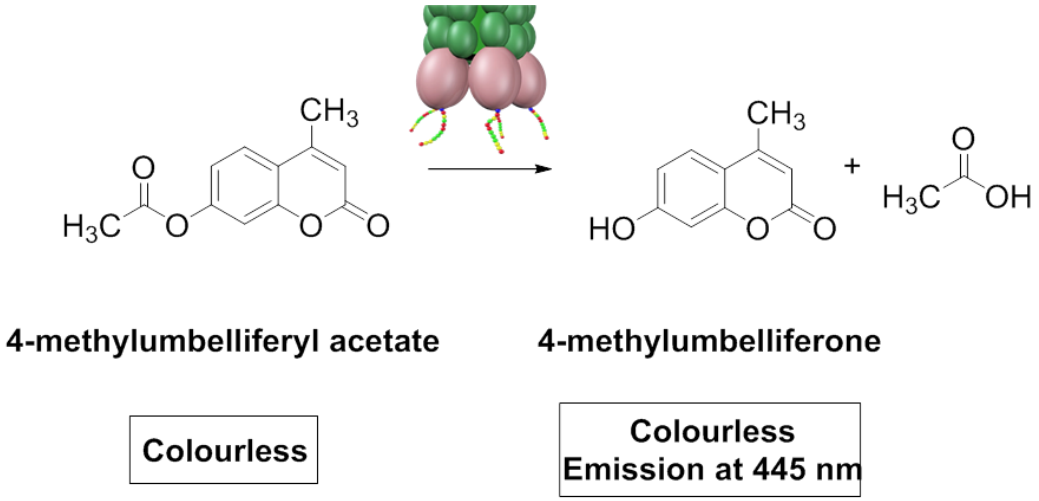

Figure 3.15. MUA hydrolysis assay. Schematic of MUA hydrolysis reaction.

Typical time courses were observed for hydrolysis of the ester bond in MUA in the presence of the catalytic phages (Figure 3.16). The fluorescence for these samples increases over time.

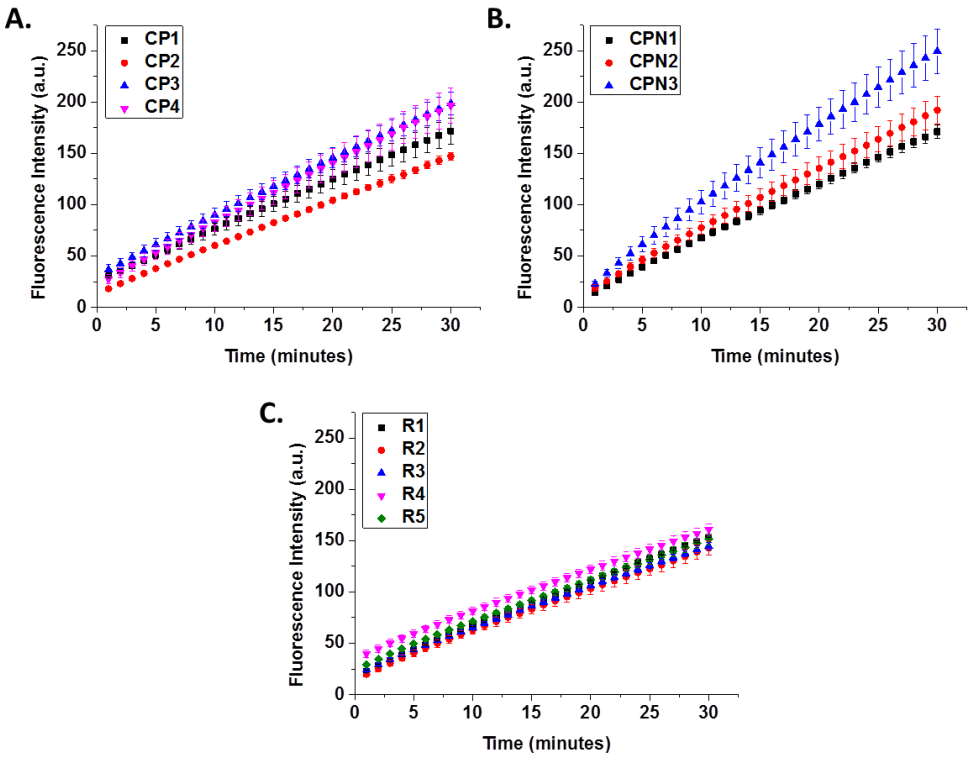

Figure 3.16. MUA hydrolysis assay. Time courses observed for the hydrolysis of methylumbelliferyl acetate (MUA) using 0.0125 μM phage and 0.25 mM MUA. Error bars are based on three repeats.

The absorbance recorded at 445 nm can be correlated to the rate of hydrolysis. The rate constant (k_{obs} in s^{-1}) for each phage (Figure 3.17) was determined from a fluorescence calibration graph of methylumbelliferone. Once again the rates are based on the concentration of the catalytic peptides (five peptides per phage).

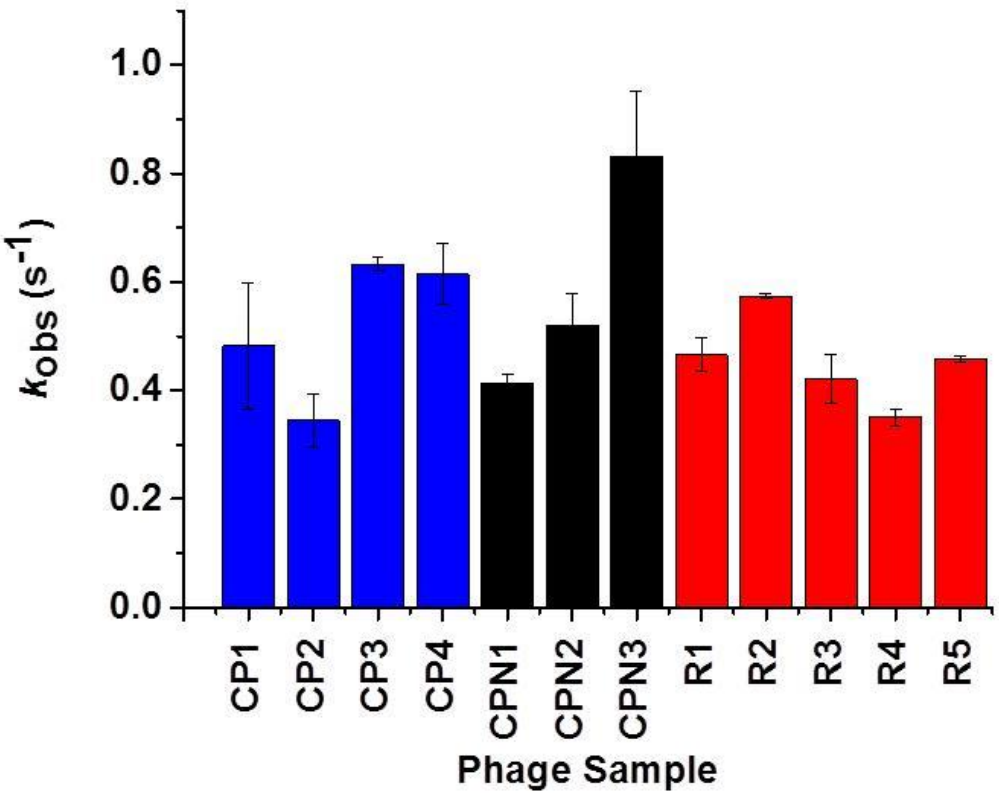

Figure 3.17. MUA hydrolysis assay. Rate data for the hydrolysis of methylumbelliferyl acetate (MUA) using 0.0125 μM phage and 0.25 mM MUA. The rate data is based on a 30 minute time course. Error bars are based on three repeats. Samples are corrected for background hydrolysis to give a true rate based on the catalyst alone.

These data confirm the trend in catalytic rates observed between the phages studied. As before, CPN3 phage showed the highest activity of the catalytic phage, this time followed by CP4 = CP3 and slightly lower again, CPN2, CPN1 and CP1 phage were in line with the control phage. Using this assay, CP3 showed an increased rate of ester hydrolysis. Both assays confirm that CPN3 is the best esterase mimic out of the catalytic phages brought forward for this study. Further investigation is required to decipher the mechanism of action and obtain an insight into the activity of this peptide sequence (chapter 4.3.3). Remarkably, the results also demonstrate that it is possible that the catalytic phages can be selective towards substrate.

3.5 Conclusions

The combination of catalytic self-assembly and phage display to create a novel screening technology successfully identified phage viruses displaying dodecapeptides at their tip with the ability to hydrolyze amide and ester bonds under physiological conditions as the results here demonstrate. These phages were isolated and extracted from a vast library of 10^9 different sequences. Only seven of over twenty sequences identified in screening were selected for further analysis so it is possible that there are still sequences which have not yet been studied for activity which possess amidase and esterase activity. This approach allows for screening and selection based on function rather than transition state binding and makes no assumption on the origin of catalysis. Function can be found in random, unevolved peptides.[74]

CPN2 was identified as the best sequence for amide hydrolysis through fluorescence assays utilizing a FRET peptide. This peptide sequence contains amino acids traditionally found in the catalytic triad of an enzyme and so it is likely that the mechanism of action for this sequence is *via* the charge relay mechanism although this has not yet been confirmed. Surprisingly CPN3 also showed some amidase activity despite lacking the catalytic residue histidine, confirming that each peptide has its own mechanism of action. With regards to esterase activity, CPN3 was identified as the most efficient sequence for esterase hydrolysis through UV and fluorescence esterase assays. There was no sequence homology between the dodecapeptides identified from the screening and selection process meaning that it is possible to find function in random, unevolved peptide sequences. At this point the mechanisms of action for these sequences has not been identified but will be discussed further in subsequent chapters. Random phage did also possess amidase and esterase activity although this can be attributed to the amino acid residues present in the coat protein of the phage. Residues traditionally found in the catalytic triad of an enzyme are also present on the surface which can catalyze hydrolysis reactions without being orientated in the scaffold of an enzyme as previously reported.

4.0 Amidase/Esterase Activity of Free Dodecapeptides Discovered by Biocatalytic Self-assembly

4.1 Introduction

The catalytic activity of an enzyme relies on precise and highly conserved positions of the catalytic residues within a semi-rigid scaffold structure. The amino acid sequence of an enzyme underpins its ability to fold into a precise structure, which holds the catalytic moieties in place for binding and catalysis to occur.[30] The primary sequences of enzymes typically exceed 100 residues in a globular protein. The design and development of minimalistic (self-assembled) peptide catalysts is becoming a widely studied field.[7] As the most extreme case, it is perhaps surprising to see that the simple dipeptide Ser-His and Ser-His-Asp tripeptides have been reported to possess hydrolytic activity for ester, amide and oligonucleotide hydrolysis.[25, 65] The results clearly illustrate that a rigid scaffold structure is not strictly necessary for catalysis to occur. Furthermore, these previous findings suggest that early precursors of enzymes could have been composed of very short peptides.

There has been a recent surge of interest in development of *de novo* short peptide catalysts typically aiming to mimic key elements of enzymes- such as the presence of certain functional groups, the organization of these groups into a favorable 3D structure that may help stabilize the transition state and the introduction of substrate binding sites. Recent examples have built upon this by providing a short peptide based supramolecular nanostructure, amongst other scaffolds, for the display of catalytic residues which in turn realizes organization of these moieties and thereby enhancing catalysis.[2-6] These *de novo* catalysts all possess histidine which is known to play a key role in the catalytic triad of numerous enzymes.[24, 28]

This study demonstrates the rate enhancement of amide and ester hydrolysis by unstructured peptides in solution that were identified by combining biocatalytic self-assembly and phage display (see chapter 3.3). Furthermore, it explores the possible mechanism of action for CPN3, which was the catalyst with the highest activity and unlike the others sequences identified contained no histidine residue.[8] Strikingly, in chapter 3.4 it was demonstrated that CPN3 was the most convincing esterase mimic from a range of peptide sequences identified.[8] Instead of histidine, this peptide contains two cysteine residues whichplay key roles in the catalytic mechanism of this

peptide[12, 13] and has catalytic rates which are on par with the best histidine containing peptide catalysts in the literature, many of which rely on self-assembly, substrate binding or multivalency to achieve this catalytic performance. Finally, the ability of this peptide to catalyze reactions in non-physiological conditions including variations in pH and temperature was studied, as well as further investigating substrate scope.

4.2 Objectives

Based on the initial studies with the peptide on phage (Chapter 3), the aims of this chapter were to:

- Characterize the activity of the catalytic peptides identified by biocatalytic self-assembly and phage display.
- Investigate mutant CPN3 sequences to gain an insight into its mechanism of catalysis.
- Study different conditions for the catalysis to understand the affect that these factor have on catalysis.

4.3 Results and Discussion

In chapter 3.4, catalytic phage systems were identified *via* a biocatalytic screening process and found to possess amidase and esterase activity. In order to gain more understanding into the role of the peptide in catalysis, the sequences displayed on the tip of the phages were synthesized and the same hydrolytic assays carried out to assess these dodecapeptides as catalysts.

4.3.1 Amidase Activity – FRET Amide Hydrolysis

The first study looked at the hydrolysis of amide bonds by the FRET fluorescence assay with peptide catalysts over time. The FRET peptide was designed to include the Thr-Leu dipeptide which was utilized for the phage panning experiments. As for the phage samples, typical time courses were observed for hydrolysis of the FRET peptide in the presence of the catalytic phages (Figure 4.1). The fluorescence signal

for these samples increases over time which can be observed in these plots. Due to the low level of activity observed it was not practical to assess catalytic activity over a short time frame. Instead conversions were assessed at 24 hour intervals.

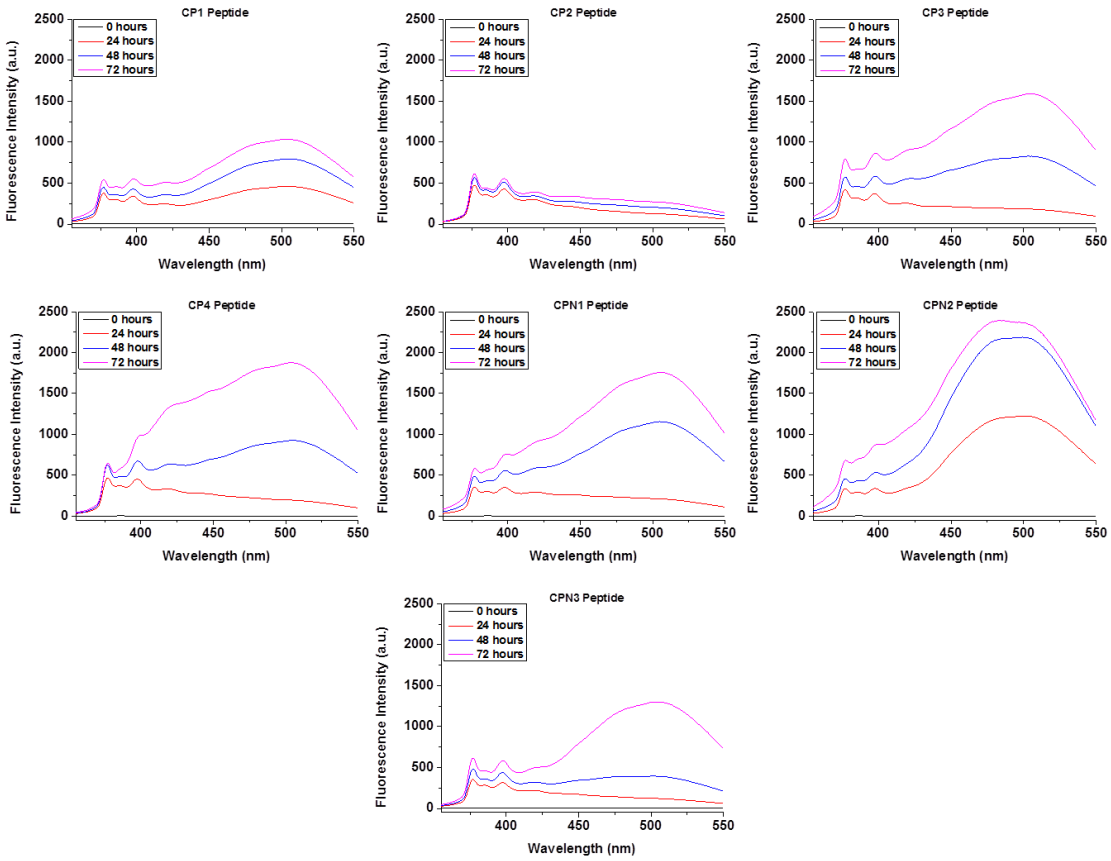

Figure 4.1. Amide hydrolysis by fluorescence. Raw data for the hydrolysis of FRET peptide using 0.4 mM peptide catalyst and 2 μM FRET peptide. Each spectrum is the average of three repeats.

The increase in fluorescence was observed over time at 493 nm to deduce the kinetic profile of the hydrolysis of the Thr-Leu peptide bond (Figure 4.2). A rate constant was determined by using a calibration graph and equation 1. All of the observed rates are based on the concentration of the catalytic peptides - this should be borne in mind when comparing directly to the rates observed using phages, which contain five peptides per phage.

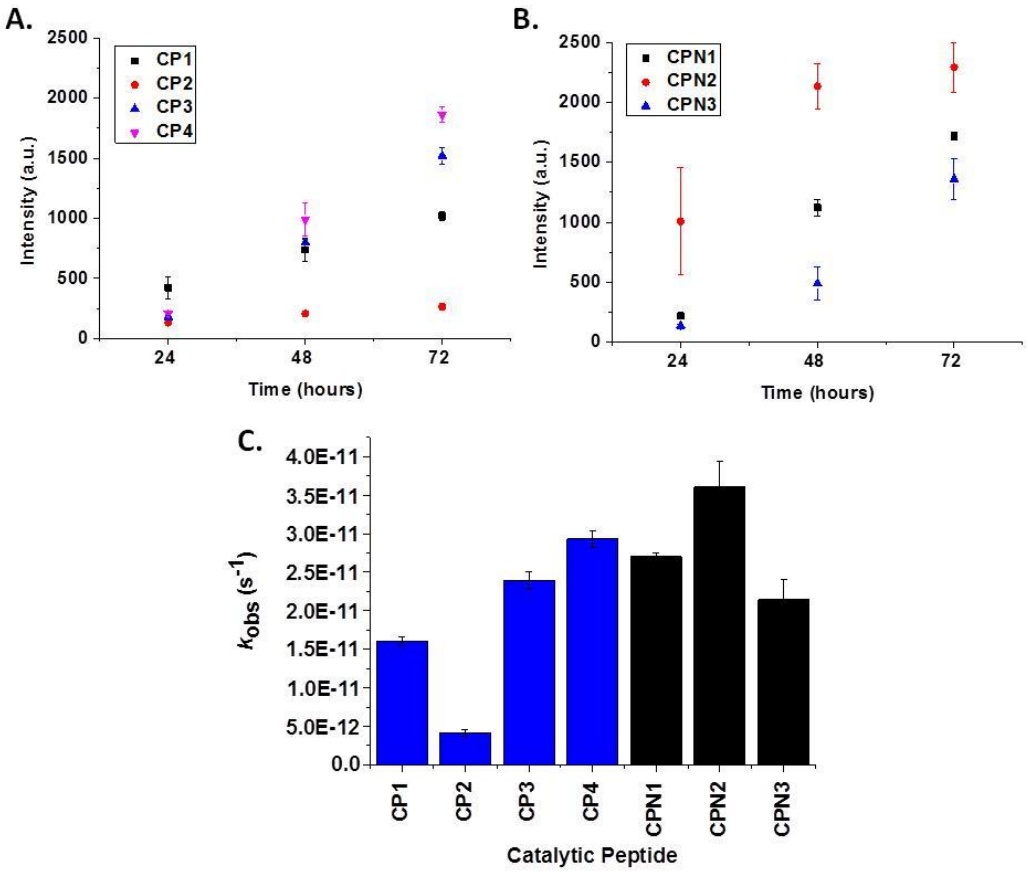

Figure 4.2. Amide hydrolysis by fluorescence. A and B. Time courses observed for the hydrolysis of FRET peptide using 0.4 mM peptide catalyst and 2 μM FRET peptide. **C.** Rate data for the hydrolysis of FRET peptide using 0.4 mM peptide catalyst and 2 μM FRET peptide. The rate data is based on a 72 hour time course. Error bars are based on three repeats. Samples are corrected for background hydrolysis to give a true rate based on the catalyst alone.

It is observed that all of the CP and CPN peptides demonstrate hydrolytic activity over time. The rate constants for the peptides (5×10^{-12} – 3.5×10^{-11} s^{-1}) are nine orders of magnitude slower than for the catalytic phage. The rates are also more variable. For the CPN peptides the trend is the same (see chapter 3.4.2, Figure 3.12), with CPN2 highlighted as the best amidase catalyst. However, for the CP peptides a different trend is observed where the activity of CP2 is considerably lower than for that of the other CP peptides. Although the rates are low, there is activity from the isolated peptides. All of the sequences have Ser-His or closely related dyads, His-Ser and Thr-His, excluding CPN3 which will be discussed later (chapter 4.3.3). It has been shown previously that the dyad Ser-His possesses hydrolytic activity in relation to DNA, proteins and esters[25, 65] and these catalytic peptides have the potential to

follow the same mechanism of action as a result of the catalytic dyads within their sequence. Histidine is known to be a fundamental amino acid required for catalysis.[15, 60] The basic nature of this amino acid can deprotonate the neighboring hydroxyl group, whether serine or threonine, increasing the nucleophilic character and priming it for nucleophilic attack on the substrate resulting in hydrolysis.[25]

4.3.2 Esterase Activity – UV-Vis Assay

Having confirmed that the free peptides demonstrate a low level of amidase activity, subsequently esterase activity of the peptide sequences was investigated over time making use of *p*-nitrophenyl acetate in a colorimetric assay following the formation of reaction product at 400 nm (Figure 4.3).

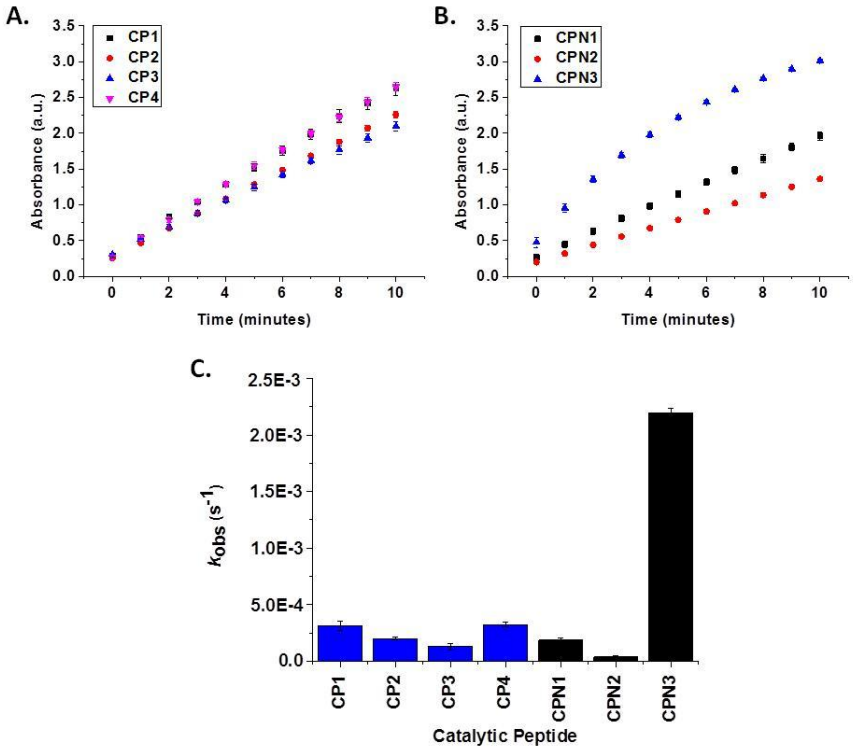

Figure 4.3. UV-Vis *p*NPA ester hydrolysis assay. A and B. Time courses observed for the hydrolysis of *p*-nitrophenyl acetate (*p*NPA) using 0.5 mM peptide catalyst and 6 mM *p*NPA. For CPN3 instrument saturation occurred and as a result only the initial linear section of the plot was used to calculate the rate. **C.** Rate data for the hydrolysis of *p*-nitrophenyl acetate (*p*NPA) using 0.5 mM peptide catalyst and 6 mM *p*NPA. The rate data is based on a 10 minute time course. Error bars are based on three repeats. Samples are corrected for background hydrolysis to give a true rate based on the catalyst alone.

The rate of ester hydrolysis by the peptidic catalysts ($3.8 \times 10^{-5} – 2.2 \times 10^{-3}$ s^{-1}) was three to five orders of magnitude lower than those observed for the catalytic phage. However, with this assay the trends observed between catalysts is remarkably similar to that observed for the catalytic phage which gives confidence that the catalytic behavior observed is indeed related to peptide sequence. What is most remarkable is that CPN3 was by far the most active esterase catalyst (followed by CP4).

These results demonstrate that despite the lower rates observed for the catalytic phage as a whole, the peptide sequence present on the tip of the phage contributes to the catalytic activity. It also confirms that the presence of the phage does enhance the catalytic properties of the peptides; most likely due to contributions of residues that compose the protein coat. The enhanced rate of CPN3 free peptide in the esterase studies is remarkable. The $k_{obs} = 2.2 \times 10^{-3}$ s^{-1} for this free peptide catalyst is only one order of magnitude lower than for the most efficient literature examples of peptidic catalysts which benefit from multivalency, metal ions and substrate binding to name a few.[3, 4]

There is extensive sequence diversity between the 'hits' identified through new combined phage display/catalytic self-assembly methodology. However, understanding the underlying mechanism of action for these catalytic phage/peptides is a considerable undertaking. Initial studies looked at whether substrate binding played a role in catalysis. This has been the focus for most enzyme designs and CPN3 was chosen to investigate this. In this instance, catalytic rates were observed at different *p*NPA concentrations for both catalytic phage and free peptides to establish whether Michaelis-Menten kinetics played a role (Figure 4.4).

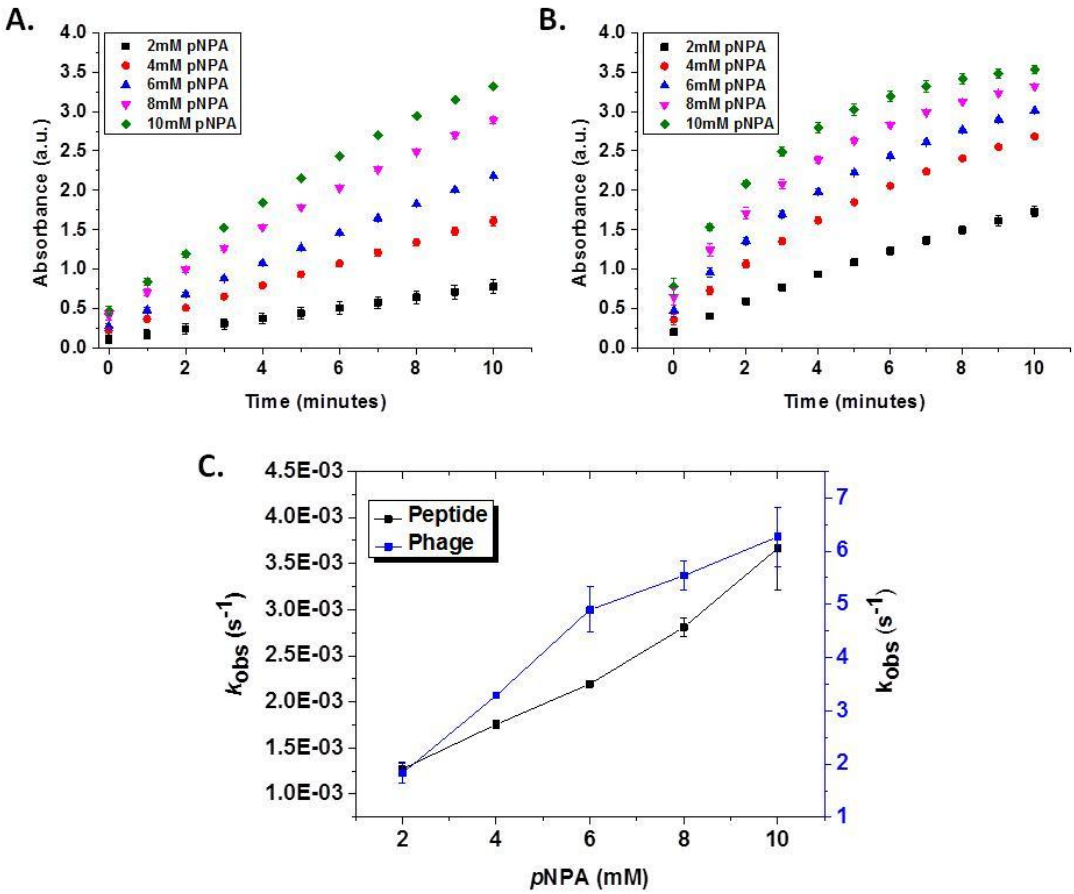

Figure 4.4. A and B. Time course observed for comparison of k_{obs} for hydrolysis of *p*NPA by CPN3 phage and peptide to assess whether substrate binding plays a role in catalysis. The peptide concentration was 0.5 mM and the phage concentration was 0.0167 μM. The substrate concentrations were 2 – 10 mM *p*NPA. **C.** Comparison of k_{obs} for hydrolysis of *p*NPA by CPN3 phage and peptide to assess whether substrate binding plays a role in catalysis. Error bars are based on three repeats. Samples are corrected for background hydrolysis to give a true rate based on the catalyst alone.

The catalytic profiles show a near-linear relationship which suggests that Michaelis-Menten kinetics is not playing a significant role in catalysis within the studied concentration range. Further investigations at increased concentrations failed since the solubility of the substrate became limited above 10 mM. This linear relationship indicates that the K_M value (the substrate concentration at which the reaction rate is half of the maximum rate achieved by the system) has not yet been reached therefore k_{cat} could not be determined. CP1-4 and CPN1 and 2 free peptides also display a linear relationship in the same concentration range. These results strongly suggest that substrate binding plays a minor role in this system if it plays a role at all. This

distinguishes these catalysts from other catalytic systems reported in the literature which exploit self-assembly[2-6, 40]; instead our catalytic phage and free peptides seem to operate more like small molecule catalysts. As discussed previously (chapter 3.3), all of the sequences, excluding CPN3, possess the dyad Ser-His or a variation on this, His-Ser and Thr-His. Histidine is a well-known amino acid that is crucial for catalysis and its basic character can increase the nucleophilic character of the neighboring serine or threonine residue. As a result, the nucleophile attacks the substrate inducing hydrolysis.

4.3.3 Esterase Activity of a Short Cysteine Peptide

CPN3 was chosen for further investigation due to its remarkable esterase catalysis (2.2×10^{-3} s^{-1}). It is very unusual for an unstructured peptide in solution (Figure 4.5) to display catalytic activity as it possesses none of the required features of a natural enzyme including binding pocket, rigid scaffold structure and resulting orientation of catalytic residues.

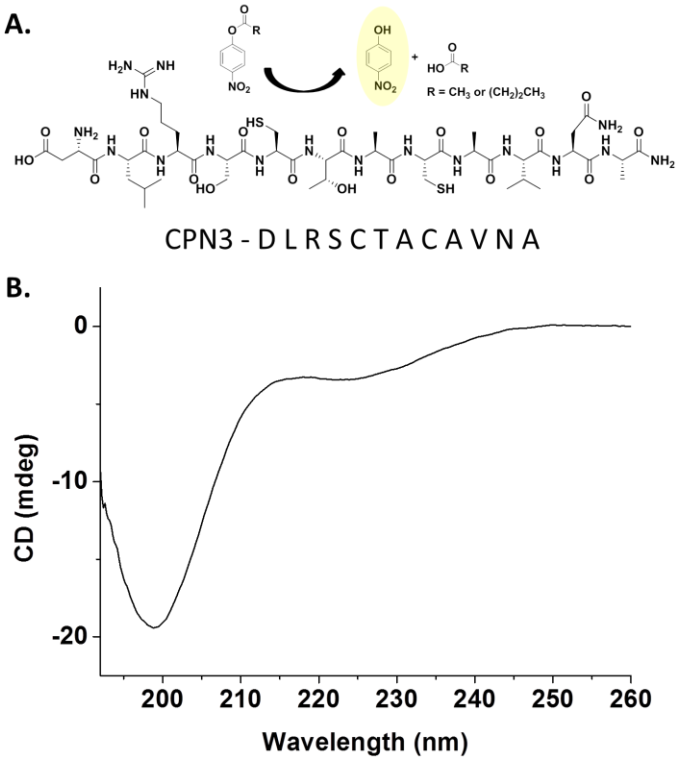

Figure 4.5. CPN3 peptide with esterase activity. A. schematic representation of the UV *p*NPA hydrolysis assay. **B.** CD spectrum of CPN3 peptide illustrating random, unfolded structure in solution.

To look at the proposed mechanism of catalysis for CPN3, a standard UV-Vis spectroscopy enzyme assay was utilized for esterase hydrolysis. The hydrolysis of *p*-nitrophenyl acetate (*p*NPA) in a colorimetric assay is well documented in literature.[3, 5, 6, 15] To determine the mechanism of catalysis, an alanine scan was first performed to assess the influence of primary sequence whereby all residues in the peptide were sequentially knocked out and replaced with alanine to determine the role that they play in catalysis using the *p*NPA assay (Figure 4.6). Here the hydrolysis of an ester bond in the presence of CPN3 is observed (Figure 4.6) and the role of the various amino acid residues hypothesized.

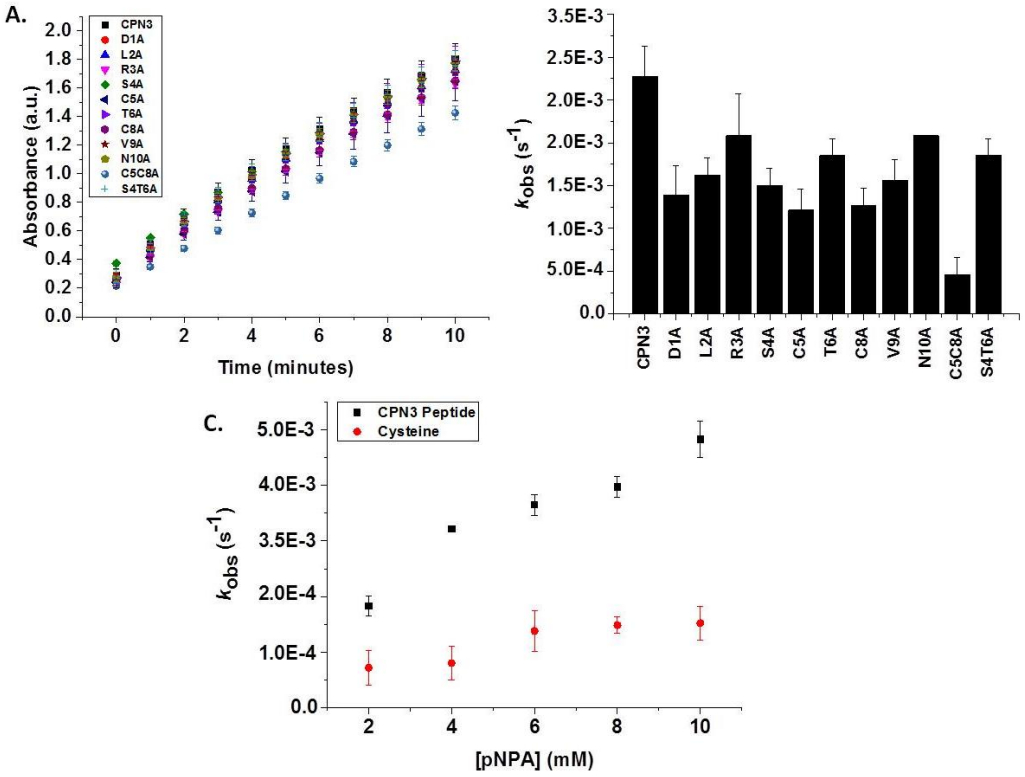

Figure 4.6. UV esterase assay to determine catalytic mechanism of the CPN3 peptide sequence. A. Time course data for ester hydrolysis by the alanine sweep peptides whereby the name of the sample indicates which amino acid which has been knocked out of the sequence. Peptide concentration was 0.018 mM and the substrate concentration was 6 mM. **B.** Catalytic rates (k_{obs}) for ester hydrolysis by the alanine scan peptides whereby the name of the sample indicates which amino acid which has been knocked out of the sequence. Peptide concentration was 0.018 mM and the substrate concentration was 6 mM. **C.** Catalytic rates (k_{obs}) for ester hydrolysis by CPN3 peptide and cysteine alone. Catalyst concentration was 0.036 mM and the substrate concentration ranged from 2 - 10 mM. Error bars are basedon three repeats. Samples are corrected for background hydrolysis to give a true rate based on the catalyst alone.

Remarkably, it was observed that upon replacing individual amino acids with alanine, the rate of hydrolysis decreased for all analogues therefore implying that every amino acid within the sequence plays a role in the mechanism of catalysis (Figure 4.6B). There are a number of possible roles that could be assigned to each residue, as summarized in Table 4.1.

It should be noted that substituting both cysteine residues for alanine had the largest effect on reducing the catalytic activity, (C5C8A) which is in agreement with the idea that the cysteine plays a major role in the catalysis. However, since there is still some activity while only one cysteine residue is substituted (C5A and C8A), this leads us to believe that these residues are in fact acting independently of one another. The importance of the cysteine residue is reinforced by the fact that cysteine alone possesses a low level of catalytic activity although not matching CPN3 (Figure 4.6C). The removal of aspartic acid also causes a reduction in activity (D1A). This residue has the potential to assist in proton extraction from a neighboring amino acid or from a water molecule as a result of the negative charge across the oxygen atoms. Although this would be unusual at physiologically pH, the aspartate protease enzyme renin operates at an optimum pH of 5.5 – 7.5 *via* a mechanism involving the deprotonation of water by an aspartate residue. The resulting anion can then catalyze the ester hydrolysis.[75-77] As hydrophobic residues, leucine and valine are unreactive however L2A and V9A mutants show that they are contributing. Their role is most likely related to the (transient) binding of the hydrophobic substrate of the reaction and enhances the opportunity for catalysis to occur, although it should be noted that substrate binding is not a major factor in these systems. Arginine substitution has only a minor effect on catalytic rates (R3A) – it has the potential to play a role in binding/stabilization with regards to the charged transition state of the substrate - as previously observed for some examples of designed self-assembled catalysts reported in literature.[7] Indeed, the guanidyl group of the arginine has previously been used as a binding site to bind the reaction transition state *via* electrostatic interactions therefore enhancing the catalysis of an ester. The overall positive charge of this amino acid can bind the negatively charged transition state. Serine[78] and threonine have the potential to act as nucleophiles in catalysis although in this case the activity

does not drop significantly (S4A, T6A, S4T6A) suggesting that these residues are not playing a key role in nucleophilic attack. However, there is still activity on substitution of the cysteine residues indicating that serine and threonine are acting as very weak nucleophiles in the absence of cysteine. Furthermore, these residues can also form weak hydrogen bonds with the NO_2 group of the substrate. Finally, substitution of asparagine does not show a significant loss in activity either. Asparagine (N10A) is known to complete catalytic triads in cysteine protease mechanisms due to its ability to orientate neighboring residues into the optimum position for catalysis to occur and to stabilize the anion as a result of its polar nature.[79] It is likely that this is the role of asparagine in this case. The terminal amine of this peptide has a pKa of 6.9-8.1.[80] As in threonine protease enzymes, this terminal group has the ability to act as a base and deprotonate water molecules. In turn, the water anion can deprotonate the nucleophilic residues within the peptide sequence initiating hydrolysis of the ester substrate.

As a result of the alanine scan, it cannot be stated categorically which specific amino acids contribute to the catalytic mechanism however it allows a picture of the potential roles to be built for each residue as summarized (Table 4.1 and Figure 4.7).

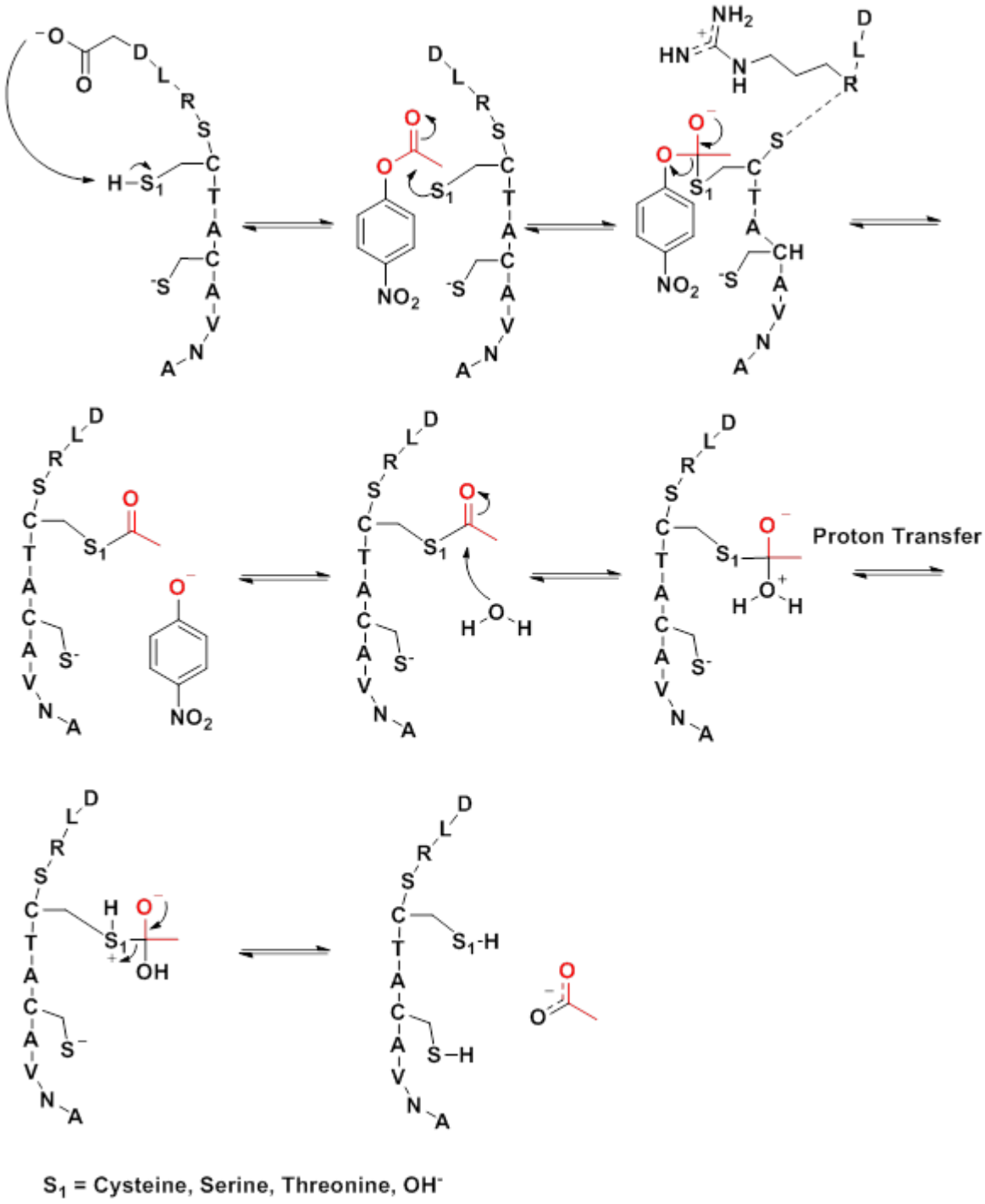

Figure 4.7. Proposed mechanism of ester hydrolysis by CPN3 indicating possible roles for each amino acid.

Cysteine, serine, threonine and water anions have the ability to act as the nucleophile after being deprotonated by another functional group in the sequence which is likely to be the terminal amine or aspartic acid. The negatively charged, nucleophilic group

can then attack the carbon of the carbonyl group initiating ester hydrolysis. The anionic transition state may be stabilized by arginine.

Table 4.1. Hypothesized roles in catalysis.

Amino Acid	Side Chain pKa	Potential Role in Catalysis		
		Nucleophile	Binding/ Stabilizing	Deprotonating
D1	3.86			X
L2	-		X	
R3	12.48		X	
S4	-	X	X	
C5/8	8.36	X		
T6	-	X	X	
V9	-		X	
N10	-		X	
NH_2 Terminus	6.9-8.0			X
OH^-		X		X

At this point it is hypothesized that catalysis is based on intramolecular interactions. This is due to the extremely low concentration of catalyst used in the reaction (0.018 mM) however this cannot be studied due to the insolubility of CPN3 at high concentrations.

Having established that cysteine is necessary for the enhancement of catalytic rates to occur, to further understand the mechanism by which the catalysis occurs, the esterase activity of the peptide was monitored at different pH values (Figure 4.8) in order to study how the protonation state of the thiol group of the cysteine impacts on the catalytic activity. The pH study demonstrates that as the pH of the reaction buffer increases, the esterase activity of the peptide also increases. This is potentially due to the protonation state of the cysteine residue. The pKa of cysteine is 8.36 and although the side chain will not be fully deprotonated, as the pH of the buffer increases so will the percentage of deprotonated thiols in solution. The remaining negatively charged sulfur atom has the ability to act as a nucleophile and attack the substrate initiating ester hydrolysis. However, the same trend can be seen when the catalyst is CPN3 peptide with both cysteine residues substituted for alanine.

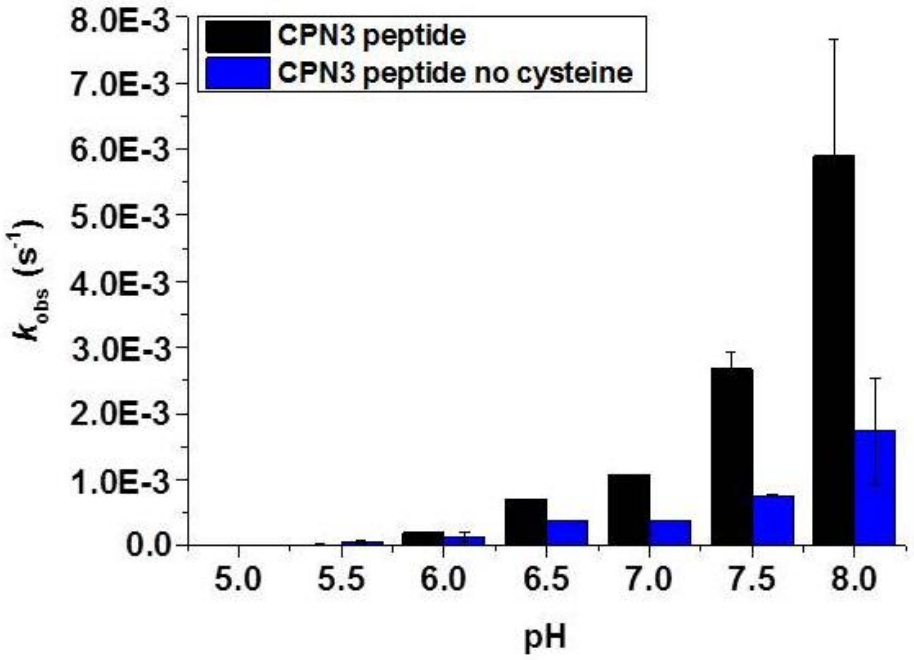

Figure 4.8. CPN3 esterase activity at different pH values. Catalytic rates (k_{obs}) for ester hydrolysis by CPN3 peptide. Peptide concentration was 0.018 mM and the substrate concentration was 6 mM. (Black) Catalytic rates (k_{obs}) for ester hydrolysis by CPN3 peptide with both cysteine residues replaced by alanine residues (C5C8A). Peptide concentration was 0.018 mM and the substrate concentration was 6 mM. (Blue) Error bars are based on three repeats. Samples are corrected for background hydrolysis to give a true rate based on the catalyst alone.

As discussed previously, serine and threonine have the potential to attack as weak nucleophiles in the absence of the major contributor cysteine. It was found that although there is an increase in activity with pH for C5C8A, this effect is enhanced in the CPN3 peptide example. The presence of CPN3 peptide doubles the rate at which activity increases with pH implying that the protonation state of the cysteine residues does in fact have an effect on the activity of this peptide reinforcing that cysteine is key for catalysis to occur. It is known that water can play an important role by either directly taking part in catalysis or alternatively providing solvation medium for reactants, transition state and products.[81] An aqueous environment is key for catalysis to occur although it is not the sole source of deprotonation of the nucleophilic cysteine.

It is apparent that deprotonation of the cysteine residue to facilitate nucleophilic attack on the substrate is a key step in the mechanism of catalysis (Figure 4.8). Based on chemical characteristics and observed effects on rates, aspartic acid could play a role here deprotonating water molecules which in turn deprotonate the cysteine residue. The terminal amine may play a similar role here deprotonating water molecules as it acts as a base. Alternatively, deprotonation has the potential to occur as a result of the pH of the aqueous environment however it is known that this is not the sole source of deprotonation since catalytic activity of cysteine alone in buffer does not match the catalytic rates of CPN3. Therefore there is an alternative source of deprotonation in the peptide sequence.

Next, the effects of temperature (Figure 4.9A) were investigated. A change in temperature does not contribute to catalytic rates and only increases background hydrolysis as temperature increases resulting in a slight loss of activity above 40 ^{o}C. At higher temperatures the peptide-substrate interaction encounters perturbation meaning that even at high temperatures which usually favor catalytic activity of synthetic catalysts, up to an optimum temperature, product formation is hindered due to entropic effects.

Since CPN3 is flexible, the active site of the peptide should be relatively unimpeded and therefore it was sought to characterize the ability of the peptide to hydrolyze substrates with varying carbon chain length. CPN3 has the ability to catalyze ester hydrolysis of a variety of substrates (Figure 4.9B). Hydrolysis of *p*NPA over a variety of substrate concentrations leads to a linear increase in activity as observed previously.[8] The hydrolysis of para-nitrophenyl butyrate (*p*NPB) also occurs in the presence of CPN3 at a lower rate than for *p*NPA. The rate is almost two times faster for *p*NPA at a substrate concentration of 1 mM (2.6×10^{-4} s^{-1} for *p*NPB in comparison to 5.2×10^{-4} s^{-1} for pNPA). This reduced activity for the substrate with a longer carbon chain length has been observed for wild-type carbonic anhydrase which has been found to catalyze *p*NPB with only 2% of the activity with which is hydrolyzes *p*NPA.[82] The larger substrate is harder to bind and therefore the efficiency of the catalyst is reduced. The substrate *p*-nitrophenyl formate was also

used for this experiment. However the ester was hydrolyzed almost instantaneously and activity could not be measured. These results allude to substrate specificity however this has not been clarified at this time.

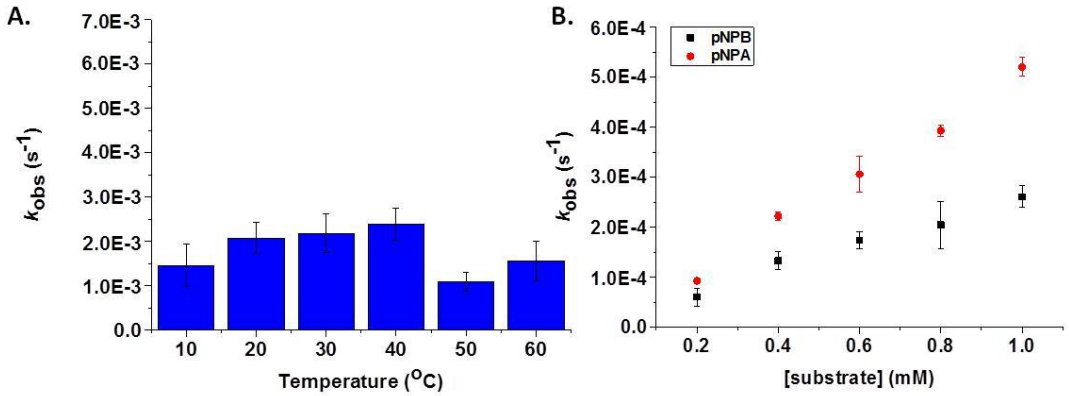

Figure 4.9. CPN3 esterase activity in alternative conditions. A. Catalytic rates (k_{obs}) for ester hydrolysis by CPN3 peptide at different temperatures. Peptide concentration was 0.018 mM and the substrate concentration was 6 mM. **B.** Time course data for ester hydrolysis by CPN3 peptide in organic solvents. Peptide concentration was 0.018 mM and the substrate concentration was 6 mM. **C.** Catalytic rates (k_{obs}) for ester hydrolysis by CPN3 peptide using different substrates. Peptide concentration was 0.018 mM and the substrate concentration ranged from 2 - 10 mM. Error bars are based on three repeats. Samples are corrected for background hydrolysis to give a true rate based on the catalyst alone.

In summary, this chapter reports a non-histidine containing peptide catalyst which has a catalytic rate of 2-3 x 10^{-3} s^{-1}. This catalytic constant is on a par for examples of short peptide catalysts in literature however those examples have an organized structure which presents catalytic moieties on the surface for catalysis in comparison to our random, unassembled peptide.

4.4 Conclusions

Removing the peptide sequences from their phage scaffold results in a decrease in activity on the scale of more than nine orders of magnitude for amidase activity and three to five orders of magnitude for esterase activity. However, the trend in the rates of activity is retained in most examples with CPN2 being the best amidase and CPN3 being the best esterase. Initial investigation into the mechanism of catalysis of the

peptides for esterase activity demonstrated that binding plays only a minor role in catalysis. Within the concentration range studied, the linear relationship indicated that the catalytic phage and free peptides behave more like small molecule catalysts.

CPN3 has a random conformation and it is this flexibility which allows for catalysis to occur. It has been identified that on the substitution of cysteine in the peptide sequence, catalytic activity dramatically reduces highlighting the importance of these residues. Cysteine alone can also hydrolyze ester bonds however this is at a lower rate than CPN3 peptide indicating that there is some transition state stabilization coming from remaining peptide residues (most likely candidate is arginine) therefore enhancing catalysis. Protonation state of the cysteine has been highlighted as key for the catalytic mechanism to take place. It is unlikely that these residues are completely deprotonated as a result of the pH of the buffer however several neighboring amino acids such as aspartic acid and the terminal amine have the potential to deprotonate the catalytic residue and facilitate nucleophilic attack on the substrate. Temperature has a minimal effect on the activity of CPN3 peptide and conformational perturbation at higher temperatures can hinder product formation. CPN3 peptide has the ability to catalyze two different substrates, *p*NPA and *p*NPB, with the difference in rate being almost two times faster for *p*NPA at a substrate concentration of 1 mM. The difference in chain length for the substrate can affect the catalytic ability of CPN3 as a result of steric hindrance for the longer chain length resulting in lower catalytic activities. CPN3 is a novel peptide catalyst which is unstructured and does not contain histidine. This provides further insight into alternative catalytic amino acids as an alternative to histidine and provides an initial understanding of the mechanism of action. It also provides some understanding of simple peptides could act as catalytic predecessors to the more complex enzymes that are known now.

5.0 A Tripeptide for Ester Hydrolysis

5.1 Introduction

The self-assembly of simple peptides into nanostructures is advantageous for many applications including biomedicine, cosmetics and nanotechnology.[39, 83-86] The combination of the 20 natural amino acids into peptide building blocks provides diversity and versatility in the form of chemical functionality of the residue side chains. Short peptides in particular, enhance the capability of rational design as well as providing robust systems which are scalable. The concept of minimalistic peptide assembly was pioneered by Gorbitz who reported the formation of peptide nanotubes by four dipeptides including Phe-Phe. These peptides crystalize with hydrogen bonded head to tail chains in the form of helices.[87] Reches and Gazit also studied the self-assembly of Phe-Phe which forms hollow tubular assemblies, noting that this dipeptide is the core recognition motif of the Alzheimer's β-amyloid peptide.[38] De Groot *et al.* reported self-assembly and gelation whilst providing an insight into the amyloid formation of the dipeptide Ile-Phe.[88] It was shown that while Ile-Phe self-assembles in an aqueous environment to form a self-supporting hydrogel, Val-Phe, with a difference of only one methyl group, does not. Study of these di-peptide building blocks, Ile-Phe and Val-Phe, provides an insight into the nucleation and growth mechanisms in the self-assembly of amyloid structures. They suggest that formation of amyloid fibrils begins with the formation of globular structures driven by less-specific hydrophobic interactions which then undergo reorganization by specific interactions for example, aromatic stacking.[88] These specific interactions then transform the globular aggregate into short fibrils. Tamamis and co-workers took this work with Phe-Phe further by studying the tripeptide Phe-Phe-Phe in aqueous solutions and demonstrated that this self-assembles into plate-like nanostructures.[89] These are planar and rich in β-sheet structures. As well as this, the tripeptide networks provide more stable nanostructures in comparison to the dipeptide system due to the difference in alignment of β-strands. The dipeptide tends to favor unaligned strands whilst the tripeptide favors aligned strands. This stems from the different sizes of the monomers for each peptide resulting in the tripeptide having additional hydrogen bonding in comparison to the dipeptide as well as an additional side chain.

Further interest in the behavior of amyloid peptides developed due to the potential applications in nanostructured materials.[20, 90] The core sequence of the Alzheimer's β-amyloid peptide, Lys-Leu-Val-Phe-Phe, has been identified as a short peptide sequence which will form amyloid fibrils and consequently hydrogels.[91] However, fragments of this pentapeptide only form hydrogels in the presence of organic solvents *e.g.* 1,1,1,3,3,3- hexafluoro-2-propanol ~2% final volume. This is due to uncapped di- and tripeptides being either too hydrophilic and readily dissolving in water or too hydrophobic and precipitating. Marchesan reports short tripeptides, Val-Phe-Phe and Phe-Phe-Val, which on the modification of the N terminal amino acid from L to D configuration form self-supporting hydrogels without the presence of organic solvents at a physiological pH.[92] The induced chirality of these structures results in the formation of twisted nanostructures with β-sheet structures. In this case, chirality is an important component for the self-assembly of tripeptides. Indeed, this does not only extend to the formation of nanostructures from random, unassembled peptides but goes further to form self-support hydrogels at physiological pH. This work has been studied further and another tripeptide, Leu-Phe-Phe, has been found to form gels on the modification of the N terminal amino acid.[93] In this case key intermolecular interactions were identified for the different supramolecular behavior of these systems. It is proposed that a phenylalanine zipper is a pivotal interaction motif for the formation of elongated fibers in the D modified peptide which initiates macroscopic gelation and subsequently the system evolved to have a higher fiber density.

Computational chemistry has been employed to screen peptides for their aggregation capability as a potential precursor to self-assembly.[94] In this example, Frederix *et al.* screened dipeptides to look at their aggregation propensity. Dipeptides which showed strong aggregation tendencies were screened for longer simulations and results were in good agreement with the literature reports. It was demonstrated that Phe-Phe is able to reproduce important features of self-assembling systems and provide an insight into this process. Initially sheets form before vesicles are observed, the precursor to nanotube formation, as a result of the sheets folding on themselves once they have reached sufficient size. Since these first examples of short peptide self-assembly,[37, 95] many of the examples in literature have been discovered by chance or

by mapping onto biological systems. A further example by Frederix and co-workers has addressed this issue by using coarse grain molecular dynamics simulations to map the entire di- and tri-peptide sequence space. This has allowed for the development of design rules that direct the probability of a short peptide forming nanostructures.[96] Their methodology makes no assumptions regarding self-assembly and as a result allows for unbiased selection. Coarse grain molecular dynamics simulations based on the Martini model[97, 98] which was developed to analyze protein folding, was applied to screen peptides for their aggregation behavior. From 8,000 tripeptides tested, sequences were selected from this initial screening for further studies into tripeptide dynamics and the ability to (experimentally) form nanostructures. A set of design rules for aggregation of peptides were established whereby aromatic residues are favorable in positions two and three of a tripeptide and positive, hydrogen bond favoring residues are found in position one (the N terminus). Residues with acidic (negatively charged) side chains are found to be advantageous in position three (C-terminus). These results were confirmed by experimental analysis which studied the hydrogelation of unprotected peptides Lys-Tyr-Phe, Lys-Tyr-Tyr, Lys-Phe-Phe and Lys-Tyr-Trp at neutral pH and in the absence of organic solvents. Good agreement was observed between the computational analysis and experimental results.

Short peptides have not only been studied for their self-assembling tendencies, but also for their catalytic propensity, as enzyme mimics. As stated above, Ser-His has been shown to possess hydrolytic activity with respect to carboxyl esters, DNA and proteins, namely BSA.[25] Histidine is known to be fundamental for catalysis to occur and this has been further studied in the field of scaffolded peptides (see chapter 2.6). Liskamp *et al*. reported on a branched structure of three tripeptide 'arms' which has the ability to hydrolyze esters.[52] A TAC-scaffold was utilized to display three tripeptides, one nucleophilic, one basic and the final one acidic in nature to mimic a catalytic triad. These peptides were prepared by the split-mix method and resulting beads characterized for hydrolytic activity using a fluorescent esterase substrate that remains localized in these beads, allowing for those with catalytic activity to be easily identified. It was found that in active tripeptides, amino acids in the acidic chain were highly conserved even though this arm was not crucial for catalysis.

Aspartate was favored over glutamate. Furthermore, histidine was once again found to be crucial for catalysis, as the number of histidine amino acids present increased, the hydrolytic activity also increased. Variation in the other tripeptide arms was shown to affect catalytic rates. The proposed mechanism of action here is deprotonation of water by the histidine which can then facilitate nucleophilic attack with assistance by very weak substrate binding although binding does not play a significant role in the mechanism. Further examples of short peptide catalysts can be found in Chapter 2.0.

In this chapter , the unexpected esterase activity of the tripeptide Lys-Tyr-Phe is reported. This was discovered by chance, the intention had been to co-assemble the catalytic peptide described in Chapter 4.3.3 into a fibrous matrix in an effort to enhance its activity, but it was found that Lys-Tyr-Phe matrix showed substantial activity in the absence of CPN3. This remarkable observation was then studied in more detail and this chapter explores the mechanism of action for the catalyst in relation to the formation of self-assembled nanostructures and peptide sequence. This peptide was identified as self-assembling by Frederix *et al*. by computational analysis. It does not contain the traditional catalytic amino acids, for example histidine, serine and aspartic acid, but instead possesses positively charged lysine and two hydrophobic, aromatic residues and has catalytic rates for ester cleavage that are only one to two orders of magnitude lower than those reported in literature.

5.2 Objectives

Based on initial results that demonstrated the ester cleavage activities of KYF, the aims of this chapter were to:

- Study Lys-Tyr-Phe (KYF) and gain an insight into the peptide's self-assembly at different concentrations.
- Assess whether the self-assembly of KYF enhances the rate at which esters are broken.
- Investigate substituted and scrambled sequences to gain an insight into its mechanism of action.

- Study different reaction conditions and also different tripeptides to understand the affect that these factors have on the rate at which esters are broken.

5.3 Results and Discussion

The ability of KYF to break ester bonds was discovered by chance during the study of multivalent display of CPN3 peptide (Chapter 4.3.3) explored in a bid to increase the hydrolytic activity of the peptide. CPN3 was modified with KYF at the C terminus of the peptide so that when mixed with KYF itself, the two peptides would co-assemble and display CPN3 in an ordered fashion at several different sites along the length of the fibers formed (results not included). In this process, it was discovered that KYF itself substantially increased the rate at which ester bonds were broken while there was no evidence of enhanced activity of CPN3 when displayed by co-assembly. Therefore, it was decided to further study this unexpected tripeptide in a bid to understand how the mechanism of action of one of the shortest peptide identified with ability to break ester bonds .

5.3.1 Self-Assembly of KYF

It was first investigated whether the peptide is structured. KYF shows a positive peak at 200 nm when analyzed by CD at concentrations below 5 mM which shows that the peptide in solution does have some conformation and is not a random, unassembled structure (Figure 5.1). As the peptide concentration increases, the spectra begin to change with the original peak at 200 nm broadening to cover the range of 200 - 240 nm and eventually splitting into two peaks, one at 200 nm and the other at 235 nm demonstrating that there is a change in conformation of the peptide as concentration increases and a supramolecular structure is beginning to form. 12.5 mM was the maximum concentration that could be analyzed due to saturation of the absorbance signal and any further data would not have been reliable. At 12.5 mM as well as the original peak splitting into two, a dip begins to develop around 280 nm. These short peptides are clearly much simpler in structure than proteins, therefore the spectra

obtained cannot be directly mapped onto traditional protein spectra to obtain information about the chirality and structures formed. This makes the results very difficult to interpret and they need further investigation, although they clearly show that a structure is formed. High tension voltage is a parameter monitored whilst taking measurements on the CD and is included here to demonstrate that the measurements taken were within the allotted parameters and are therefore reliable (less than 1000 V, Figure 5.1B)

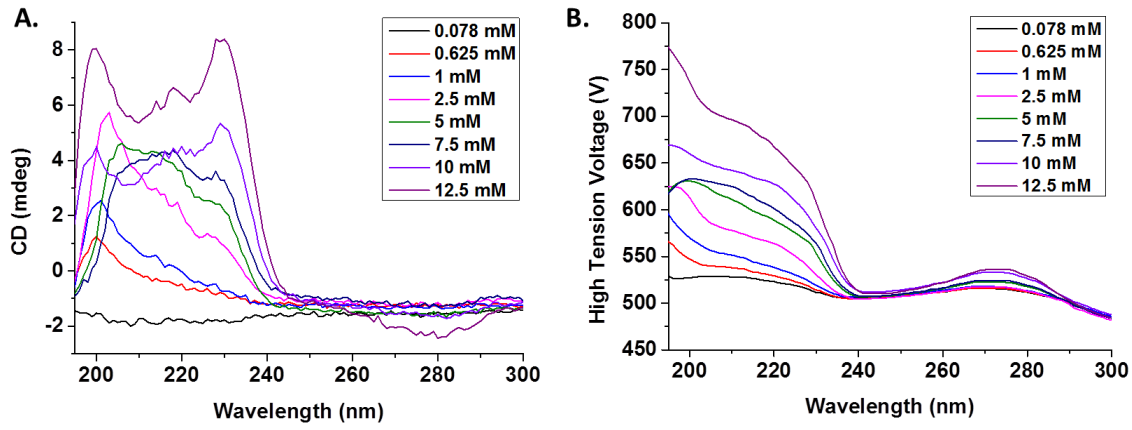

Figure 5.1. A. CD spectra of KYF peptide illustrating that the peptide has conformation in solution. **B.** High tension voltage spectra of KYF peptide illustrating that the peptide has conformation in solution.

As well as investigating conformations by CD, TEM was also utilized to visualize any nanostructure formation in the samples. TEM shows that even at very low concentrations (1 mM KYF) short, flat sheet-like structures are present in the sample and with increasing concentration, fiber formation occurs resulting in a self-supporting hydrogel (Figure 5.2). 10 mM KYF results in a viscous sample whilst 1 mM KYF is a liquid. The scale of these images is 2 µm for the sheet like structures at 1 and 10 mM KYF in comparison to 0.5 µm for the fibers at 20 mM KYF concentration. This demonstrates that these sheet-like formations are large structures, greater than 2 microns in size, whereas the fibers are long and very narrow, ~ 10 nm in diameter and over microns in length. These high concentration samples are highly organized into very narrow but long fibers whereas the lower concentration samples appear to be more aggregated due to non-specific interactions including aromatic

interaction. This is in line with the observations by CD illustrating KYF has some conformation at concentrations of 10 mM and below but does not self-assemble into fibers until 20 mM concentration.

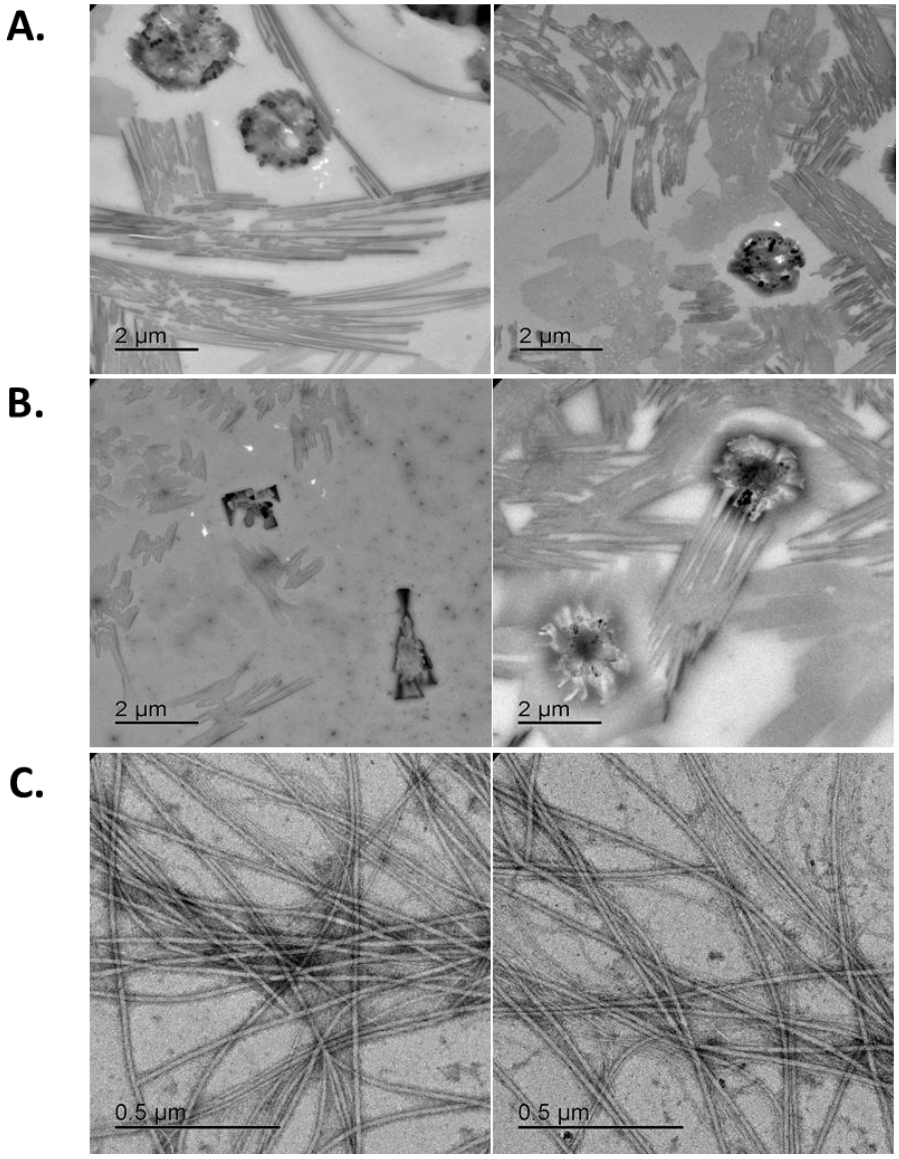

Figure 5.2.TEM images of KYF at different concentrations. A. 1 mM KYF in PBS. **B.** 10 mM KYF in PBS. **C.** 20 mM KYF in PBS forms a self-supporting hydrogel.

Fluorescence and UV-Vis spectroscopy provide a further insight into the self-assembly process of KYF. It can be seen by fluorescence emission that on increasing peptide concentration, the fluorescence of the tyrosine residue[100] in the peptide sequence is quenched (excluding that of 0.1 mM KYF which has reduced

fluorescence due to the very low concentration of peptide (Figure 5.3A)). This is the maximum signal that can be obtained for the low concentration sample. Fluorescence significantly increases at 1 mM and then quenches with increasing peptide concentration. The most pronounced drop in signal occurs from 2.5 – 5 mM which is indicative of the peptide conformation developing into supramolecular, self-assembled nanostructures, which is in agreement with the concentration at which a change in CD spectra is observed (5 mM and above). The aromatic residues interact with one another *via* π stacking[101] and the fluorescence intensity decreases suggesting self-assembly.

On incubation with ThioflavinT, low concentrations of KYF (0.078 – 5 mM) show no fluorescence however at 7.5 mM KYF and above, fluorescence is emitted strongly from the samples (Figure 5.3B and C). ThioflavinT is a widely used dye for the identification of β-amyloid structures[102] and has been known to be used for demonstrating the aggregation of oligopeptides[103] due to the enhancement of its fluorescence as a consequence of binding to amyloid-like fibrils. The emission of fluorescence is caused by the restriction of free rotation of the two rings in ThioflavinT upon binding to a hydrophobic surface. The mechanism of interaction is not fully understood and therefore it is unclear whether the dye interacts with β-sheets specifically or with a hydrophobic domain in a non-specific manner.[104, 105] However, it does indicate self-assembly and formation of a hydrophobic domain. Therefore, it can be determined that KYF does indeed self-assemble with the formation of a hydrophobic domain when the concentration of peptide is above 7.5 mM. KYF has some conformation at lower concentrations (1, 2.5 and 5 mM, see Figure 5.3A) but these samples do not form supramolecular structures and as a result do not possess a significant hydrophobic domain for ThioflavinT to bind to therefore, there is no fluorescence signal (Figure 5.3B and C). When the tyrosine amino acid is excited directly, quenching of the fluorescence is observed even at low concentrations, 1 – 5 mM KYF, as described previously (Figure 5.3A) and so the peptide conformation is changing in this concentration range even though this cannot be measured with ThioflavinT. This suggests that the long narrow fibers at high concentrations have more hydrophobic surface area than the larger, sheet-like structures. UV-Vis spectroscopy confirms the self-assembly occurring above 7.5 mM

KYF (Figure 5.3D). Measuring at 800 nm, the turbidity of the sample can be measured which is indicative of self-assembly in the sample.

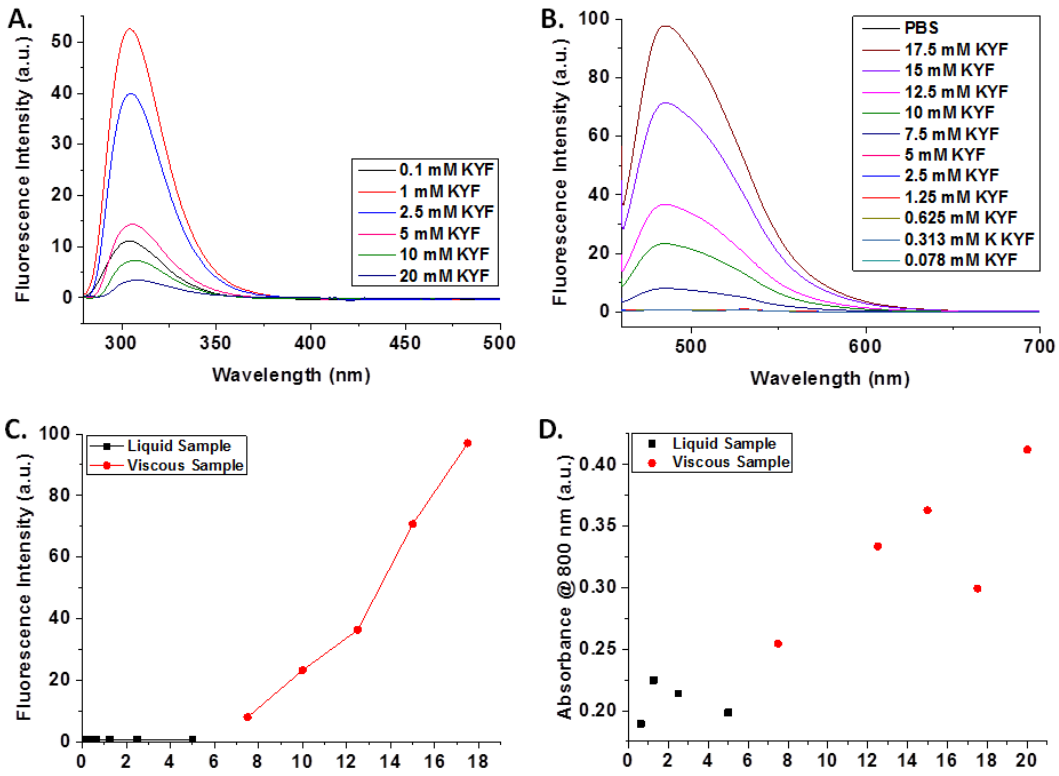

Figure 5.3. Spectroscopic study into the self-assembling propensity of KYF. A. Fluorescence spectra of increasing KYF concentrations at an excitation wavelength of 274 nm for the tyrosine residue. **B.** Fluorescence spectra of KYF at different concentrations in the presence of ThioflavinT which demonstrates self-assembly and formation of a hydrophobic domain at concentrations greater than 7.5 mM. **C.** Fluorescence data showing the increasing fluorescence vs. increasing peptide concentration to reveal the critical aggregation concentration. **D.** UV-Vis data demonstrating the formation of self-assembled structures.

The self-assembly data has been summarized in table 5.1 to make a comparison between techniques and the concentration at which a change can be seen in the structures formed by KYF. For CD and fluorescence, the critical concentration is found to be between 5 and 7.5 mM. TEM does not illustrate a change in structure until the concentration is above 10 mM. In conclusion to this, the critical concentration for self-assembly of KYF is in the range of 5 mM – 7.5 mM.

Table 5.1. Comparison of techniques used to study KYF structure and critical concentrations reported.

Technique	Critical Concentration of KYF (mM)	Consistency of Sample
CD	5 – 7.5 mM	Viscous
TEM	> 10 mM	Viscous - Gel
Fluorescence varying KYF Concentration	> 5 mM	Viscous - Gel
Fluoresence with ThT	7.5 mM	Viscous

5.3.2 Hydrolytic Activity of KYF

KYF forms a gel at 20 mM which has hydrolytic activity. Introduction of the substrate onto the surface of the gel, results in diffusion of the substrate through the hydrogel and ester cleavage of the substrate to the yellow nitrophenol product. The substrate has completely diffused through the sample after 2 hours and continues to become a more intense color as time passes. It is not possible to measure this activity by UV-Vis spectroscopy and so a hydrolytic rate cannot be calculated for this process however it is clear that the peptide gel possesses esterase activity.

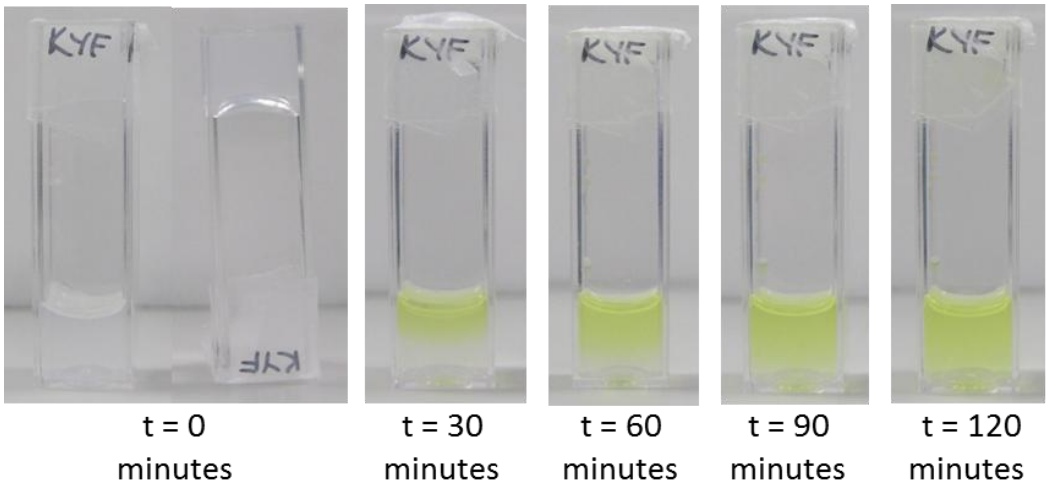

Figure 5.4. Esterase activity of a 20 mM KYF gel over two hours.

Informed by the structural studies and the fact that a 20 mM KYF gel possesses the ability to hydrolyze ester bonds, the esterase activity of the peptide was investigated at concentrations above and below the critical aggregation concentration (7.5 mM)

utilizing the UV spectroscopic study of *p*NPA (Figure 5.5). Samples were prepared at final concentrations of 2, 3, 4, 5, 6 and 7 mM peptide concentration after being diluted from 4 – 14 mM (UV cannot be used to follow cleavage within a gel and so samples must be diluted). Remarkably, it could be concluded that the self-assembly state of the peptide does not contribute to the esterase activity.

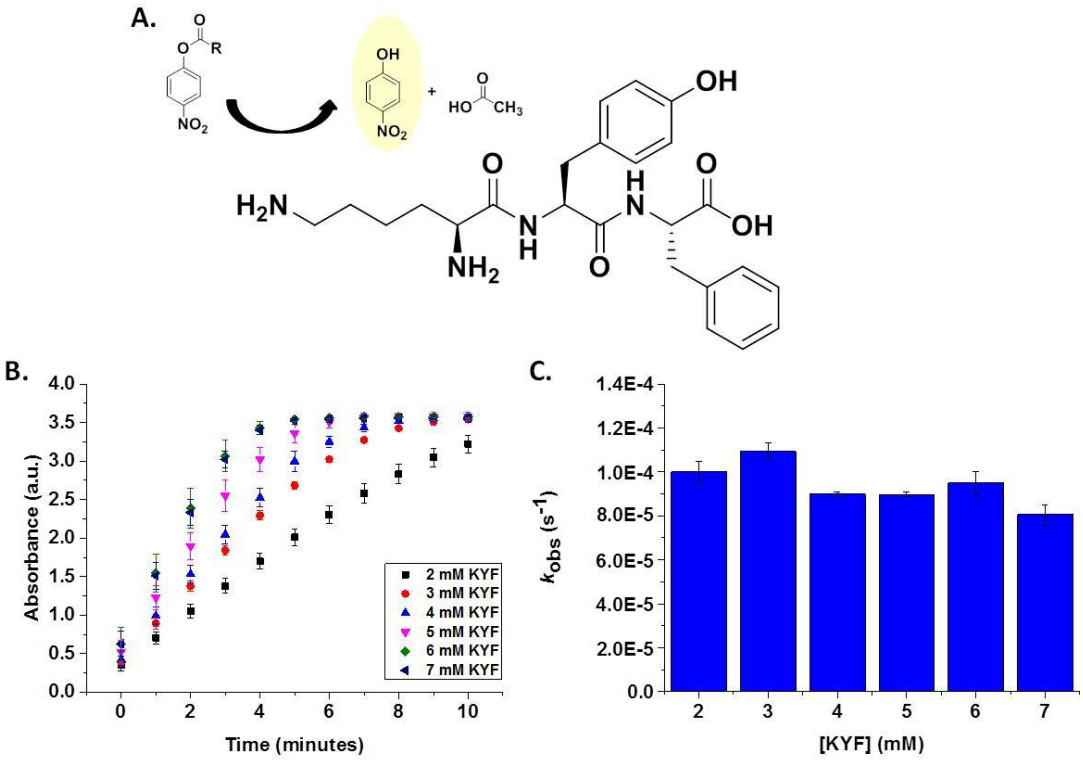

Figure 5.5. A. schematic representation of the UV *p*-NPA cleavage assay. **B.** Time course data for ester cleavage by KYF. Final peptide concentration varied from 2 – 7 mM after being diluted from 4 – 14 mM samples that were left overnight to self-assemble. The substrate concentration was 6 mM. **C.** Rates (k_{obs}) for ester cleavage by KYF. Peptide concentration varied from 2 – 7 mM and the substrate concentration was 6 mM.Error bars are based on three repetas. Samples are corrected for background hydrolysis to give a true rate based on the peptide alone.

It can be seen that the concentration of peptide in the sample does not contribute to the overall (concentration corrected) rate of esterase breakage (1 x 10^{-4} s^{-1}) (Figure 5.5B and C). There is a slight downward trend as peptide concentration increases. Therefore it suggests that self-assembly may inhibit the activity slightly, perhaps due to restricted substrate diffusion when fibers are present, and so lower concentrations of peptide were utilized to further investigate the activity.

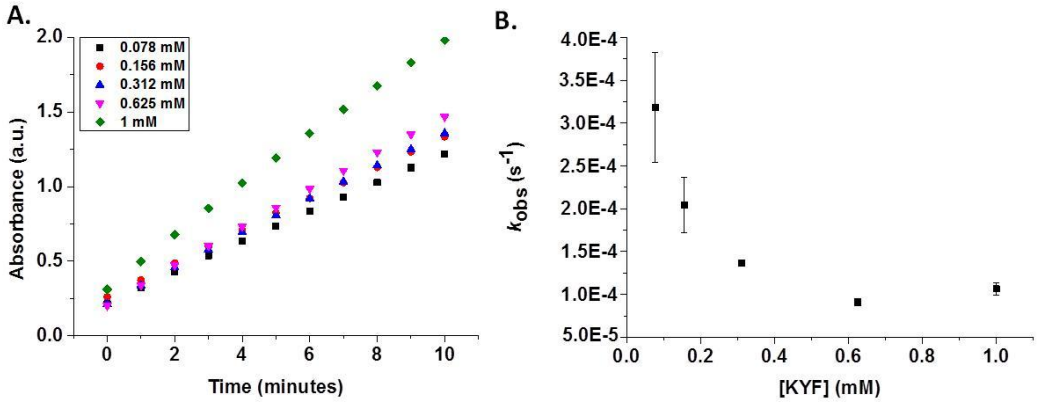

Figure 5.6. A. Time course data for ester cleavage by KYF. Peptide concentration varied from 2 – 7 mM and the substrate concentration was 6 mM. **B.** Rates (k_{obs}) for ester cleavage by KYF. Peptide concentration varied from 2 – 7 mM and the substrate concentration was 6 mM. Error bars are based on three repeats. Samples are corrected for background hydrolysis to give a true rate based on the peptide alone.

As KYF concentration decreases the activity increases (up to 3.1 x 10^{-4} s^{-1}) indicating that self-assembly does not enhance the rate of ester cleavage in this case (Figure 5.6). However, at these low catalyst concentrations the data become less reproducible due to the background hydrolysis and for this reason 1 mM was selected as the concentration for further study of this peptide.

It is clearly unexpected for a tripeptide that does not contain traditional hydrolytic amino acids to demonstrate esterase cleavage activity. Substituted peptides (Figure 5.7A) were designed to delineate the role that each functional group plays in ester cleavage and propose a mechanism of action for the activity (Figure 5.7B and C).

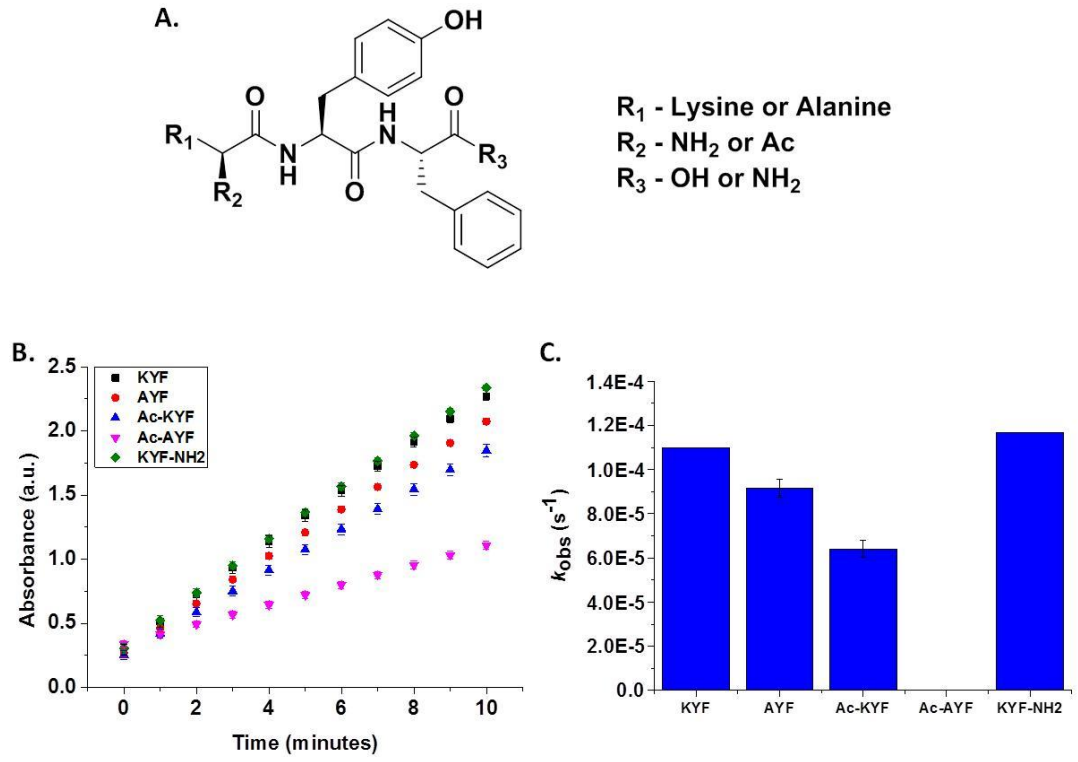

Figure 5.7. A. KYF substitutions. **B.** Time course data for ester cleavage by KYF. Peptide concentration was 1 mM and the substrate concentration was 6 mM. **C.** Rates (k_{obs}) for ester cleavage by KYF. Peptide concentration was 1 mM and the substrate concentration was 6 mM.Error bars are based on three repeats. Samples are corrected for background hydrolysis to give a true rate based on the peptide alone.

It is shown that the terminal acid group of the peptide plays no role in ester cleavage as on amidation of this functional group the hydrolytic activity of KYF remains constant. On substitution of lysine with alanine, there is a slight decrease in the activity implying that lysine does contribute to cleavage[106-108] although is it not the main functional group involved in this process. Lysine in close proximity to the terminal amine contributes to reducing the pK_a of the terminal amino group (typically pK_a 6.9 - 8.1)[80] resulting in deprotonation[109, 110] and possible nucleophilic attack by NH_2. The general hydrophobic environment provided by the Phe and Tyr residues may further contribute to suppressed ionization. Another mechanism of action which is possible is that basic lysine deprotonates water which can also act as a nucleophile in ester cleavage. Lysine has also been known to form part of a condensation reaction with a carbonyl group of a reaction substrate forming and imine or Schiff base[111] although this mechanism seems unlikely when taking pK_a

into account. Lysine has a side chain pKa of 10.53 in comparison to the terminal amino of a polypeptide which has a pK_a of 6.9 - 8.1[80] therefore it is more likely that the terminal group will be deprotonated and act as a nucleophile for cleavage. This was confirmed by acylation of the terminal amino group which results in a more significant decrease in activity implying that the terminal amino group has a key role in esterase activity.[107] Finally, acylation of the terminal amino and substitution of the lysine residue simultaneously results in complete deactivation of the peptide. It can therefore be concluded that the terminal amino group plays a key role in ester cleavage whilst lysine plays a secondary role in the local microenvironment. This result is reinforced by the fact that lysine itself has (limited) activity with respect to ester cleavage.

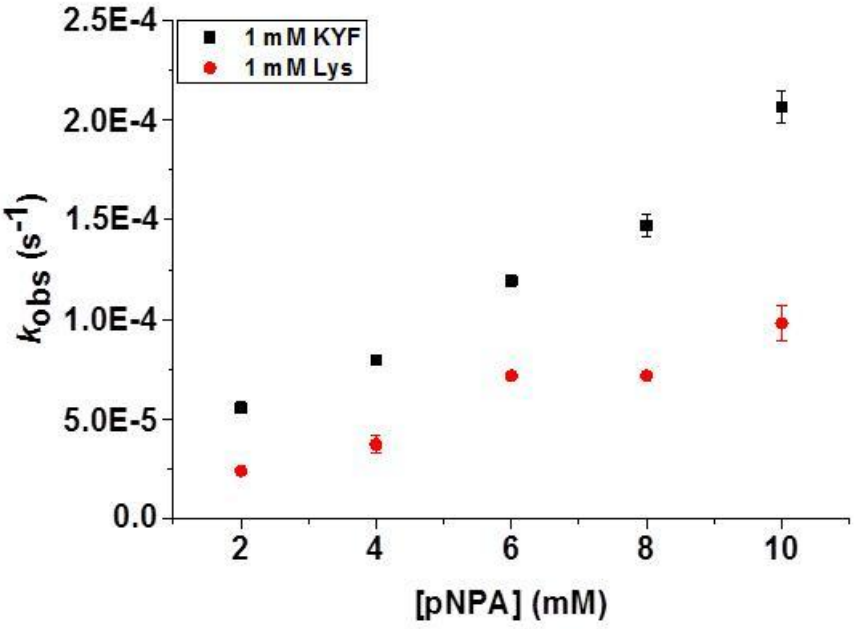

Figure 5.8. Rates (k_{obs}) for ester cleavage by KYF and lysine alone. Catalyst concentration was 1 mM and the substrate concentration ranged from 2 - 10 mM. Error bars are based on three repeats. Samples are corrected for background hydrolysis to give a true rate based on the peptide alone.

A linear trend is observed for the cleavage of esters by KYF at 1 mM concentration and by 1 mM Lys (Figure 5.8). This suggests that at this concentration, binding is not

playing a significant role in the mechanism of action within the concentration range of 2 – 10 mM *p*NPA.

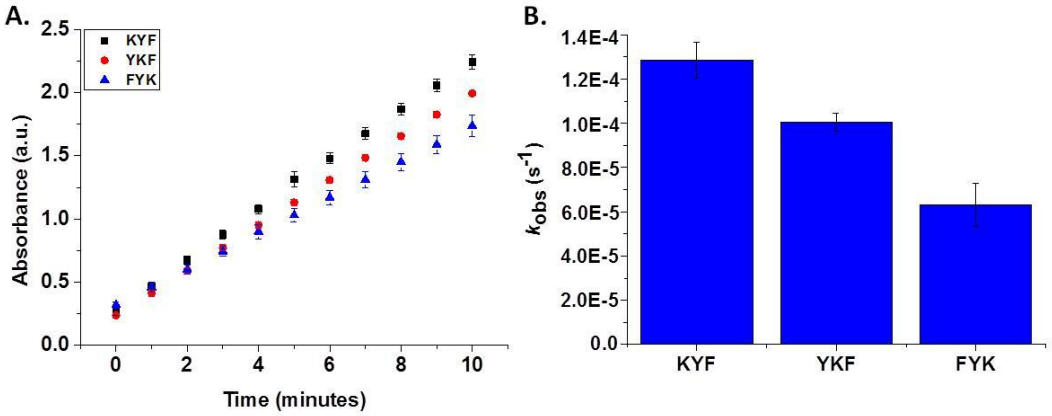

Figure 5.9. A. Time course data for ester cleavage by KYF scrambled sequences. Peptide concentration was 1 mM and the substrate concentration was 6 mM. **B** Rates (k_{obs}) for ester cleavage by KYF scrambled sequences. Catalyst concentration was 1 mM and the substrate concentration was 6 mM.Error bars are based on three repetas. Samples are corrected for background hydrolysis to give a true rate based on the peptide alone.

Furthermore, scrambled sequences have been tested for esterase cleavage. Scrambling the sequences affects the activity of the peptide. As the lysine residue moves further away from the N terminus the activity decreases. Essentially the basic environment provide by the lysine side chain is moving further away from the terminal amino group therefore the pKa of the amino group will increase to the original value of ~ 8.0 as expected for polypeptides. Due to this, it is more likely to be protonated in reaction conditions at pH 7.4 and less likely to be able to catalyze the ester cleavage . This can be seen as the activity decreases from KYF, to YKF and finally FYK. At the point where lysine becomes C terminal, the activity is at its lowest confirming that the basic microenvironment that the lysine side chain creates is important to prepare the terminal amino group for cleavage.

KYF is a hydrophobic peptide and these hydrophobic residues have not yet been accounted for in the mechanism of action. It can be seen that on deletion of one of the aromatic residues from the sequence KYF, the rate of activity decreases although some activity is maintained. This demonstrates that the presence of both of the aromatic residues is fundamental for the peptide to work at full efficiency. This is

confirmed by the decrease in activity seen for KLL where both aromatic residues are replaced with leucine. In each case, KLL, KY and KF, the activity is in the same region as for lysine alone and so the presence of only a single aromatic group does not enhace cleavage. It is possible, that an aromatic 'sandwich' is forming whereby the substrate interacts with tyrosine and phenylalanine by moving in between those amino acids. This acts as a transient binding state which can enahnce cleavage. The deletion of tyrosine has the most dramatic loss of activity which could be due to the removal of the hydroxyl group which has the ability to hydrogen bond with the substrate as another method of transient interaction.

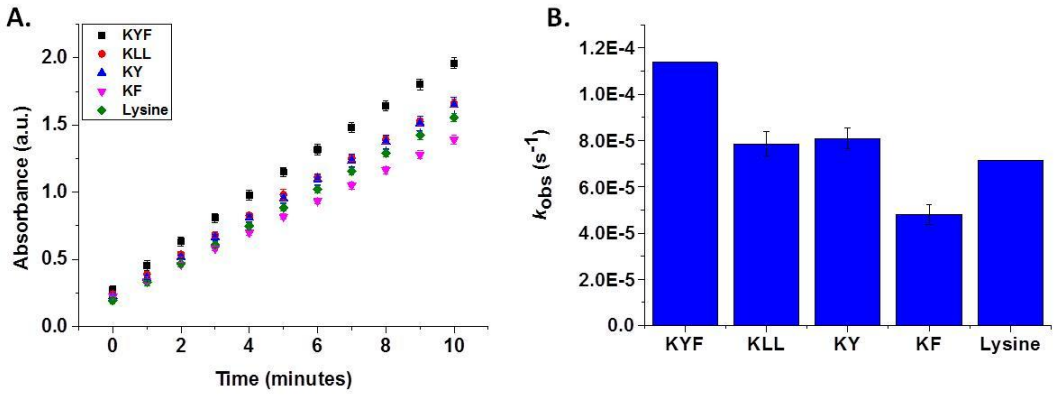

Figure 5.10. A. Time course data for ester cleavage by KYF, KY, KF and Lysine. Peptide concentration was 1 mM and the substrate concentration was 6 mM. **B** Rates (k_{obs}) for ester cleavage by KYF, KY, KF and Lysine. Catalyst concentration was 1 mM and the substrate concentration was 6 mM. Error bars are based on three repeats. Samples are corrected for background hydrolysis to give a true rate based on the peptide alone.

A peptide with two aromatic residues creates the opportunity for π-π interactions with an aromatic substrate, in this case *p*NPA. Fluorescence spectroscopy was utilized to monitor interactions between the aromatic residues and the substrate for ester cleavage. In this case the excitation wavelength chosen was 274 nm to excite at the tyrosine residues as this fluorescence is stronger than for phenylalanine.[100] Since the aromatic residues are in close proximity to one another, tyrosine absorbs at 257 nm, the excitation for phenylalanine, therefore strong fluorescence overshadows the weak signal from phenylalanine.[112]

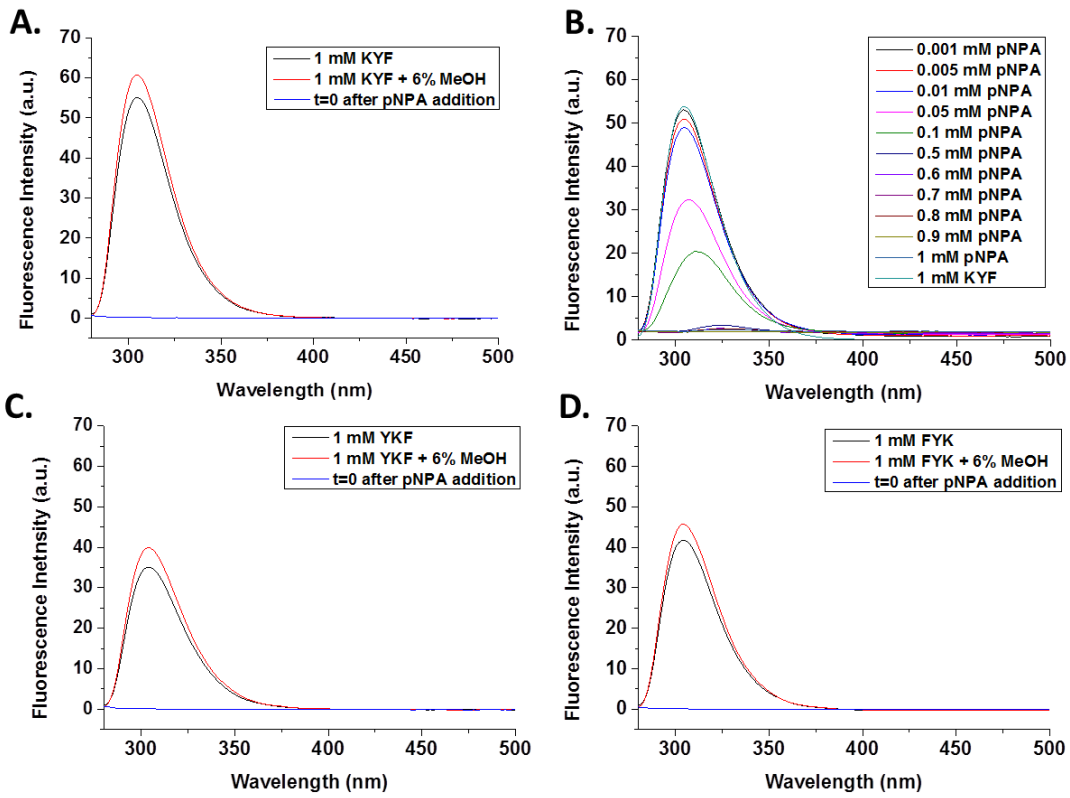

Figure 5.11. Substrate interaction with aromatic residues of KYF by fluorescence A. Fluorescence of KYF, KYF interaction with 6% MeOH and KYF interaction with 6% *p*NPA in MeOH. KYF concentration was 1 mM and the substrate concentration was 6 mM. **B.** Fluorescence of KYF interaction with *p*NPA in MeOH. KYF concentration was 1 mM and the substrate concentration varied from 0.001 – 1 mM. **C.** Fluorescence of YKF, YKF interaction with 6% MeOH and YKF interaction with 6% *p*NPA in MeOH. YKF concentration was 1 mM and the substrate concentration was 6 mM. **D.** Fluorescence of FYK, FYK interaction with 6% MeOH and FYK interaction with 6% *p*NPA in MeOH. FYK concentration was 1 mM and the substrate concentration was 6 mM.

It can be seen that on the addition of 6% methanol to KYF there is no change in the intensity of the fluorescence signal. Methanol, as expected, does not interfere with the tyrosine signal. On the addition of 6% *p*NPA in methanol (100 mM) to 1 mM KYF the fluorescence signal is quenched immediately. Nitrobenzene is a well-known fluorescence quencher.[113-115] Quenching can occur through the mechanism of electron transfer,[113, 116] in this case photo-induced electron transfer. This demonstrates that the aromatic residues and the nitrobenzene substrate are in close enough proximity for electron transfer to happen. This is as a result of the hydrophobic and π-π interactions which result in transient binding of the substrate

which is sufficiently long for the cleavage to occur. An alternative method of quenching is the result of energy transfer to the nitrobenzene. As molecules collide, energy is transferred to nitrobenzene forming the excited state of the molecule before return to the ground state through internal conversion of the energy. This quenching effect is concentration dependent. KYF signal intensity is maintained at a nitrobenzene concentration of 0.001 mM. Upon increasing the substrate concentration to 1 mM, the fluorescence decreases until the tyrosine peak has been completely quenched. The substrate concentration used in the activity assays is 6 mM therefore it can be expected that the aromatic residues interact with the substrate in a manner that brings them close enough for transient binding and electron transfer to occur.

Having established that lysine and the terminal amino group are key for cleavage to occur, an investigation into pH was carried out to further understand the mechanism of action. This study demonstrates that as pH increases the activity of KYF also increases however there is a significant difference between pH 7.5 and pH 8. At pH 8, the terminal amino group is fully deprotonated and therefore has a better nucleophilic capability. pH 8 is the optimum pH studied and increases the activity from 9.26×10^{-5} s^{-1} to 3.26×10^{-4} s^{-1} which is 3 and a half times faster than for pH 7.5. This trend is also observed for background activity however the introduction of KYF into the sample shows an enhancement of that effect. Therefore pH and protonation state of the terminal amino group are very important for cleavage to occur and as the pH is increase the optimum conditions are reached for the range studied. Increasing the pH further would also increase activity however the background will come in line with the peptide sample at some point and it would not be possible to measure the activity at this point.

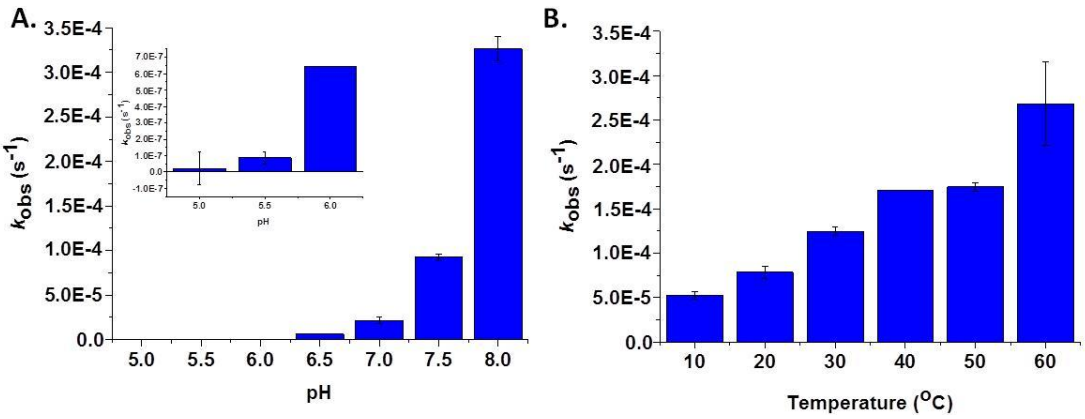

Figure 5.12. A. Rates (k_{obs}) for ester cleavage by KYF. Peptide concentration was 1 mM and the substrate concentration was 6 mM. **B.** Hydrolytic rates (k_{obs}) for ester cleavage by KYF at different temperatures. Peptide concentration was 1 mM and the substrate concentration was 6 mM. Error bars are based on three repeats. Samples are corrected for background hydrolysis to give a true rate based on the peptide alone.

The effects of temperature were also studied. As temperature increases there is a small increase in cleavage activity up to 40 ^{o}C. At this temperture the activity of the peptide plateaus and does not vary significantly. At increased temperatures the peptide-substrate interaction encounters perturbation meaning that even at high temperatures which usually favor cleavage activity of synthetic catalysts, product formation is hindered due to entropic effects.

Finally, other tripeptides were studied for esterase cleavage at 1 mM concentration including KYW, KFF, DFF and FFD.[99] The activity for these peptides did not match that of KYF but showed a decrease in activity for all sequences tested.

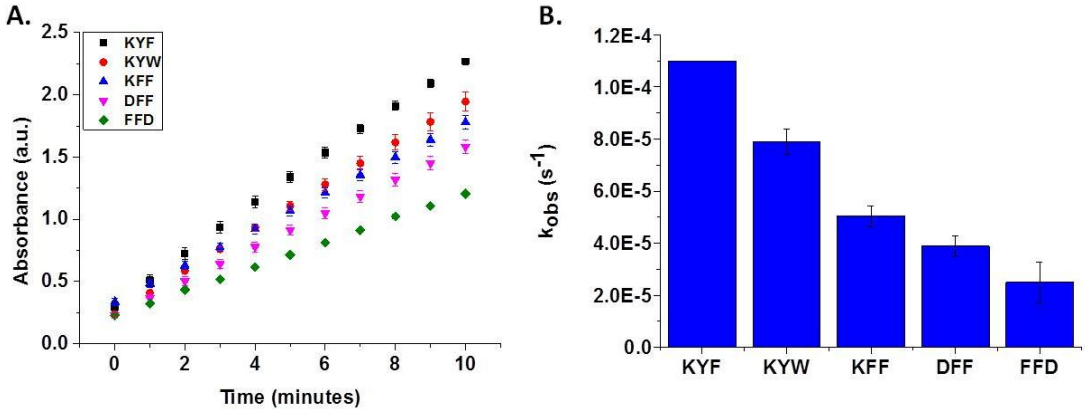

Figure 5.13. A. Time course data for ester cleavage by alternative tripeptides. Peptide concentration was 1 mM and the substrate concentration was 6 mM. **B** Rates (k_{obs}) for ester cleavage by alternative tripeptides. Catalyst concentration was 1 mM and the substrate concentration was 6 mM.Error bars are based on three repeats. Samples are corrected for background hydrolysis to give a true rate based on the peptide alone.

On substitution of phenylalanine to tryptophan, the activity of the peptide decreases. This is due to tryptophan being a bulkier amino acid which potentially alters the aromatic substrate – peptide interactions resulting in less efficient cleavage. For KFF the activity decreases further due the loss of heteroatoms capable of hydrogen bonding with the substrate and transiently binding it whilst cleavage takes place. Hydrophobic interactions between the substrate and aromatic amino acids are not enough for the catalyst to work to effectively. The introduction of an acidic residue instead of lysine results in reduced activity since the local environment becomes acidic meaning that the acidic residue is more likely to be deprotonated than the terminal amino group which is fundamental for cleavage although there is still measurable activity.

These results allow a mechanism to be proposed for the hydrolytic activity of KYF.

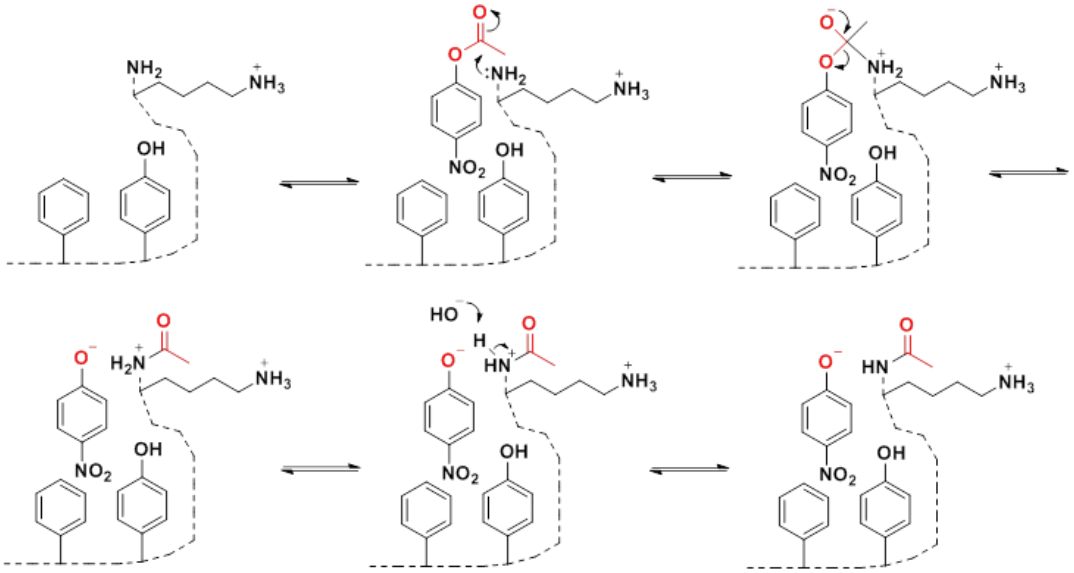

Figure 5.14. Proposed mechanism of ester cleavage by KYF indicating possible roles for each amino acid.

The pK_a of the terminal amino group is lowered as a result of the basic environment provided by the lysine side chain and is therefore more likely to be deprotonated than in an ordinary polypeptide.[110] This allows for the nucleophilic attack of the substrate by the lone pairs on the nitrogen atom. The electrons flow onto the oxygen of the carbonyl group which then flow back into the core of the transition state promoting the leaving of the bound catalyst in the form of an amide. This is known as aminolysis and is not a catalytic process but instead sacrificial.[117-119] Mass spectroscopy was used to confirm the formation of the amide final product. Ten minutes after addition of the substrate to the peptide, formation of the amide product (final mass 498 g/mol) can be detected in the positive and negative ion spectra with a mass of $[M+H]^+$ m/z 499 and $[M-H]^-$ m/z 497, respectively. This can also be found as the reaction is followed over eight and twenty-four hours ($[M+H]^+$ m/z 499 and $[M-H]^-$ m/z 497 in both cases). The amide bond that forms is extremely difficult to break and as a result it is presumed that this is the final product and no further cleavage takes place. Ester cleavage in this example is as a result of aminolysis and not catalysis. The terminal amino group is sacrificed for cleavage to occur and cannot be recovered.

Further study is required to confirm that aminolysis is the mechanism by which esters are cleaved by KYF. UV-Vis studies can be used to look at the process for longer to see whether the absorbance plateaus before the threshold value indicating that all of the amino groups have been sacrificed by aminolysis.

5.4 Conclusion

KYF self-assembles into nanofibers and consequently forms hydrogels at peptide concentrations above 10 mM. However, this self-assembly is not limited to the formation of gel materials. At concentrations below 10 mM self-assembly was also observed by CD, TEM and fluorescence. Although hydrogels are not formed, short fibrils have been observed and so it can be said that self-assembly occurs even at very low peptide concentrations.

Studies were carried out with peptide concentrations above and below the critical aggregation concentration. It was found that self-assembled formation of nanofibers does not enhance the enzymatic activity of the peptide and may have some inhibiting effect as the concentration of peptide increases. As the concentration of the peptide decreases there is an increase in activity however this is less reproducible than for the higher peptide concentrations, so 1 mM was the concentration chosen for future studies.

Mutation and scrambling of the original peptide sequence gave an insight into the mechanism of action for ester cleavage. Mutation of lysine and the N terminal amino group simultaneously result in complete loss of activity which demonstrates that both of these functionalities are required for the catalyst to work at maximum efficiency. However, the amino group plays a key role in cleavage whilst the lysine's role is secondary; lysine's highly basic nature causes the resulting pK_a of the terminal amino group to decrease and therefore it is more likely to be activated as a nucleophile than the lysine. The activity was also seen by lysine alone although the rate was reduced. The C terminal acid group plays no role in cleavage with the rate remaining unchanged on amidation. Scrambled sequences confirmed the interaction of the lysine and the amino group. As the lysine and consequently the basic environment

move away from the amino group the activity decrease as the pK_a increases and the functional group is less susceptible to deprotonation resulting in a lower rate of cleavage. These studies allowed a hypothetical mechanism to be developed in which the terminal amino nitrogen uses lone pairs of electrons to attack the substrate and consequently initiate ester cleavage. KYF is a hydrophobic peptide and fluorescence studies demonstrated that these amino acids do indeed interact with the substrate in a transient binding situation.

pH and temperature studies demonstrate the esterase cleavage activity of KYF in less conventional conditions. As pH increases the activity of the peptide also increases up to pH 8 which is not unsurprising since this increase in pH is optimal for the deprotonation of the terminal amino group known to be key for cleavage to occur. This trend has also been observed for background activity however introduction of the peptide enhances this considerably. pH and protonation state are very important if cleavage is going to be carried out efficiently. As temperature increased the esterase activity increased slightly up to 40 ^{o}C. The peptide substrate-interaction is perturbed at high temperatures hindering product formation and the background activity increases significantly. The proposed mechanism of action for ester hydrolysis is aminolysis. This study of KYF provides an insight into tripeptides as predecessors to more complex enzymes and provides an initial understanding of their mechanism of action which can be applied to the design if future *de novo* enzymes.

6.0 Search for Catalytic Phages for Phosphatase Activity by Biocatalytic Self-Assembly*

* Declaration of contribution to chapter: Any reproduced practical work I was solely responsible for, unless otherwise stated. Prof. Hiroshi Matsui, Dr. Yuka Kanetsuki and Dr. Ana Pina collaborated on phage display panning.

6.1 Introduction

In nature, enzymes rely on relatively simple organic functionality in the amino acid side chains of *e.g.* histidine, aspartic acid and serine to achieve substrate binding and subsequently catalysis of chemical reactions and biological pathways. While selective binding of substrates requires a complex 3D surface which provides complementary shape and chemical functionality, it seems reasonable that catalytic functions can be achieved using simpler structures. Therefore, there is an increasing level of interest in reducing protein complexity and mimicking their activity utilizing small peptide based catalysts. Few examples of peptide catalysts in aqueous environments have been reported, as summarized in Chapter 2.0. Those identified use catalytically active peptide fragments *e.g.* Ser-His incorporated into a dendrimer structures to achieve multivalency,[58] as well as taking advantage of hydrophobic interactions to achieve substrate binding and consequently catalysis.[120] Recently it has been demonstrated that these enzymatic traits are not necessary for catalysis to occur (chapters 2.0, 3.4 and 4.3). It was also demonstrated that random, unassembled dodecapeptides also have (limited) amidase and esterase activity based on amino acid functionality alone rather than being displayed in a multivalent fashion due to the formation of self-assembled nanostructures. It is possible to look for peptides with alternative enzymatic activities.

Studies have been undertaken in a bid to screen combinatorial libraries to reveal peptide-based catalysts with phosphatase activity.[121] Schmuck and co-workers introduced a screening method to identify octapeptides from an on bead split-mix-combinatorial library that have the ability to hydrolyze phosphorester bonds in an aqueous environment. A $_{D}$-Pro-Aib turn was incorporated into the sequence to induce a folded conformation in solution whilst the other positions were made up of different combinations of His, Ser, Glu, and Asp as catalytically active residues and Phe, Val to provide a less polar microenvironment to favor binding. A colorimetric assay was used to observe the successful hydrolysis of a phosphorester by the identified octapeptides in an aqueous and metal free environment giving rise to an initial rate of 5.3×10^{-5} s^{-1} by the most active peptide Cbz-His-Gly-Gua-$_{D}$-Pro-Aib-Gua-Gly-Val-NH_2 (where Gua is an artificial arginine analogue). Further studies are

required to expand the scope and determine a mechanistic understanding of catalysis which could help to rationally modify and improve the rate of the identified peptide.

In particular, phosphatase activity is of interest due to its wide range of applications including the degradation of organo-phosphorus neurotoxins in the case of bioremediation of agricultural and chemical warfare agents.[122, 123] in addition to the general role in adenosine triphosphate (ATP) hydrolysis which is a key process in energy supply of living systems.[124-126] As well this, phosphatase activity is interesting for use in biological applications. Biocatalytic self-assembly and disassembly of peptide precursors can take place in the presence of a number of different enzymes including phosphatases.[70, 127, 128] Gulseren *et al.* make use of peptide nanofibers to mimic alkaline phosphatase activity for differentiation of bone cells.[60] Bone formation requires the coordination of several molecular and biological systems[129] and alkaline phosphatase plays several roles in this process. The enzyme cleaves non-specific phosphate esters which elevates the local concentration of inorganic phosphate in turn promoting the formation of hydroxyapatite, an essential building block of bone tissue.[130] Alkaline phosphatase also demonstrates the ability to induce osteoblast differentiation and to play a role in the deposition of bone matrix.[131] Gulseren *et al*. designed a bioactive, multivalent and functional peptide nanofiber, lauryl-Val-Val-Ala-Gly-His-NH_2, which possesses both the catalytic and bio-mineralization-enhancing effect of alkaline phosphatase. The nanofiber was decorated with histidine residues in a multivalent fashion where they can cooperate and mimic catalytic activity of the natural enzyme. Catalytic activity of this phosphatase mimic was demonstrated by the fibers, 1.83×10^{-5} s $^{-1}$, using a colorimetric nitrophenyl phosphate substrate. This technology has led to a versatile peptide platform that can be used for the development of new materials for biomedical applications.

In this study, the scope of the previous combinatorial technique of phage display and biocatalytic self-assembly (see chapter 3.3) is broadened to investigate phage libraries for phosphatase activity. Herein the characterization of two phosphorylated gelators is described, one of which is novel whilst the other is well reported in

literature,[14] using fluorescence, rheology, transmission electron microscopy (TEM), infra-red spectroscopy (IR) and high performance liquid chromatography (HPLC). Furthermore studies into the feasibility of using these catalytically formed gelators to extract phage with dodecapeptide sequences of interest from the library, as carried out previously for amidase/esterase activity (chapter 3.3) was undertaken. The catalytic activity of the phage extracted from the bulk library was assessed using HPLC and UV-Vis spectroscopy. Overall this study demonstrates that sequences can be extracted from the bulk library with duplicate sequences obtained. An effective UV-Vis phosphatase assay was developed however the results did not yield reproducible phosphatase activity over the background hydrolysis that takes place as a result of the phage presence. HPLC demonstrated a low percentage of conversion to the product. The panning process will require optimization for the new gelators to identify phage with significant activity.

6.2 Objectives

As a result of successful identification of amidase and esterase phages (Chapter 3), the aim of this chapter was to:

- Design and characterize phosphatase-responsive gelators to be used in the phage display panning experiments.
- Carry out phage display panning for the identification of phage with phosphatase activity.
- Characterize the phage identified by the panning process for phosphatase activity by HPLC and UV-Vis spectroscopy.
- Optimize the phage display panning process for phosphatase activity.

6.3 Results and Discussion

6.3.1 Characterization of the Peptidic Precursors for Panning

The first example of a phosphatase triggered supramolecular transformation was presented by Yang *et al.* whereby on the addition of alkaline phosphatase to Fmoc-Tyr$(PO_4)^{3-}$, the ionic phosphate group on the amino acid derivative was converted to a neutral OH group leading to the formation of supramolecular hydrogels.[132] A further study on a related system by Sadownik *et al*. reported the phosphatase-driven supramolecular transformation whereby Fmoc-Phe-Tyr$(PO_4)^{3-}$-OH undergoes dephosphorylation and changes from a solution of micelles to a fibrous gel phase (Figure 6.1).[14] This peptide building block was chosen for the biocatalytic screening of a phage library alongside an unreported peptide building block, Fmoc-Tyr$(PO_4)^{3-}$-Ala-OH. The addition of a second self-assembling building block was due to the fact that Fmoc-Phe-Tyr$(PO_4)^{3-}$-OH precursor has been reported to assemble in absence of a phosphatase enzyme.[133]

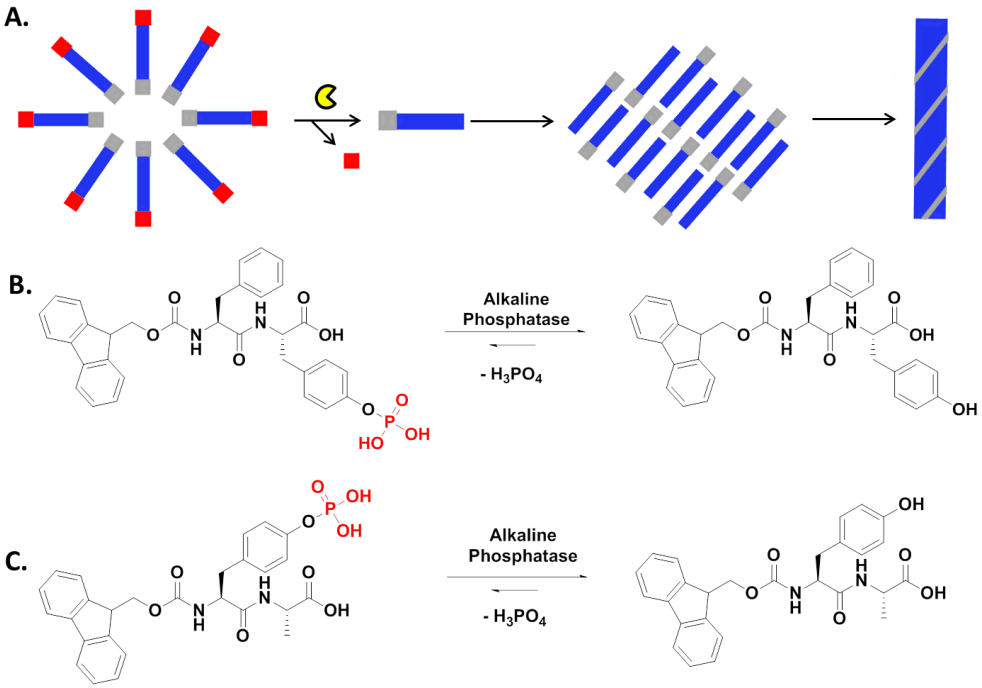

Figure 6.1. Biocatalytic self-assembly of aromatic peptide amphiphiles. A. Schematic representation of self-assembly process catalyzed by the presence of an enzyme *e.g.* phosphatase. The addition of the enzyme results in a hydrolysis reaction transforming a non-gelator into a gelator. **B.** Self-assembly of Fmoc-Phe-Tyr$(PO_4)^{3-}$-OH to form self-supporting gel. **C.** Self-assembly of Fmoc-Tyr$(PO_4)^{3-}$-Ala-OH to form self-supporting gel.

Furthermore, variations of Fmoc-Tyr(PO_4)$^{3-}$-Ala were synthesized including the methyl ester and amide versions. Mass spectroscopy and HPLC were used to identify the correct mass and the purity of the peptides. NMR was attempted for further confirmation that the correct peptides had been made however there were solubility issues when preparing the sample of analysis. It is thought that this is down to spontaneous micelle forming characteristics of the peptides at the high concentrations required to obtain an NMR spectrum. A sepctrum could not be obtained. These modifications were utilized to change the properties of the peptide and ultimately to reduce solubility and therefore the likelihood of diffusion away from the tip of the phage during the catalytic assembly process which is exploited during panning. Both of these peptide building blocks formed gels however neither were suitable for the panning process. Fmoc-Tyr(PO_4)$^{3-}$-Ala-OMe did not fully dissolve in buffer therefore there was particulate material in the final gel. This would interfere with the centrifugation process in the panning methodology as the particulate would also sediment out from the bulk material and interfere with the extraction of the phage from the bulk solution. Fmoc-Tyr(PO_4)$^{3-}$-Ala-NH_2 was also unsuitable as the gel also contained a small quantity of particulate material.

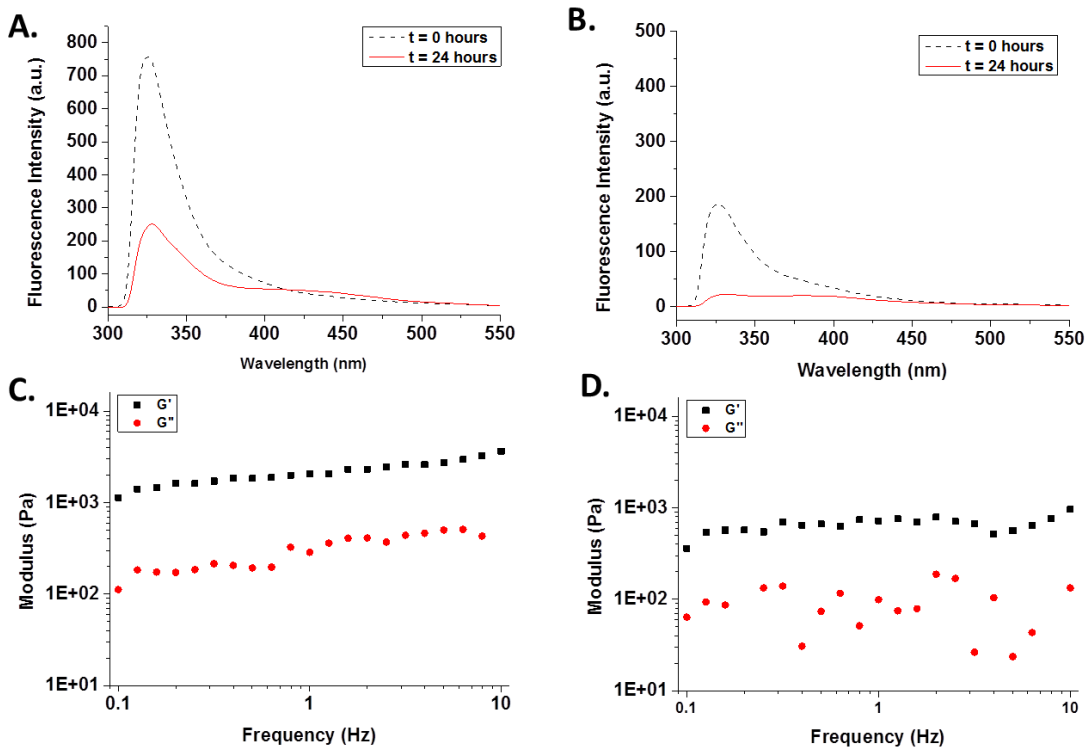

Figure 6.2. Fmoc-Tyr-Ala-OMe/NH_2 characterization. A. Fluorescence spectra of Fmoc-Tyr-Ala-OMe at t = 0 and 24 hours. **B.** Fluorescence spectrum of Fmoc-Phe-Tyr-NH_2 at t = 0 and 24 hours. **C.** Rheology of Fmoc-Tyr-Ala-OMe after 24 hours. **D.** Rheology of Fmoc-Phe-Tyr-NH_2 after 24 hours.

These variations were partially characterized before being dismissed for use in the panning process. Fluorescence spectroscopy for both samples demonstrates quenching of the Fmoc peak at 320 nm which is indicative of self-assembly of the aromatic groups. As the Fmoc groups stack in a π-π arrangement, their signal diminishes due to quenching of fluorescence by the other aromatic groups in the arrangement. Another observation is that there is no shoulder peak at 370 nm which is unusual for these particular Fmoc dipeptides. Other known examples reported previously,[14, 134] form micelles in solution, indicated by a shoulder peak, and over time this diminishes due to the formation of an extended fiber arrangement. This is not observed here which could be due to the poor solubility of these materials. The strength of the resulting gels was recorded with G' (storage modulus) being greater than G'' (elastic modulus) for both materials. Fmoc-Tyr-Ala-OMe has strength 2.2 kPa and Fmoc-Tyr-Ala-NH_2 strength 0.6 kPa. Although these gels are weak, this does not discount them for the panning process since localized aggregation is required and not bulk gelation. The mitigating factor in the process of selecting

gelators for the phage display panning experiment is their insolubility in phosphate buffer.

The selected precursors were fully characterized at a 20 mM concentration before use. The dephosphorylation reaction (Figure 6.1) was followed by HPLC for both and showed 99.6% and 92.2% conversion to the reaction product for Fmoc-Tyr-Ala-OH and Fmoc-Phe-Tyr-OH, respectively (Figure 6.3). Initial velocity (V_0) of reaction for the conversion to Fmoc-Tyr-Ala-OH and Fmoc-Phe-Tyr-OH was 0.006 mM s^{-1} and 0.004 mM s^{-1}, respectively. TEM was used to observe that dephosphorylation and gel formation results in nanoscale fibers.[135, 136]

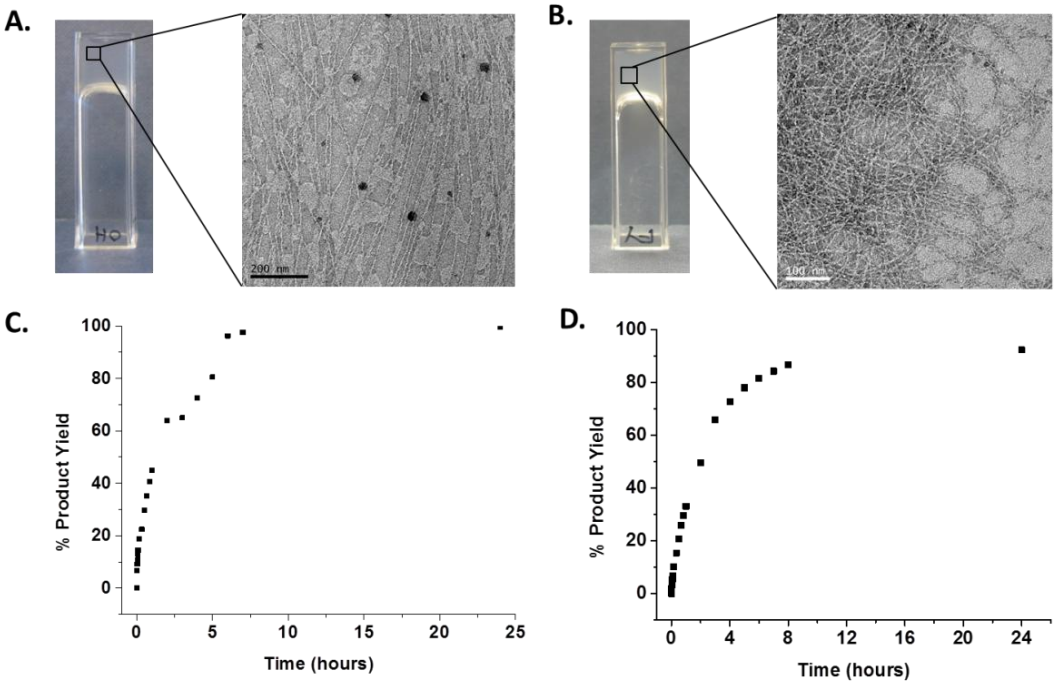

Figure 6.3. A. Image of Fmoc-Tyr-Ala-OH and TEM of Fmoc-Tyr-Ala-OH showing fibers. B. Image of Fmoc-Phe-Tyr-OH and TEM of Fmoc-Phe-Tyr-OH showing fibers. **C.** % conversion to reaction product Fmoc-Tyr-Ala-OH over 24 hours. **D.** % conversion to reaction product Fmoc-Phe-Tyr-OH over 24 hours.

The hydrogels were further characterized by fluorescence due to the expectation of spectroscopic changes over time as a result of changes in the fluorenyl environment.[14] The samples were excited at 295 nm and spectra obtained after 0 and 24 hours (Figure 6.4). Firstly, the shoulder peak at 370 nm which is associated with the parallel stacked Fmoc group in a micellar organisation[14, 134] disappears over time,

which is indicative of micelles transforming into fibers and extended π-π interactions forming. The peak at 320 nm is present as a result of the fluorescence from the fluorenyl groups of the Fmoc group. Over time the intensity of the peak decreases as the fluorescence of the aromatic group is quenched as the peptides become involved in extended π stacked arrangements. At 0 hours, the peptide is in a micellar organization which minimizes aromatic interactions allowing a stronger fluorescent signal. Over time as π-π interactions become more important, the intensity of this peak decreases as a result of molecular association of the Fmoc groups which results in self-quenching. This indicates the π stacking of 1D aggregates which result in the formation of a gelating network.

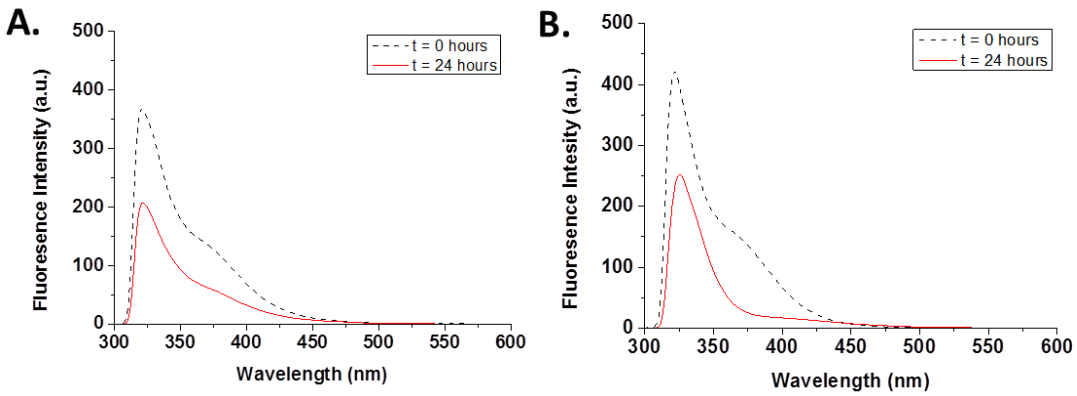

Figure 6.4. A. Fluorescence spectra of Fmoc-Tyr-Ala-OH at t = 0 and 24 hours. **B.** Fluorescence spectra of Fmoc-Phe-Tyr-OH at t = 0 and 24 hours.

Rheology was used to characterize the resulting gels for both peptide building blocks after 24 hours (Figure 6.5).[128, 137] It can be seen that for both peptide building blocks, the G' value is greater than the G'' value therefore the material can be classed as a gel. Fmoc-Tyr-Ala-OH had strength of 6.3 kPa and Fmoc-Phe-Tyr-OH had strength of 13.7 kPa. The latter is in line with previously reported values for Fmoc-dipeptides whilst Fmoc-Tyr-Ala-OH is a weak gel.[138] It has been reported that on varying the enzyme concentration for the formation of Fmoc-Phe-Tyr-OH, the strength of the resulting gels is in the region of 14 – 16 kPa. In comparison to other peptide gels, Fmoc-Phe-Phe and Fmoc-Phe-Phe-Lys which have strengths of 21.2 and 12.3 kPa, respectively,[139] the strength recorded for Fmoc-Phe-Tyr is in the range of expected values.

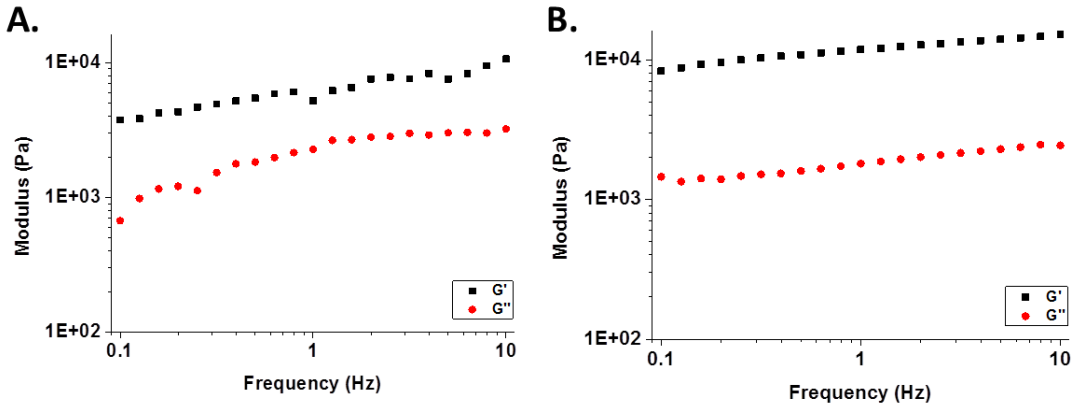

Figure 6.5. A. Rheology of Fmoc-Tyr-Ala-OH after 24 hours. **B.** Rheology of Fmoc-Phe-Tyr-OH after 24 hours.

Finally, FTIR was used to indicate hydrogen bonding within the final gels (Figure 6.6). Both peptide spectra show two peaks in the amide I region, one at 1630 cm^{-1} and the other at 1680 cm^{-1}. The first is attributed to the formation of β sheets whilst the latter is arises from the carbamate moiety of the Fmoc group hydrogen bonding into the β sheet configuration.[140, 141]

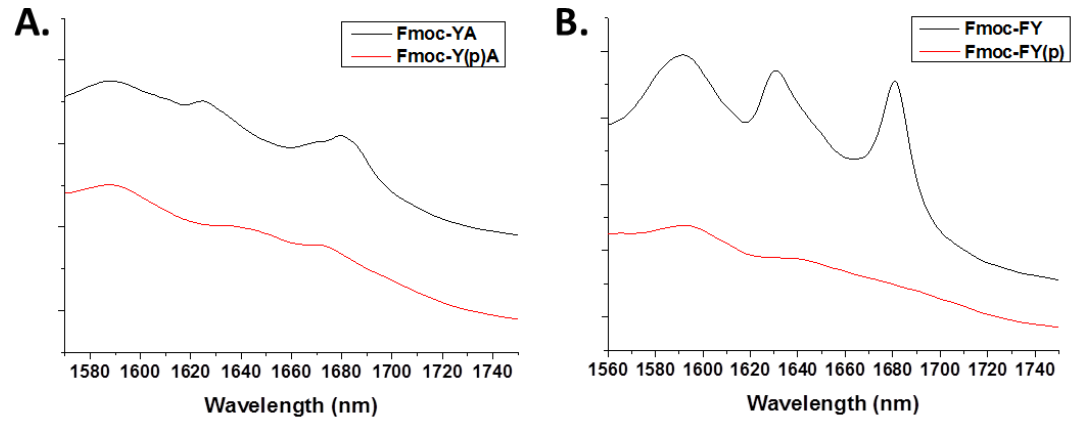

Figure 6.6. A. FTIR of Fmoc-Tyr-Ala-OH after 24 hours. **B.** FTIR of Fmoc-Phe-Tyr-OH after 24 hours.

In conclusion, both peptide building blocks form gels on dephosphorylation of the starting materials. Both self-assembling dipeptides were selected for combination with a phage display library to screen for phage viruses which have the ability to catalyze the dephosphorylation of peptidic precursors.

6.3.2 Phage Display Panning Combined with Catalytic Gelation of Peptides*

* in collaboration with Prof. Hiroshi Matsui, and Dr. Yuka Kanetsuki.

As discussed in chapter 3.3,[8] the library of phage viruses was incubated with the soluble, peptidic gel precursors Fmoc-Tyr(PO_4)$^{3-}$-Ala-OH and Fmoc-Phe-Tyr(PO_4)$^{3--}$ OH. Upon catalysis of the dephosphorylation reaction by selected peptides at the tip of the phage, it would be expected that an aggregate of the dipeptide Fmoc-Tyr-Ala-OH or Fmoc-Phe-Tyr-OH formed. Due to the self-assembling propensity and poor solubility in aqueous media, the resulting catalyst/product aggregate should remain localized at the site of catalysis *i.e.* at the tip of the phage. This localized aggregation facilitates isolation of the phage virus of interest from the extensive library being screened. Centrifugation is employed to ensure separation and isolation of these specific phage viruses, a technique that has previously been used successfully.[16] As before, the aggregate is removed from the tip of the phage by incubation with 50:50 acetonitrile/water resulting in dissolution of the aggregate material.[8] Amplification of the phage viruses was carried out in *Escherichia coli.*,[142,143] the viruses were titrated and colonies selected for sequencing (Table 6.1).

Table 6.1. Peptide sequences selected by the catalytic self-assembly screening process. YA sequences were selected using phosphorylated Fmoc-Tyr$(PO_4)^{3-}$-Ala-OH and the FY sequences were selected using Fmoc-Phe-Tyr$(PO_4)^{3-}$-OH. Sequences from both the first and second rounds of panning are recorded. Histidine is highlighted in red, cysteine in blue and duplicate sequences in bold italics.

YA 2nd round		FY 1st round		FY 2nd round	
Name	**Sequence**	**Name**	**Sequence**	**Name**	**Sequence**
YA 1	NSGKTHTDMASN		INSNVRATTTYI	**FY 4**	GGQNPADDYRQP
YA 3	VQVVAVEWTRHA	**FY 2 1st**	***TTRLHHSSPFTT***	**FY 6**	AYQYPAHNSSVL
YA 5	LPNSQTMRADDP		VRVMDPGIRHND	**FY 7**	GFAVGARDSLMF
YA 8	GGGGGIDYISLS		STYLPQMSVWQP	**FY 8**	***VVSPDMNLLLTN***
YA 11	NASPGARSLFYM		DVGYPKWHYYSR	**FY 12**	MMTDMFMERKFG
YA 12	THPPIGPMHDSL		SRDYSLANLVGE	**FY 16**	ADPGRVVIIIC
YA 13	WSGPDLRRGTNP		MSRTHPDSRPIS	**FY 17**	***AYPQKFNNNFMS***
YA 16	DQFVHDVKGTKH		GPTLWPIAVERH	**FY 18**	DLSALVDMDSHD
YA 17	SGDVLKVRQTIH		TYARSDGDTHKR	**FY 19**	HSANAPGSHYSV
YA 18	TTYNAEHQR*KV		TSNVIHNLLDFS	**FY 20**	***AYPQKFNNNFMS***
YA 19	***AYPQKFNNNFMS***		ASYTNLDDTWKS	**FY 22**	VSPPTACHYSNM
YA 21	GGPPPLDLKKKW	**FY 18 1st**	***TTRLHHSSPFTT***	**FY 23**	***VVSPDMNLLLTN***

As the rounds of panning progress, the library of phage becomes enriched with the sequences which possess the desired activity.[144] It can be seen that in both round one and two of the YA panning there is no sequence duplication indicating that the sequences with phosphatase activity are not being extracted from the bulk library *via* the panning process and therefore the library of phage for the next round of panning

is not enriched with sequences of interest. As for the FY panning, in the first round duplicate sequences already occur. Although this sequence does not appear in the second round of panning two more duplicate sequences are observed indicating that the library is indeed being enriched and sequences with phosphatase activity and being extracted from the bulk sample. All of the sequences reported here are very different. There is no sequence homology amongst the library of sequences taken on for further study. Therefore, sequence cannot be linked to function which correlated with what was found in the amidase and esterase panning (chapter 3.4).

Initially the duplicate sequences from the first and second round of FY panning were taken forward to investigate phosphatase activity as they were the most likely to possess the desired function. These will be referred to as the FY phage.

6.3.3 Phosphatase Activity – Dephosphorylation Reaction by HPLC

Before studying the catalytic activity of the selected phages from the screening process, they were amplified and transferred into buffer from LB media.

Proof of concept experiments were carried out as the initial study to investigate the ability of the FY phage to catalyze the dephosphorylation reaction used in the panning process (Figure 6.7). Phage were mixed with the gel precursors in individual vials and HPLC was used to follow the dephosphorylation reaction and quantify the percentage conversion of starting material to product due to the phosphorylated precursor and the reaction product having different retention times[145] (Figure 6.7).

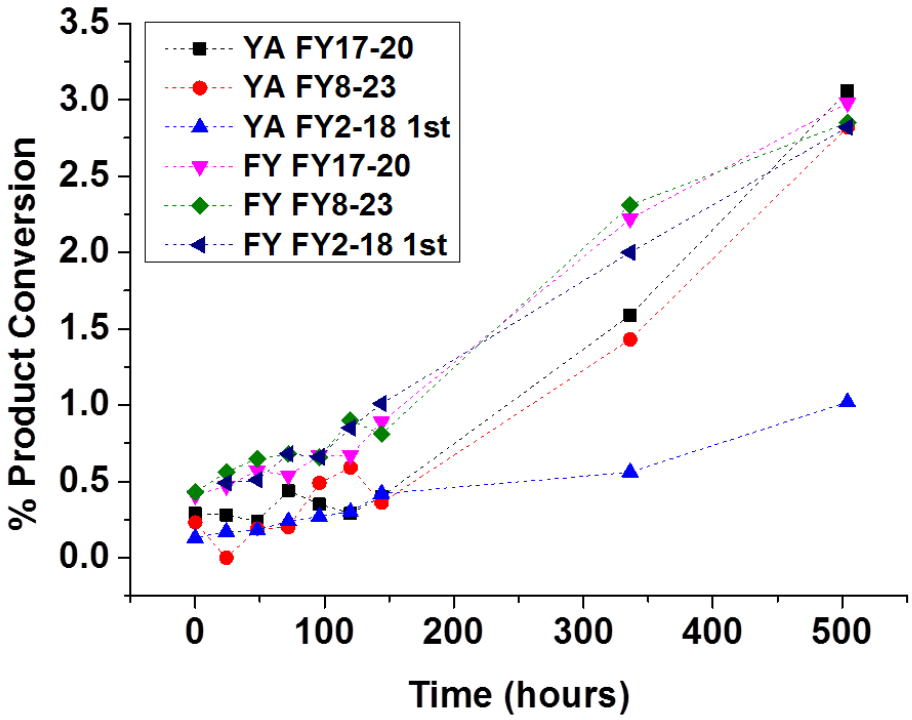

Figure 6.7. Dephosphorylation by HPLC. The graph shows % conversion to the reaction product Fmoc-Tyr-Ala-OH and Fmoc-Phe-Tyr-OH over time.

After 336 hours, dephosphorylation is observed for FY17-20 in both Fmoc-Tyr$(PO_4)^{3-}$-Ala-OH and Fmoc-Phe-Tyr$(PO_4)^{3-}$-OH up to 1.59 and 2.2%, respectively. For FY8-23, dephosphorylation is also observed for both Fmoc-Tyr$(PO_4)^{3-}$-Ala-OH and Fmoc-Phe-Tyr$(PO_4)^{3-}$-OH up to 1.43 and 2.31%, respectively. Finally, for FY2-18 1st, very little conversion is observed for Fmoc-Tyr$(PO_4)^{3-}$-Ala-OH, up to 0.56% in comparison to 2% for Fmoc-Phe-Tyr$(PO_4)^{3-}$-OH. It is clear here that the dephosphorylation process is taking place however the rate at which the starting materials are converted into the product is extremely slow. This does not indicate that the sequences selected have the phosphatase activity that was desired at the beginning of this study with final results obtained indicating up to a maximum of 3% conversion after 3 weeks incubation. Random sequences showed equivalent conversion up to 96 hours.

6.3.4 Phosphatase Activity – Dephosphorylation Reaction by UV-Vis Spectroscopy

Dephosphorylation assays that make use of UV-Vis spectroscopy[146, 147] are available to assess phosphatase activity. *p*-nitrophenyl phosphate (*p*NPP) was used to investigate dephosphorylation by all of the phage viruses sequenced from the second round of panning for both Fmoc-Tyr$(PO_4)^{3-}$-Ala-OH and Fmoc-Phe-Tyr$(PO_4)^{3-}$-OH (Figure 6.8). This includes the duplicate sequence which means that some of the sequences are run twice. Similar to the *p*NPA assay used in chapter 3.4, 4.3 and 5.3, this assay works on the basis that the hydrolysis product is yellow and can be measured by UV-Vis spectroscopy.

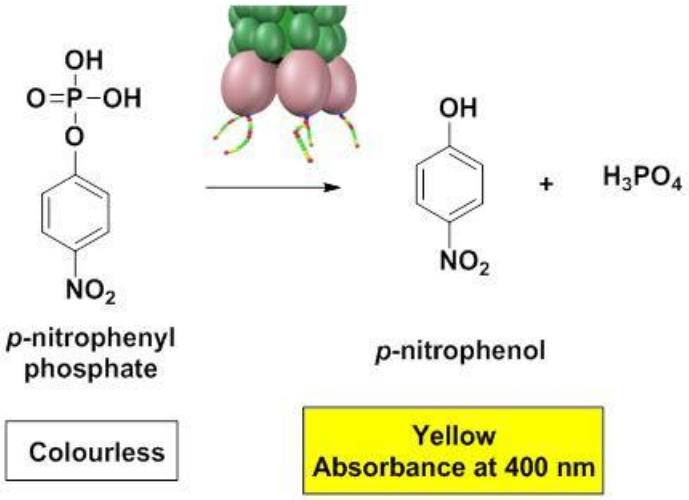

Figure 6.8. UV-Vis *p*NPP ester hydrolysis assay. Schematic of *p*NPP dephosphorylation reaction.

Typical time courses were observed for hydrolysis of the ester bond in *p*NPP in the presence of the catalytic phages (Figure 6.9A). The absorbance for these samples increases over time which can be observed in these plots.

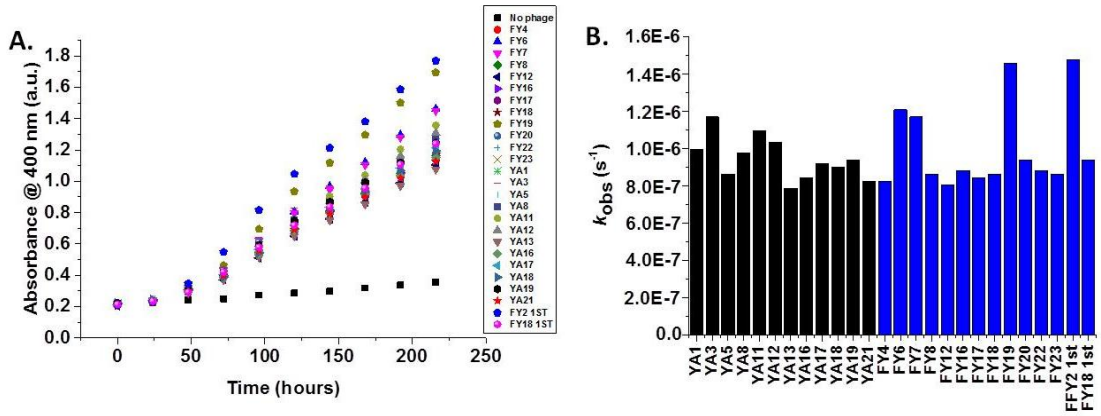

Figure 6.9. UV-Vis *p*NPP dephosphorylation assay. A. Time courses observed for the hydrolysis of *p*-nitrophenyl phosphate (*p*NPP) using varying μM phage and 10 mM *p*NPP. **B.** Rate data for the hydrolysis of *p*-nitrophenyl phosphate (*p*NPP). The rate data is based on a 10 minute time course. Samples are corrected for background hydrolysis to give a true rate based on the catalyst alone.

The absorbance recorded at 400 nm can be correlated to the rate of dephosphorylation. The rate constant (k_{obs} in s^{-1}) for each phage (Figure 6.9B) was determined from a UV-Vis calibration graph of *p*-nitrophenol and Equation 1. The rates observed are based on the concentration of the catalytic peptides (five peptides per phage). From the time courses it can be seen that the background dephosphorylation is an extremely slow process. They also demonstrate that there is little difference in rate between each phage sequence, although there are two that stand out. These are one of the duplicate sequences, FY18 1st and FY19. This is unusual since the duplicate of FY 18 1st, which is FY 2 1st, does not show this same enhancement of activity over the remaining sequences. It can also be seen that the observed rate for this reaction is low (10^{-7} s^{-1}) and takes place over an extended length of time up to 10 days. This again indicates that the selected phage do not possess the desired activity to a significant extent that was panned for in the initial experiment.

Sequences were selected based on preliminary results to be taken forward and further investigated to ensure that the results obtained previously, indicating low levels of

activity, were indeed correct. The sequences chosen were those which showed the most promise including FY18 1st and FY19 (Figure 6.10).

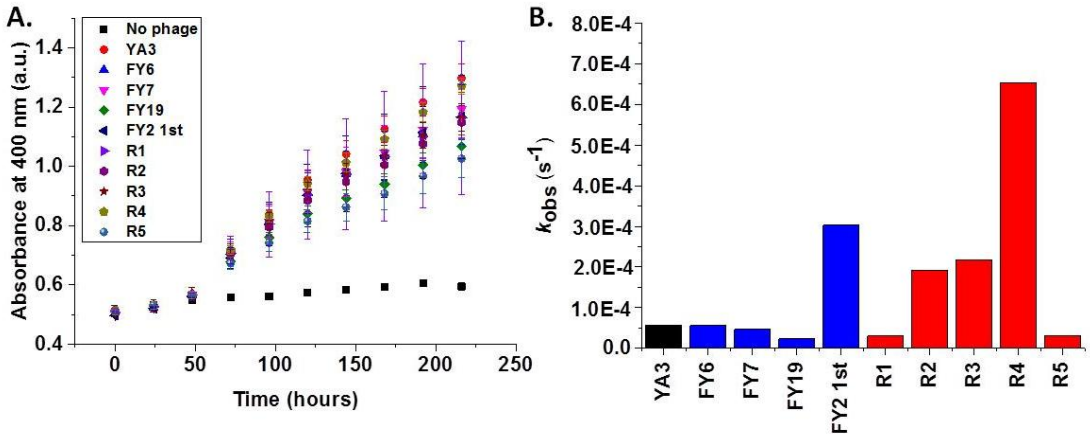

Figure 6.10. UV-Vis *p*NPP dephosphorylation assay. A. Time courses observed for the hydrolysis of *p*-nitrophenyl phosphate (*p*NPP) using varying μM phage and 10 mM *p*NPP. **B.** Rate data for the hydrolysis of *p*-nitrophenyl phosphate (*p*NPP). The rate data is based on a 10 minute time course. Error bars are based on three repeats**.** Samples are corrected for background hydrolysis to give a true rate based on the catalyst alone.

Again these demonstrate that the rate at which dephosphorylation of *p*NPP occurs is slow over an extended period of time. Although it seems that there is an increase in rate from 10^{-7} s^{-1} to 10^{-4} s^{-1}, this may simply reflect the variation on phage concentration which is taken account of in the rate calculation. Since the activity of these sequences is so low, the difference in concentration between phage samples can have a considerable effect on the reported rate of dephosphorylation. In this case, control sequences were run side by side with the catalytic sequences. These randomly selected phages also demonstrated some phosphatase activity confirming that the phage identified by the screening approach did not possess phosphatase activity but showed an equivalent background rate. Random phages show activity in the same range as for the catalytic phage. It has been previously hypothesized that the coat protein of the phage plays a role in catalysis due to the numerous catalytic histidine residues displayed on its surface.

Overall, this assay has demonstrated limited activity by the conversion to product followed by HPLC and also by the UV-Vis results. It is likely that the panning

process did not successfully identify sequences which possess phosphatase activity and this will have to be optimized for further experiments and investigation to take place.

6.3.5 Phage Display Panning Combined with Catalytic Gelation of Peptides - Optimization*

* in collaboration with Dr. Ana Pina from UCIBIO, Requimte, Departamento de Química, Faculdade de Ciências e Tecnologia-UNL, Portugal.

The initial panning experiment to select sequences which possess phosphatase activity was unsuccessful. Therefore, the panning process must be optimized to be able to achieve our goal and identify sequences which can indeed carryout dephosphorylation.

The first stage was to investigate whether the optimal gelator had been selected for the panning experiment and whether the conditions were appropriate for the gel to form but not affect the interaction between the peptide and the phage. Initial panning was carried out in 0.6 M phosphate buffer which was necessary in relation to the enzymatic gelation process on the basis of literature research and not related to the phage. However, this is an unusually high salt concentration for a buffer. The high salt concentration should not affect the phage, since they undergo precipitation in 2.5 M NaCl. However it is possible that it could interfere with interactions taking place in the panning environment. Fmoc-Phe-Tyr$(PO_4)^{3-}$-OH in 0.1 M phosphate buffer was selected for the optimized panning process and the gel was fully characterized.

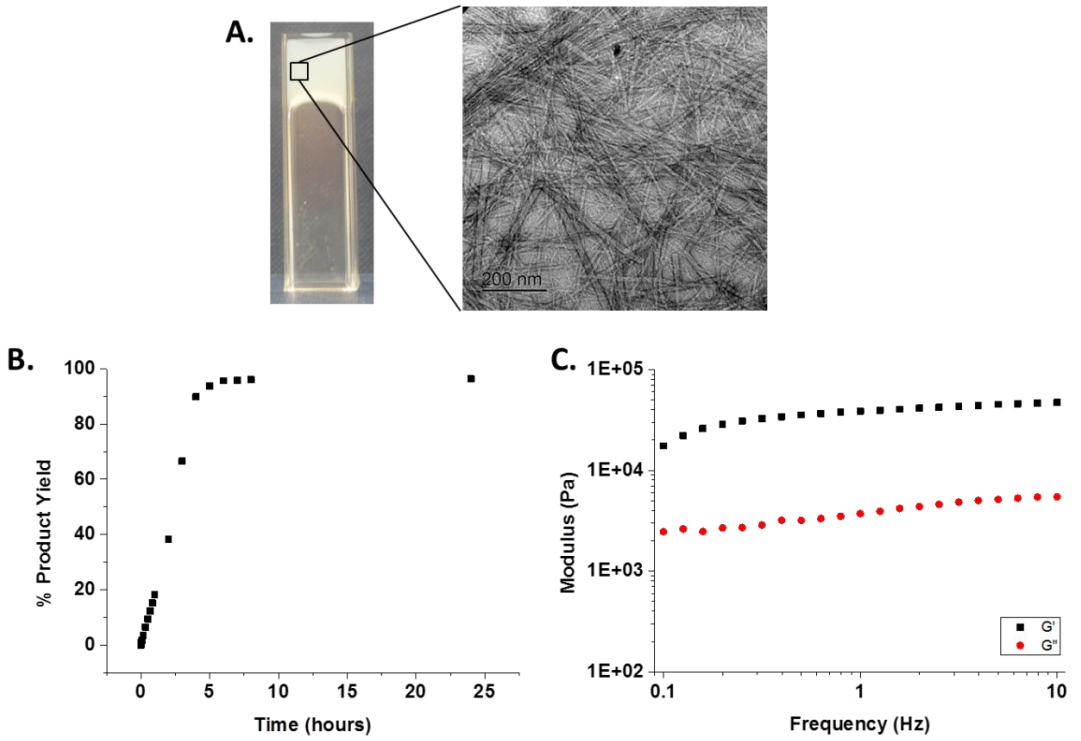

Figure 6.11. Full characterization of Fmoc-Phe-Tyr-OH in 0.1 M Phosphate Buffer. A. Image of Fmoc-Phe-Tyr-OH hydrogel and TEM of Fmoc-Phe-Tyr-OH gel sample showing fibers. **B.** % conversion to reaction product Fmoc-Phe-Tyr-OH over 24 hours. **C.** Rheology of Fmoc-Phe-Tyr-OH after 24 hours.

TEM analysis indicates that the gel product is made up fibers on the nanoscale (Figure 6.11A) and by using HPLC to follow the reaction and conversion of Fmoc-Phe-Tyr$(PO_4)^{3-}$-OH to the dephosphorylated product it can be shown that the reaction reaches 96.4% conversion after 24 hours (Figure 6.11B) with an initial reaction velocity of 0.001 mM s^{-1}. This is 4 times slower than for Fmoc-Phe-Tyr-OH in 0.6 M phosphate buffer (0.004 mM s^{-1}) suggesting that the high salt concentration enhances the initial reaction velocity although maximum conversion is obtained within 24 hours for both samples.

Rheology was also used to characterize the final product after 24 hours. This had a G' of 39.4 kPa which is almost three times more elastic than for the Fmoc-Phe-Tyr-OH gel in 0.6 M phosphate buffer (Figure 6.11C). In comparison with the previously mentioned literature values for Fmoc-Phe-Tyr-OH (in 0.6 M phosphate buffer) this value is higher than expected however, when considering other Fmoc-dipeptide gels,

this sample is within the observed range.[11] Fmoc-Thr-Phe and Fmoc-Thr-Leu have G' of 100 kPa and 90 kPa, respectively therefore, Fmoc-Phe-Tyr-OH gel in 0.1 M phosphate buffer is in the middle of the literature range. These reported gels were made in 0.1M phosphate buffer indicating that salt concentration can play a role in the resulting gel properties.

Fluorescence spectroscopy shows a prominent peak at 320 nm, which is due to the Fmoc group. At time zero these groups are in a parallel, micellar organization and so fluorescence emission is at its maximum however as time passes at the gel forms this peak is quenched as a result of the molecular association of these aromatic groups. This indicates the π-stacking of aggregates and formation of extended fibers. Another change that occurs to the spectra over time is the disappearance of the shoulder peak at 370 nm. Initially the formation of micelles in solution causes this shoulder peak however as these transform into nanoscale fibers the peak disappears indicating that extended π-π interactions are forming (Figure 6.12A). It can be seen that in the original 0.6 M sample quenching, occurs however this effect is more prominent in the 0.1 M sample confirming that aromatic stacking is more efficient in the 0.1 M sample, probably due to the hydrophobic effect (Figure 6.12B).

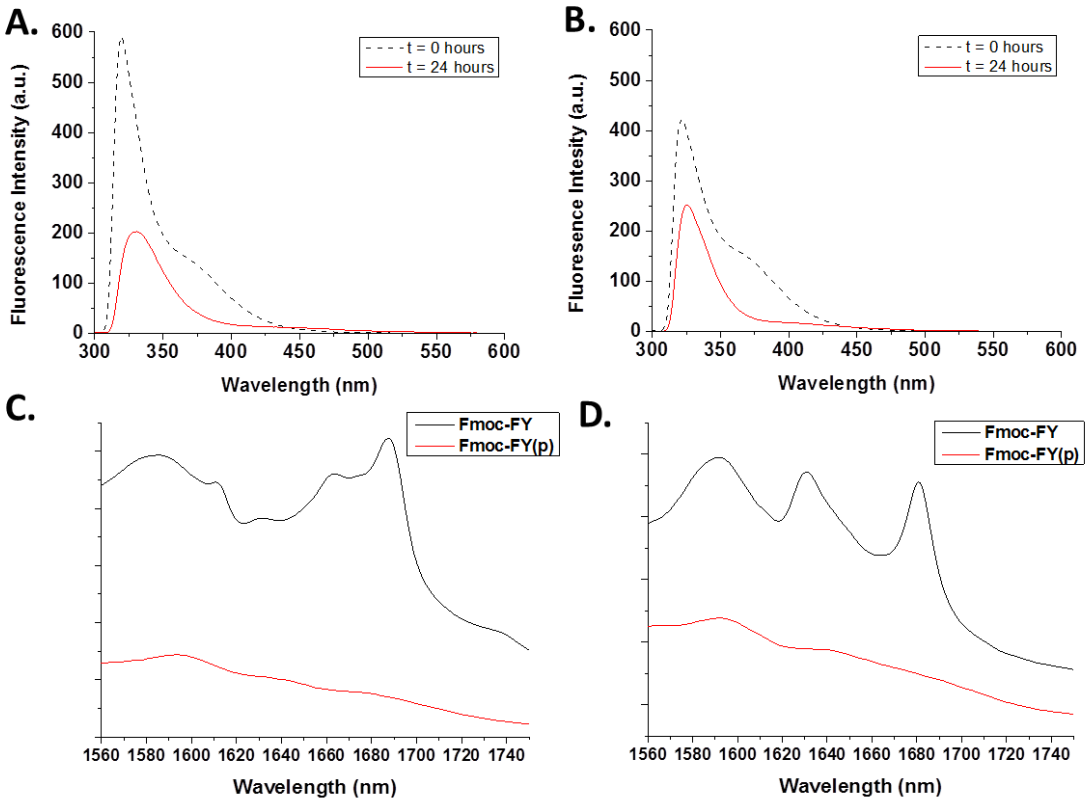

Figure 6.12. Comparison between Fmoc-Phe-Tyr-OH in 0.1 and 0.6 M phosphate buffer. A. Fluorescence spectra of Fmoc-Phe-Tyr-OH in 0.1 M phosphate buffer at t = 0 and 24 hours. **B.** Fluorescence spectra of Fmoc-Phe-Tyr-OH in 0.6 M phosphate buffer at t = 0 and 24 hours. **C.** FTIR of Fmoc-Phe-Tyr-OH in 0.1 M phosphate buffer after 24 hours. **D.** FTIR of Fmoc-Phe-Tyr-OH in 0.6 M phosphate buffer after 24 hours.

Finally FTIR was used to indicate hydrogen bonding between peptide backbones (Figure 6.12C). In this case three peaks appear in the amide I region. The first peak at 1630 cm^{-1} is attributed to the formation of β sheets whilst the second peak at 1680 cm^{-1} arises from the carbamate moiety of the Fmoc group hydrogen bonding into the β sheet configuration.[140, 141] In this case, the third peak at 1665 cm^{-1} can be attributed to free amide functionality that is not involved in hydrogen bonding. Peptide gelators in 0.1 M phosphate buffer in comparison to 0.6 M (Figure 6.12D) will have different electrostatic interactions. In the lower concentration buffer, electrostatic interactions are increased in comparison to the higher concentration where electrostatics are reduced therefore the peaks in the amide I region are less prominent in the 0.1 M sample due to increased repulsion. In this case the formation of the gel is more likely

to be a hydrophobic effect[148] and additionally π-stacking of the aromatic groups complemented with hydrogen bonding.

Phosphate is a 'water structure maker' meaning that it has the capability to form hydrogen bonds with water. It is also known to induce hydrophobic collapse. At increased phosphate concentrations, the hydrophobic collapse is induced more quickly, which can be seen by the HPLC results. This in turn leads to the formation of a less organized and therefore weaker structure which can been seen by the rheology results whereby the gel in 0.6 M phosphate buffer is considerably weaker than in the 0.1 M phosphate buffer. At the lower salt concentration, the hydrophobic collapse occurs in a slower, more controlled manner and allows the peptide to organize itself into a very stable structure as seen by the increased strength of the gel in 0.1 M phosphate buffer. It is possible that a critical salt concentration has been breached in the 0.6 M buffer and is not optimal for gel formation. Therefore, the 0.1 M phosphate buffer was used for the optimized phage panning process.

Further improvements were also made to the panning process. In the original procedure the sample was left to incubate for 3-4 days. This extended time for the sample to be left allowed more time for the aggregate to diffuse from the tip of the catalytic phage and attach to another phage in the vicinity meaning that it was possible to misidentify sequences as catalytic due to non-specific interaction. It also allowed for the breakdown of aggregate materials. On addition of enzyme to the phosphorylated Fmoc-peptide, gels form within 6 hours with near complete conversion observed by HPLC. Although the phage would not be expected to have the same catalytic efficiency as an enzyme would, it is unlikely that localized aggregation would take 3-4 days to occur at the tip of the phage and this extended incubation time deviates from traditional panning methods. It also allows the aggregate enough time to form and diffuse from the catalyst. Therefore, this incubation time was reduced to 1-2 days which still gives the aggregate time to form but less time to diffuse back into solution and bind non-specifically. A shorter incubation time is in line with traditional panning processes although this is still significantly longer than for most experiments.

In the original procedure, the phage peptide mixture was centrifuged to extract the phage carrying the assembled aggregates from the bulk mixture. This results in a pellet in the microfuge tube which was washed with phosphate buffer in the first panning experiment. Washing the pellet allows for the removal of any non-specific binding e.g. Fmoc binding to phage and it is unlikely that phosphate buffer alone would remove this. In the optimization process washing the pellet multiple times with Tris buffer saline + 0.1% Tween 20 was introduced. Tween 20 is a surfactant which helps to prevent non-specific binding.[149] By introducing this step, it also increases the ability of the washing to remove any unwanted, bound Fmoc groups and any non-selective binding in comparison to phosphate buffer alone. The pellet, after washing with Tris buffer saline + 0.1% Tween 20, was then re-suspended in phosphate buffer so the rest of the panning can continue as per the previous method.

Another change that was made to the panning process was that instead of incubation with 50:50 acetonitrile/water to remove the gel product, the phage pellet was incubated with 10 mg/mL chymotrypsin. Initially the acetonitrile mixture was used to perturb the gel and result in dissolution from the tip of the phage. Chymotrypsin cleaves peptide bonds C terminal to phenylalanine[30] therefore can insure that the gel is dispersed from the tip of the phage before the next step takes place.

Finally, input titrations were carried out as well as the output titrations which were undertaken in the previous procedure. This ensures that there are phages from the first round of panning to be used as an input library for the next stage of the process. It also allows the number of phages involved in the panning process to be followed. After the first round of panning it would be expected to see a decrease in the number of phage in the mixture due to the panning procedure isolating only sequences that have the desired function. These would then be amplified and input into the next round of panning. After the initial decrease in phage concentration an increase in phage in the input and output titrations would be expected. This is due to the catalytic sequences being amplified and therefore more prominent in the solution. As the number of catalytic sequences increases, the number of phages identified from the mixture by the formation of a localized aggregate increases and duplicate

sequences appear when sequenced. An increase in concentration of these phages is expected through subsequent rounds of panning and titration. These modifications were made to the panning process as well as an additional round of panning. Amplification of the phage viruses was carried out in *Escherichia coli*, the viruses were titrated and colonies selected for sequencing before further study on their phosphatase activity was carried out.

The library of phage viruses was incubated with the soluble, peptidic gel precursors Fmoc-Phe-Tyr$(PO_4)^{3-}$-OH. The panning procedure was carried out as before with the new modifications to the procedure as described above (in particular, lower incubation time and reduced buffer concentration). Each clone was then assessed for catalytic activity.

Table 6.2. Peptide sequences selected by the catalytic self-assembly screening process using Fmoc-Phe-Tyr$(PO_4)^{3-}$-OH. Histidine is highlighted in red and cysteine in blue.

Name	Sequence
P2	H H L R I P Y A L D Q T
P3	D S A P S Y N Y R P S Y
P6	***D Y H D P S P P T L R K***
P7	K V Y F S I P W R V P M
	R D Y H P R D H T A T W
P8	W S S V V G Q N F R S Q
	Q V N G L G E R S Q Q M
P9	H S N D P R L I T M R K
P10	T C F A H T H N N F G H
P11	***D Y H D P S L P T L R K***
P12	***D Y H D P S L P T L R K***
P13	***G N N P L H V H H D K R***
P17	***G N N P L H V H H D K R***
P19	***R D Y H P R D H T A T W***
P25	***D Y H D P S L P T L R K***
P27	***D Y H D P S L P T L R K***
P28	I P G T A P P L A R T G
P31	V R A F S G E H S F V S
Other clones	M13 non-display phage

As was observed previously, there is no sequence homology amongst the identified peptide sequences. Several duplicate sequences appear from the panning which is

promising for phosphatase activity. However, these are rich in aromatic amino acids which could also be plastic binders that interact with the polystyrene walls of the reaction vessels used.[150, 151] These plastic binders are often selected when there is in an absence of a strong preference for the target. Numerous clones that were picked from the titration were identified as non-display phage. This is a problem with the library used for the phage display panning.

6.3.6 Phosphatase Activity – Dephosphorylation Reaction by HPLC

Again, the ability of the new phage to catalyze the same dephosphorylation reaction used in the panning process was tested. Phage were mixed with the gel precursors in individual vials and HPLC was used to follow the dephosphorylation reaction and quantify the percentage conversion of starting material to product due to the phosphorylated precursor and the reaction product having different retention times.[145] In this case, the conversion was too small to measure and therefore is not recorded here. It is clear that the conversion from the precursor to the product is extremely low, implying that the phage once again do not have the desired activity. However, the low conversion rate could be down to localized aggregation at the tip of the phage which prevents the catalytic peptide from dephosphorylating the precursor further and therefore no conversion is recorded. The phages identified in the panning process were taken on for UV-Vis studies to confirm whether they possessed the desired activity it not.

6.3.7 Phosphatase Activity – Dephosphorylation Reaction by UV-Vis Spectroscopy

Dephosphorylation of the phosphatase substrate was monitored by UV-Vis spectroscopy.[146, 147] *p*-Nitrophenyl phosphate (*p*NPP) was used to investigate dephosphorylation by all of the phage viruses sequenced from the second panning experiment with Fmoc-Phe-Tyr$(PO_4)^{3-}$-OH.

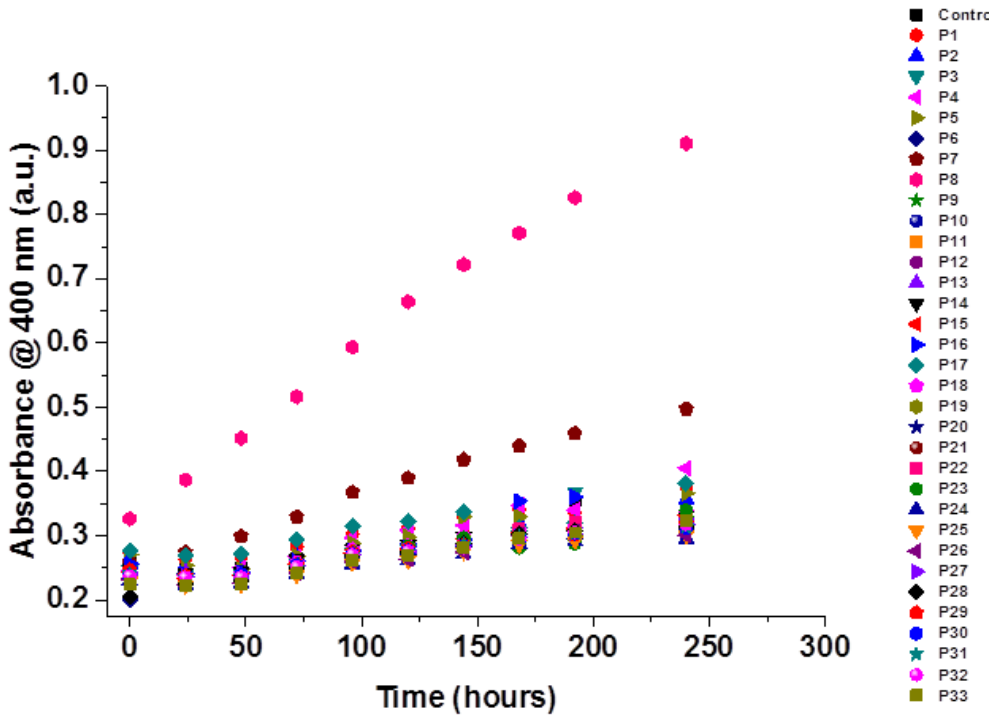

Figure 6.13. UV-Vis *p*NPP dephosphorylation assay. Time courses observed for the hydrolysis of *p*-nitrophenyl phosphate (*p*NPP) using varying μM phage and 10 mM *p*NPP.

The absorbance recorded at 400 nm can be correlated to the rate of dephosphorylation. The rate constant for P7 and P8 were determined from a UV-Vis calibration graph of *p*-nitrophenol and Equation 1. Once again the rates are calculated based on the concentration of the catalytic peptides (five peptides per phage).

From the time courses it was confirmed that the background dephosphorylation is an extremely slow process. It also demonstrates that there is little difference in rate between each phage sequence however there are two that stand out, these are P7 and P8. It can also be seen that the observed rate for this reaction is extremely low and takes place over an extended length of time up to 10 days. The rates for the P7 and P8 which possess the desired activity are 1.33×10^{-2} s^{-1} and 6.22×10^{-2} s^{-1}. This is considerably higher than for the phages for the first panning experiment however again the concentration of the phage in the sample is extremely low and can therefore alter the rate in a significant way making it very difficult to compare to the original data set.

P8 shows the highest activity for phosphatase however this is not reproducible. On further investigation the rate of activity was in line with background rate. The sample was titrated on agar plates and several colonies lifted for cloning to identify whether the sequence had mutated over time which is a possibility after multiple rounds of amplification. In this case, it was found that the sequence had indeed mutated and several variations of the sequence were identified. As a result, the original sequence of the P8 phage was lost and no further studies could be carried out. The activity of the P7 phage was reproducible and the sequence remained constant after amplification. As observed previously in chapter 3.3 there is significant sequence diversity within the sample of phage sequences from the panning process and it is difficult to understand why some sequences possess activity whilst others do not. Given the poor rates observed and difficulties in reproducing catalytic data it was decided to discontinue the search for phosphatase activity.

6.4 Conclusions

The combination of catalytic self-assembly and phage display were utilized to screen a phage display library for phosphatase activity. The phage with the specified activity were isolated and extracted from the bulk library of 10^9 different sequences.

In the first panning experiment several sequences of interest were identified from the panning experiment. Several duplicate sequences were identified which was promising and indicated enrichment of the phage library and as panning progressed. These sequences were amplified and studied for phosphatase activity by HPLC and UV-Vis spectroscopy. Unfortunately, none of the selected phage showed the desired activity above background rates and in comparison to random sequences that were previously selected.

The panning experiment was optimized in several ways including conditions for panning, isolation and extraction and following the panning process closely to assess whether enrichment of the library was occurring throughout the process. A second panning experiment was then carried out to see if the improved conditions could

identify any phage with phosphatase activity. Although duplicate sequences were identified throughout the process, these did not possess any catalytic activity above the background rate. The extraction of these duplicate sequences could be as a result of them having the potential to be plastic binders or to possess the ability to bind to the phage in a non-specific manner. Two sequences showed promise however the activity of P8 was not reproducible. P7 proved to be a more robust choice and showed improved rates above those of the first panning experiment. However, this could be due to the very low concentration of phage in the sample which is taken into consideration when calculating the k_{obs}. It is not possible to categorically state that the panning process has yielded sequences which possess phosphatase activity. Further optimization must be carried out to improve this technology.

7.0 Conclusions and Future work

7.1 Conclusions

Whilst peptides have been proven to be versatile building blocks for the synthesis of *de novo*, synthetic enzyme mimics, further investigation into screening directly for enzymatic function was required in order to study whether a direct link between function and peptide sequence could be established. The first aim of this research was to screen phage display peptide libraries to identify catalytic peptides for amidase and esterase function. The focus also included mechanistic studies to gain an insight into the catalytic mechanism of these peptides. This was achieved by combining precursors of peptidic gelators (Fmoc-Thr and Leu-OMe to form gelator Fmoc-Thr-Leu-OMe) with a phage display library and carrying out several rounds of panning. The identified phage were sequenced and then characterized for amidase and esterase activity using HPLC, TEM, and fluorescence and UV-Vis spectroscopy. All identified peptides possessed the desired activity, albeit at low level. The activities of the peptides off phage (i.e., produced by solid phase peptide synthesis) were also characterized and the overall trend in activity found to be almost identical to that of the on phage samples (with the exception of CPN3, see below). This indicates that although rates were enhanced on the phage, the peptide sequence alone does dictate the trend of activity.

CPN3 esterase activity stood out both on and off phage with the rate off phage enhanced in comparison to the remaining peptides by almost seven times. This was unexpected as CPN3 has been identified as a random, unassembled structure (as confirmed by CD) and the peptide does not contain histidine like the remaining peptides but instead, contains two cysteine residues. An alanine scan identified that all of the amino acids play a role in the esterase catalysis however cysteine plays the key role. On substitution of both cysteine residues, the activity of the peptide decrease significantly. Individual substitution of the cysteine residues resulted in decrease activity but not to the extent of the double mutant. This indicates that these catalytic residues are working independently of one another and a disulphide bridge does not form in these peptides. This provides evidence that cysteine can be used as a convincing alternative to histidine when designing synthetic peptide mimics.

KYF was discovered by chance to show ester hydrolysis. This tripeptide has a conformation even at low peptide concentrations (1 mM) however structure does not play a role in catalysis. Mutant sequences demonstrate that lysine and the terminal amino group are key for catalysis in this example. In polypeptide sequences the pK_a of the terminal amino group is 6.9 – 8.1,[80] in comparison to the side chain of lysine which is 10.53, therefore the terminal amino group is likely to be deprotonated and able to nucleophilically attack the substrate to induce hydrolysis. It can be seen that as the lysine residue is moved further away from the amino group the catalysis decreases as a result of the removal of the basic environment and in turn the initiation of catalysis. Mass spectroscopy results confirm that the proposed mechanism of action for ester hydrolysis is aminolysis. Other tripeptides are able to hydrolyze ester bonds however bulky or acidic side chains are not optimal for activity.

Finally, phage display panning was undertaken to screen for phosphatase activity by using newly designed phosphatase responsive gelators. A number of sequences could be identified after panning (followed by an optimized panning process) and the identified sequences were characterized for the desired activity on phage. The phosphatase activity is very low and requires monitoring over a number of days instead of a number of minutes. This data is not reproducible and therefore the panning process requires further optimization to identify sequences with the desired activity.

7.2 Future Work

The conclusions drawn from this work offer opportunities for future work and further development of this project. This section discusses the future direction of the project and a possible agenda for the work. Phage libraries are good biochemical toolkits and offer a versatile platform for biocatalytic engineering and screening technology. Panning experiments to identify catalytic peptides from a phage library were successful however on characterization of the sequences on phage; it was found that the presence of the phage scaffold enhanced catalysis. Further study into the protein

coat of the phage and in turn the catalysis that comes from the protein itself is necessary. It is possible that these phages can themselves be used for biocatalysis.

The next step would be to study CPN3 peptide in more detail. Other physical techniques, for example NMR, could be used to look at interactions on CPN3 with itself, other peptides in solution and even the substrate itself enhancing what is already known about the mechanism of action. It would also be interesting to modify the peptide to identify the minimal residues required for catalysis to occur and even to enhance catalysis by removing unnecessary amino acids. It is possible that an even shorter version of this random, unassembled peptide possesses esterase activity. Based on what has been learned about CPN3 peptide it might be possible to now design a *de novo* peptide with new characteristics which are more suited to esterase activity, incorporating cysteine into the sequence. Self-assembly has been proven to be beneficial for catalysis and the design of a new self-assembling peptide which presents cysteine on its surface could have enhanced catalytic rates.

Although this peptide has esterase activity in line with examples in the literature, it would be useful to try to improve the activity above this rate and bring it in line with enzyme rates. This could be achieved by multivalent display of the peptide on a surface including gold nanoparticles or even the solid resin support used for synthesis. These are options for the free peptide however the peptide on phage also offers advantages that can be utilized to display the peptide in a multivalent fashion. The major coat protein of a phage virus is made up of 2700 copies of one protein sequence. Mutation of this sequence to display the peptide in a multivalent way 2700 time rather than 5 times as on the P3 coat protein could enhance catalysis considerably. It is beneficial for peptide display on phage viruses as they offer environmental compatibility, novel chemical activity and thermal stability. Another option is to introduce metal ions into the system to see if their presence has an effect on catalysis.

KYF has been developed as an esterase mimic however self-assembly of this system is not beneficial to catalysis in this case. After careful study of this peptide and its mechanism it is possible to incorporate lysine and terminal amino group key hydrolytic residues. Further study of this system could develop a hydrolytic gel

which would be useful for biological applications. It is currently seen that on addition of substrate on top of the gel it diffuses through the self-assembled network and hydrolysis of esters occurs. If the product can be separated from the gel material, it is possible that a reusable material could be developed. However, it will be difficult to separate the two components without significantly altering the concentration of the catalyst before reuse.

Finally, it would be interesting to look further into phage display panning for different activities. Phosphatase activity has proven difficult to pan for however optimization to this system could result in phosphatase mimics. Gelator choice, as well as other conditions, has already been optimized for this system however it requires further work to successfully identify peptides with the desired activity. Once phage display panning has been optimized it will provide a useful platform technology to pan for a multitude of different enzymatic activities and result in numerous peptidic catalysts which directly relates sequence to function. This will provide a further insight into mechanism of action for different activities however it may be the case that each peptide carries out the same enzymatic function *via* a different mechanism. Numerous sequences identified will require mechanistic analysis to develop an understanding into how activity can be related to function. This study would be pertinent as these peptides can be used for numerous applications including industrial and biomedical opportunities.

8.0 Materials and Methods

All solvents used were purchased from either Sigma-Aldrich or Rathburn Chemicals Ltd. All substrates were purchased from Sigma-Aldrich and catalytic peptides were custom made by Almac and China Peptides Ltd. Phage display kits were bought from New England BioLabs.

8.1 Methods and Materials Associated with the Study of Discovery of Catalytic Phages by Biocatalytic Self-Assembly (Chapter 3.0)

8.1.1 Phage Display Panning

200 μL of 10 mM Fmoc-Thr-OH and 40 mM Leu-OMe/Leu-NH_2 in pH 8.0 100 mM phosphate buffer was added to a microfuge tube. 10 μL of Ph.D 12 10^9 library was added to the gel precursors and this was mixed gently with the pipette tip. The mixture was left to incubate for 3 days. The sample was centrifuged at room temperature, 14,000 rpm for 30 minutes until a phage pellet formed. The supernatant was removed and the pellet was then washed with pH 8.0 100 mM phosphate buffer (PB) before being suspended in 200 μL of 1 μg/mL subtilisin and incubated overnight, in the case of Leu-OMe. Since the gelator Fmoc-Thr-Leu-NH_2 is not readily hydrolyzed by subtilisin, the pellet was suspended in 50:50 acetonitrile/water for 30 minutes. The eluted phages were amplified by infection into *E. Coli* (which is removed by centrifugation), followed by purification by precipitation with polyethylene glycol (PEG) solution (see 8.1.3). The amplified phages were titrated (see 8.1.2) on Lysogeny Broth (LB) plates containing Xgal (5-bromo-4-chloro-3-indolyl-β-D-galactoside) and IPTG (isopropyl-β-D-thiogalactopyranoside) to obtain individual plaque DNA for sequencing and also to determine the concentration of the sample. The DNA products were amplified by polymerase chain reaction (PCR). This process was then repeated for the second round of panning.

8.1.2 Phage Titration

5 mL of LB medium was transferred to a 50 mL falcon tube. 3-5 colonies of *E. Coli* were transferred to the tube. This was left to shake at 200 rpm for 4-8 hours (until OD_{600} ~0.5) LB + IPTG/Xgal agar plates (10 g of LB broth + 7.5 g agar in 500 mL distilled water plus 500 μL of IPTG/Xgal stock) were left to warm in the 37^{o}C incubator. Top agar (28 g of nutrient broth in 1 L distilled water) was melted in a microwave for 10-30 seconds and 3 mL transferred to a 15 mL sterile tube, one per phage dilution. The top agar was maintained at 45^{o}C until required. Once the OD of the *E. Coli* is greater than 0.5 the phage dilutions were prepared. These ranged from $10^{6} – 10^{16}$.

- 10 μL phage sample into 990 μL LB = 10^{2}
- 10 μL of 10^{2} into 990 μL LB = 10^{4}
- 10 μL of 10^{4} into 990 μL LB = 10^{6} etc.

200 μL of *E. Coli* was transferred to microfuge tubes, one for each phage dilution. To infect the *E. Coli* with phage 10 μl of phage dilution (*e.g.* 10^{4}) was added to the corresponding tube containing *E. Coli*. Samples were vortexed quickly and incubated at room temperature for 1-5 minutes. The infected cells were transferred to the tubes containing the top agar, vortexed briefly and immediately poured onto the warm LB + IPGT/Xgal plate. The top agar was spread the evenly and the plates allowed to cool for 5 minutes, inverted and left to incubate at 37^{o}C overnight. This was done for each phage dilution. The plates were then removed from incubator to see if blue plaques had formed. To calculate the concentration of the sample, the plaques were counted for each sample.

8.1.3 Phage Amplification, Purification by PEG Precipitation

250 μL of *E. Coli* (overnight culture) was transferred to a 50 mL falcon tube. 25 mL of LB medium (10g of LB broth in 500 mL distilled water) was also added to the tube so that the dilution was 1:100 of *E. Coli* to LB medium. Culture tubes were

placed in a holder and 1 mL of *E. Coli*/LB was transferred into each tube. Individual plaques from the titer plates were placed into the tubes, one per tube, and vortex for a few seconds. The tubes were then incubated at 37^{o}C with shaking (200 rpm) for 4.5-5 hours (no longer). After incubation the cultures were transferred to microfuge tubes and centrifuged at 14,000 rpm for 2 minutes. The supernatant was transferred to a fresh tube and re-spun. The top 80% of the supernatant was transferred to a fresh tube. This is the amplified phage stock and can be stored in the fridge for several weeks with little loss of titer. For long-term storage dilute 1:1 with sterile glycerol and store at -20^{o}C.

To remove the phage from the LB media and suspend in buffer 1/6 volume of 20% PEG/2.5 M NaCl was added to precipitate the phage (this was left overnight). The PEG precipitation was centrifuged at 12,000 rpm for 15 minutes at 4^{o}C. The supernatant was removed to leave a white smear on the side of the tube, which was the phage. The pellet was re-suspended in 1 mL of pH 7.4 10 mM phosphate buffered saline (PBS). This was centrifuged at 14,000 rpm for 5 minutes at 4^{o}C to remove any residual *E. Coli* cells. The supernatant was transferred to a fresh tube and re-precipitated again by adding 1/6 volume of PEG/NaCl. This was incubated on ice for 1 hour and then centrifuged at 14,000 rpm for 15 minutes at 4^{o}C. The supernatant was discarded and the tube re-spun briefly to precipitate the phage smear on the side of the tube. The phage was suspended in PBS, centrifuged for 1 minute at room temperature to precipitate any insoluble material left in the sample and then the supernatant was transferred to a fresh tube. This was the phage particles in buffer which were then used in the activity assays.

8.1.4 Calculation of Phage Concentration

E.g. 100 plaques were counted on the plate which was made from 10^{9} dilution sample. This can be translated to 1 x 10^{11}. Initially the concentration was calculated with respect to the peptide on the tip of the phage therefore the concentration is multiplied by five to account for the five copies of the peptide on display.

Concentration = 1 x 10^{11} pfu (plaque forming unit)/10 µL

1 x 10^{13} pfu/1000 µL

5 x (1 x 10^{13}) = 5 x 10^{13} pfu/1000 µL

5 x 10^{16} pfu/1000 mL

5 x 10^{16} / 6.02 x 10^{23} = 8.3 x 10^{-8} M stock of phage

8.1.5 Phage DNA sequencing

A single plaque from a titer plate was suspended in 1 mL 1:100 *E. Coli*/LB medium. This was amplified and transferred into buffer as chapter 8.1.3 PCR was used to amplify the DNA.

Table 8.3. PCR sample composition.

PCR component	Quantity (µL)
Pure water	13.3
5X Phusion High-Fidelity Buffer	4
dNTPs	0.4
+133gIII primer 5'GTT GTC ATT GTC GGC GCA AC 3' (10 pmol/µl)	1
-142gIII primer 5' GTA CCG TAA CAC TGA GTT TCG 3'(10 pmol/µl)	1
Polymerase	0.1
DNA	0.2
Total Volume	20

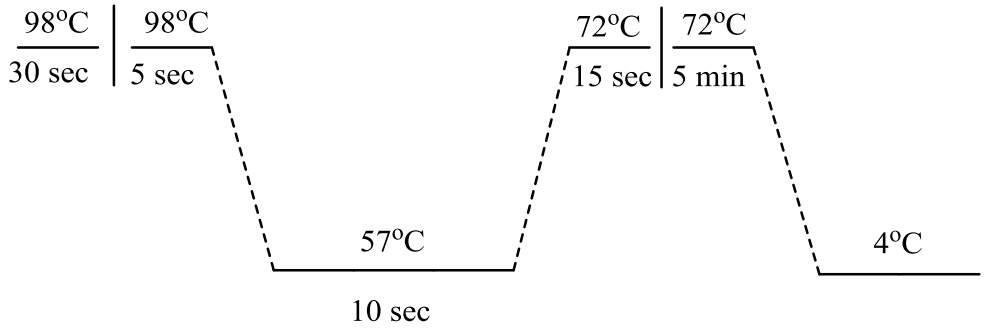

Repeat steps 2 – 4 for 35 cycles.

The PCR products were run on a 2 % agarose gel at 100 volts for 40 minutes using a 500 – 50 base pair ladder and loading dye. The DNA was then purified using a Promega 'Wizard SV Gel and PCR clean up kit' before sequencing by Genewiz.

8.1.6 TEM

TEM analysis of the eluted phage was carried out using a concentration of 10^{10} pfu. The phage was mixed with the precursors Fmoc-Thr-OH and Leu-OMe using the same conditions as for the panning process. The sample was left to incubate at room temperature and samples were taken at various time points including 10 minutes, 30 minutes and 60 minutes. 3 µL of the sample was applied to a carbon-coated copper TEM grid (Electron Microscopy Sciences, PA) and dried. The phage sample was stained with 2% uranyl acetate and then studied on a TEM (JEOL 2100) at 200 kV.

8.1.7 Amide Condensation by Catalytic Phages

The precursors Fmoc-Thr (10 mM) and Leu-NH_2 (40 mM) were mixed (at 1:4 ratio) in a glass vial. The mixture was suspended in 950 µL of pH 8.0 100 mM PB with the addition of 50 µL of the phage solution (10^{11} p.f.u.). The mixture was vortex mixed for 1 minute to ensure dissolution. Samples were incubated at room temperature and samples (25 µL of gel/viscous solution was dissolved in 975 µL of 50:50 acetonitrile water mixture having 0.1 % TFA) were taken after 24, 48,

72 and 216 hours for reverse phase HPLC analysis to determine the percentage conversion. The samples were analyzed by reverse phase HPLC using a Dionex P680 system operating with a Macherey-Nagel 250 Å, 4.6 x 250 mm, C18 column. The mobile phase of water and acetonitrile was ramped from 20-80 % over 46 minutes at a flow rate of 1 mL min^{-1}. Detection of the product peaks was carried out using a UVD170U UV-Vis detector at 225, 265, 280 and 310 nm wavelengths.

8.1.8 FRET Assay

The FRET substrate, Glu(EDANS)-Gly-Thr-Leu-Gly-Lys(DABCYL), was purchased from Almac. Catalytic phage (300 µL, working concentration 0.01667 µM) was added to FRET substrate (6 µL, working concentration 2 µM) in pH 8.0 100 mM PB (1194 µL) and incubated at 37 ˚C over a period of three days. The emission spectrum for each sample was recorded on a Jasco-FP-8500 spectrophotometer at 24 hour intervals. The FRET fluorescence parameters are excitation at 340 nm and emission between 355 and 550 nm. The emission peak is at 493 nm. An excitation and emission bandwidth of 5 nm was used with a medium sensitivity. Light was measured orthogonally to the excitation light with a scanning speed of 500 nm min^{-1}.

The curve was fit using equation 1 in the main text (Chapter 3). Since the product of the cleavage was not available, the FRET peptide was incubated with chymotrypsin and the fluorescence measured over time to obtain a calibration plot. The slope of this plot was then input into the equation as the gradient of the calibration sample. The gradient of the sample was obtained by measuring the fluorescence over time and obtaining the slope of the plot. This was also input into the equation along with the concentration of the catalyst and a rate was obtained as a function of time. This is the method used for all of the FRET samples in this thesis.

8.1.9 FITC-Casein Assay

The FITC–Casein kit was purchased from Sigma Aldrich, which included all substrate and buffer required for this assay. 10 µl of catalytic phage was added to 20 µL of the FITC substrate and 20 µl of incubation buffer. This was incubated at 37 ˚C for 24 hours resulting in the cleavage of the FITC-labelled casein substrate into smaller fragments. After incubation the sample was acidified with trichloroacetic acid and centrifuged so that any undigested substrate formed a pellet and any small acid soluble fragments remained in solution. 10 µl of supernatant was transferred into 1 mL of assay buffer so that the fluorescence could be recorded. The emission spectrum for each sample was recorded on a Jasco-FP-6500 spectrophotometer. The excitation wavelength was 485 nm and the emission wavelength was 535 nm. The spectra were recorded over a range of 500-600 nm.

8.1.10 *p*NPA UV-Vis Esterase Assay

The UV substrate, *p*-nitrophenol acetate (*p*NPA), was purchased from Sigma Aldrich. 300 µL of catalytic phage (working concentration 0.01667 µM) in pH 7.4 PBS was added to 600 µL pH 7.4 PBS. 40 µl methanol was added to the peptide and buffer mix. Finally 60 µL of 100 mM *p*-NPA in methanol (working concentration 6 mM) was added to the sample. Samples were run on a Jasco V-660 spectrophotometer at 400 nm over a course of 10 minutes, 1 scan per minute. The bandwidth is 2.0 nm with a scan speed of 400 nm min^{-1} and medium sensitivity.

The curve was fit using equation 2 in the main text (Chapter 3). Since the product of the cleavage was available, concentrations from 0.0 - 0.1 mM were prepared and the absorbance measured on the UV-Vis spectrometer. The slope of this plot was then input into the equation as the gradient of the calibration sample. The gradient of the sample was obtained by measuring the absorbance over time and obtaining the slope of the plot. This was also input into the equation. Finally, background hydrolysis was measured and subtracted from the catalytic sample (as see in equation 2 whereby the gradient of background hydrolysis is subtracted from the gradient of the catalytic

sample) to obtain the true rate of the catalyst and to account for background hydrolysis which occurs in solvent only. These values, along with the concentration of the catalyst, were input into equation 2 and a rate was obtained as a function of time. This is the method used for all of the ester cleavage samples in this thesis.

8.1.11 MUA Fluorescence Esterase Assay

The fluorescent substrate, 4-methylumbelliferone acetate (MUA), was purchased from Sigma Aldrich. 400 μL of catalytic phage (working concentration 0.01249 μM) in pH 7.4 PBS was added to 1500 μL pH 7.4 PB. 50 μL of MUA in DMSO (working concentration 0.25 mM) was added to the sample along with 50 μL DMSO (maintaining a total volume of 100 μL DMSO). The emission spectrum for each sample was recorded on a Jasco-FP-6500 spectrophotometer. The excitation wavelength was 365 nm, the emission wavelength was 445 nm and the fluorescence intensity was measured over a course of 30 minutes, 1 scan per minute. An excitation and emission bandwidth of 3 nm was used with a medium sensitivity.

8.2 Methods and Materials Associated with the study of a Non-Histidine containing Short Peptide Catalyst for Esterase Activity (Chapter 4)

8.2.1 FRET Assay

The FRET substrate, Glu(EDANS)-Gly-Thr-Leu-Gly-Lys(DABCYL), was purchased from Almac. 300 μL of catalytic peptide (working concentration 0.5 mM) was added to 6 μL of FRET substrate (working concentration 2 μM) and 1194 μL pH 8.0 100 mM PB and incubated at 37 ˚C over a period of three days. The emission spectrum for each sample was recorded on a Jasco-FP-8500 spectrophotometer at 24 hour intervals. The FRET fluorescence parameters are excitation at 340 nm and emission between 355 and 550 nm. The emission peak is at 493 nm. An excitation

and emission bandwidth of 5 nm was used with a medium sensitivity. Light was measured orthogonally to the excitation light with a scanning speed of 500 nm min^{-1}.

8.2.2 *p*NPA UV-Vis Esterase Assay

500 µl of 1 mM catalytic peptide (0.036 mM for CPN3) in PBS pH 7.4 was added to 400 µl PBS. 40 µl methanol was added to the peptide in buffer. Finally 60 µl of 100 mM *p*-NPA in methanol was added to the sample. Samples were run on a Jasco V-660 spectrophotometer at 400 nm over a course of 10 minutes, 1 scan per minute. All samples were carried out at 25^{o}C. The bandwidth is 2.0 nm with a scan speed of 400 nm min^{-1} and medium sensitivity.

8.2.3 Circular Dichroism

CD experiments were performed using Jasco J-810 spectrometer for solution of CPN3 peptide prepared in 0.2 cm cell. Measurements were performed at room temperature and spectra were recorded from 190 to 260 nm.

8.2.4 *p*NPA UV-Vis Esterase Assay with CPN3 Alanine Scan Peptides

500 µl of 0.072 mM CPN3 alanine sweep peptides in PBS pH 7.4 was added to 400 µl PBS. 40 µl methanol was added to the peptide in buffer. Finally 60 µl of 100 mM *p*-NPA in methanol was added to the sample. Samples were run on a Jasco V-660 spectrophotometer at 400 nm over a course of 10 minutes, 1 scan per minute. All samples were carried out at 25^{o}C. The bandwidth is 2.0 nm with a scan speed of 400 nm min^{-1} and medium sensitivity.

8.2.5 *p*NPA UV-Vis Esterase Assay with L-Cysteine

500 µl of 0.036 mM cysteine in PBS pH 7.4 was added to 400 µl PBS. 40 µl methanol was added to the peptide in buffer. Finally 60 µl of 100 mM *p*-NPA in methanol was added to the sample. Samples were run on a Jasco V-660 spectrophotometer at 400 nm over a course of 10 minutes, 1 scan per minute. All samples were carried out at 25^{o}C. The bandwidth is 2.0 nm with a scan speed of 400 nm min^{-1} and medium sensitivity.

8.2.6 *p*NPA UV-Vis Esterase Assay with CPN3 Peptide and CPN3 Peptide Cysteine Substitute at Different pH Values

500 µl of 0.036 mM CPN3 alanine sweep peptides in phosphate buffer, pH ranging from 5 to 8, was added to 400 µl phosphate buffer of the corresponding pH. 40 µl methanol was added to the peptide in buffer. Finally 60 µl of 100 mM *p*-NPA in methanol was added to the sample. Samples were run on a Jasco V-660 spectrophotometer at 400 nm over a course of 10 minutes, 1 scan per minute. All samples were carried out at 25^{o}C. The bandwidth is 2.0 nm with a scan speed of 400 nm min^{-1} and medium sensitivity.

8.2.7 *p*NPA UV-Vis Esterase Assay with CPN3 Peptide at Different Temperatures

500 µl of 0.036 mM CPN3 peptide in PBS pH 7.4 was added to 400 µl PBS. 40 µl methanol was added to the peptide in buffer. Finally 60 µl of 100 mM *p*-NPA in methanol was added to the sample. Samples were run on a Jasco V-660 spectrophotometer at 400 nm over a course of 10 minutes, 1 scan per minute. Samples were carried out at different temperatures ranging from 10 - 60^{o}C. The bandwidth is 2.0 nm with a scan speed of 400 nm min^{-1} and medium sensitivity.

8.2.8 UV-Vis Esterase Assay with *p*NPA and *p*NPB by CPN3 Peptide

500 µl of 0.036 mM catalytic peptide in PBS pH 7.4 was added to 475 µl PBS. 0 - 20 µl DMSO was added to the peptide in buffer. Finally 5 - 25 µl of 40 mM *p*-NPA/*p*-NPB in DMSO was added to the sample. Samples were run on a Jasco V-660 spectrophotometer at 400 nm over a course of 10 minutes, 1 scan per minute. All samples were carried out at 25^{o}C. The bandwidth is 2.0 nm with a scan speed of 400 nm min^{-1} and medium sensitivity.

8.3 Methods and Materials Associated with the study of Tripeptide Esterase Mimic (Chapter 5)

8.3.1 Preparation of KYF Samples

Dissolve the required amount of KYF peptide in PBS and use NaOH to bring the pH to 7.5. Hand mix and leave samples overnight for gelation to occur.

8.3.2 Circular Dichroism

CD experiments were performed on a Jasco J-810 spectrometer for a solution of KYF peptide prepared in a 0.2 cm cell. Measurements were performed at room temperature and spectra were recorded from 190 to 260 nm.

8.3.3 TEM

TEM analysis of KYF was carried out at concentrations of 1, 10 and 20 mM peptide. The peptide was mixed in PBS and NaOH added to bring the pH to 7.5. The samples were left at room temperature overnight. Carbon-coated copper grids were glow discharged in air for 30 seconds. 5 µL of sample was applied to the TEM grid and

excess removed by filter paper. Samples were then stained (1% aqueous methylamine vanadate obtained from Nanovan, Nanoprobes) before being left to dry. The samples were studied by TEM FEI TECNAI TEO microscope operating at 200 kV.

8.3.4 Fluorescence of KYF at Different Concentrations

0.1, 1, 2.5, 5, 10 and 20 mM KYF samples in PBS were monitored by fluorescence spectroscopy. The emission spectrum for each sample was recorded on a Jasco-FP-6500 spectrophotometer. The samples were excited at 274 nm and emission between 280 and 500 nm. The emission peak is at 303 nm. An excitation bandwidth of 1 nm and emission bandwidth of 5 nm was used with a medium sensitivity. Light was measured orthogonally to the excitation light with a scanning speed of 500 nm min^{-1}.

8.3.5 Fluorescence of KYF at Different Concentrations in the Presence of ThioflavinT

0.078, 0.313, 0.625, 1.25, 2.5, 5, 7.5, 10, 12.5, 15, 17.5 and 20mM KYF samples in PBS were monitored by fluorescence spectroscopy with the addition of 0.01 mM ThioflavinT. The emission spectrum for each sample was recorded on a Jasco-FP-6500 spectrophotometer. The samples were excited at 450 nm and emission between 455 and 700 nm. The emission peak is at 485 nm. An excitation and emission bandwidth of 3 nm was used with a medium sensitivity. Light was measured orthogonally to the excitation light with a scanning speed of 500 nm min^{-1}.

8.3.6 Measuring Turbidity of KYF samples by UV-Vis Spectroscopy

1 mL samples of 0.625, 1.25, 2.5, 5, 7.5, 12.5, 15, 17.45 and 20 mM of KYF were prepared in PBS. NaOH was added to bring the pH to 7.4. Samples were run on a

Jasco V-660 spectrophotometer from 300 – 800 nm. The bandwidth is 2.0 nm with a scan speed of 400 nm min^{-1} and medium sensitivity.

8.3.7 *p*NPA UV-Vis Esterase Assay with KYF Gel

A 20 mM gel of KYF was prepared in PBS pH 7.4. 60 µl of 100 mM *p*-NPA in methanol was pipetted onto the surface of the gel and the sample monitored visually over 120 minutes.

8.3.8 *p*NPA UV-Vis Esterase Assay with KYF

Samples of 0.156, 0.312, 0.625, 1.25, 2, 4, 6, 8, 10, 12 and 14 mM samples were prepared and left overnight. 2 mL of PBS was added to the sample to dilute to the desired concentration. 60 µl of 100 mM *p*-NPA in methanol was added to 940 µl of 0.078, 0.156, 0.312, 0.625, 1, 2, 3, 4, 5, 6 or 7mM KYF in PBS pH 7.4. Samples were run on a Jasco V-660 spectrophotometer at 400 nm over a course of 10 minutes, 1 scan per minute. All samples were carried out at 25^{o}C. The bandwidth is 2.0 nm with a scan speed of 400 nm min^{-1} and medium sensitivity.

8.3.9 *p*NPA UV-Vis Esterase Assay with Mutant KYF Sequences

60 µl of 100 mM *p*-NPA in methanol was added to 940 µl of 1 mM KYF, AYF, Ac-KYF, Ac-AYF and KYF-NH_2 in PBS pH 7.4. Samples were run on a Jasco V-660 spectrophotometer at 400 nm over a course of 10 minutes, 1 scan per minute. All samples were carried out at 25^{o}C. The bandwidth is 2.0 nm with a scan speed of 400 nm min^{-1} and medium sensitivity.

8.3.10 *p*NPA UV-Vis Esterase Assay with L-Lysine

60 µl of 100 mM *p*-NPA in methanol was added to 940 µl of 1 mM lysine in PBS pH 7.4. Samples were run on a Jasco V-660 spectrophotometer at 400 nm over a course of 10 minutes, 1 scan per minute. All samples were carried out at 25^{o}C. The bandwidth is 2.0 nm with a scan speed of 400 nm min^{-1} and medium sensitivity.

8.3.11 *p*NPA UV-Vis Esterase Assay with KYF, YKF and FYK

60 µl of 100 mM *p*-NPA in methanol was added to 940 µl of 1 mM KYF, YKF or FYK in PBS pH 7.4. Samples were run on a Jasco V-660 spectrophotometer at 400 nm over a course of 10 minutes, 1 scan per minute. All samples were carried out at 25^{o}C. The bandwidth is 2.0 nm with a scan speed of 400 nm min^{-1} and medium sensitivity.

8.3.12 *p*NPA UV-Vis Esterase Assay with KLL, KY and KF Sequences

60 µl of 100 mM *p*-NPA in methanol was added to 940 µl of 1 mM KLL, KY and KF in PBS pH 7.4. Samples were run on a Jasco V-660 spectrophotometer at 400 nm over a course of 10 minutes, 1 scan per minute. All samples were carried out at 25^{o}C. The bandwidth is 2.0 nm with a scan speed of 400 nm min^{-1} and medium sensitivity.

8.3.13 Fluorescence of KYF, YKF and FYK in the Presence of *p*NPA

1 mM samples of KYF in PBS with concentrations of *p*NPA 0.001 – 1 mM were monitored by fluorescence spectroscopy. The emission spectrum for each sample was recorded on a Jasco-FP-6500 spectrophotometer. The samples were excited at 274 nm and emission between 280 and 500 nm. The emission peak is at 303 nm. An excitation bandwidth of 1 nm and emission bandwidth of 5 nm was used with a

medium sensitivity. Light was measured orthogonally to the excitation light with a scanning speed of 500 nm min^{-1}.

8.3.14 *p*NPA UV-Vis Esterase Assay with KYF at Different pH Values

60 µl of 100 mM *p*-NPA in methanol was added to 940 µl of 1 mM lysine in phosphate buffer ranging from pH 5 to 8. Samples were run on a Jasco V-660 spectrophotometer at 400 nm over a course of 10 minutes, 1 scan per minute. All samples were carried out at 25^{o}C. The bandwidth is 2.0 nm with a scan speed of 400 nm min^{-1} and medium sensitivity.

8.3.15 *p*NPA UV-Vis Esterase Assay with KYF at Different Temperatures

60 µl of 100 mM *p*-NPA in methanol was added to 940 µl of 1 mM KYF, YKF or FYK in PBS pH 7.4. Samples were run on a Jasco V-660 spectrophotometer at 400 nm over a course of 10 minutes, 1 scan per minute. Samples were carried out at different temperatures ranging from 10 - 60^{o}C. The bandwidth is 2.0 nm with a scan speed of 400 nm min^{-1} and medium sensitivity.

8.3.16 *p*NPA UV-Vis Esterase Assay with KYW, KFF, DFF and FFD

60 µl of 100 mM *p*-NPA in methanol was added to 940 µl of 1 mM KYF, KYW, KFF, DFF and FFD in PBS pH 7.4. Samples were run on a Jasco V-660 spectrophotometer at 400 nm over a course of 10 minutes, 1 scan per minute. All samples were carried out at 25^{o}C. The bandwidth is 2.0 nm with a scan speed of 400 nm min^{-1} and medium sensitivity.

8.4 Methods and Materials Associated with the Discovery of Catalytic Phages for Phosphatase Activity by Biocatalytic Self-Assembly

8.4.1 Fmoc-Tyr(PO_4)$^{3-}$-Ala-OH

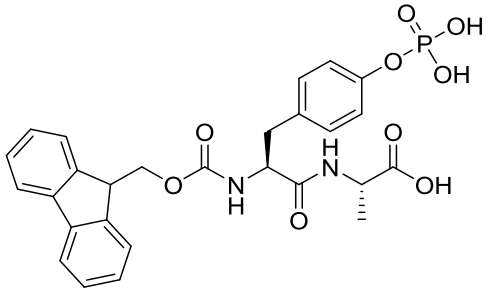

Fmoc-Tyr($PO(NME_2)_2$)-OH (0.5 g, 0.93 mmol), H-Ala-OtBu (0.2 g, 1.11 mmol), HBTU (0.423 g, 1.11 mmol) and DIPEA (420 μL, 2.3 mmol) were dissolved in anhydrous DMF (10 mL) and left to stir over night. The DMF was removed by evaporation *in vacuo*. The resulting mixture was dissolved in ethyl acetate (50 mL) and washed with equal volumes of saturated sodium bicarbonate, brine and hydrochloric acid (1 M) and brine. The organic layer was dried with magnesium sulfate. The ethyl acetate was then removed by evaporation *in vacuo*. The resulting solid was purified by column chromatography using 1:20 methanol/DCM mixture as eluent. Then the deprotection of t-Bu and $PO(NME_2)_2$ groups was carried out by an overnight reaction with 10 mL TFA followed by the addition of 1 mL of water and again an overnight stirring. The TFA and water was then removed by evaporation *in vacuo*. The excess TFA was removed by dissolving the solid in toluene followed by evaporation as azeotropic mixture. The resulting solid was characterized by HPLC and LC-MS. ESI MS +ve $[M+H]^+$ m/z 555 and $[M-H]^-$ m/z 553. Mass spectroscopy and HPLC were used to identify the correct mass and the purity of the peptides. NMR was attempted for further confirmation that the correct peptides had been made however there were solubility issues when preparing the sample of analysis. It is thought that this is down to spontaneous micelle forming characteristics of the peptides at the high concentrations required to obtain an NMR spectrum. A sepctrum could not be obtained.

8.4.2 Fmoc-Tyr(PO_4)$^{3-}$-Ala-OMe

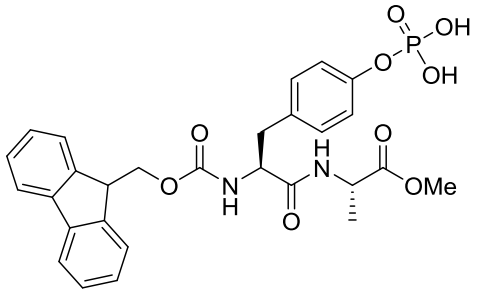

Fmoc-Tyr(PO(NME_2)$_2$)-OH (0.5 g, 0.93 mmol), H-Ala-OMe (0.153 g, 1.11 mmol), HBTU (0.423 g, 1.11 mmol) and DIPEA (420 μL, 2.3 mmol) were dissolved in anhydrous DMF (10 mL) and left to stir over night. The DMF was removed by evaporation *in vacuo*. The resulting mixture was dissolved in ethyl acetate (50 mL) and washed with equal volumes of saturated sodium bicarbonate, brine and hydrochloric acid (1 M) and brine. The organic layer was dried with magnesium sulfate. The ethyl acetate was then removed by evaporation *in vacuo*. The resulting solid was purified by column chromatography using 1:20 methanol/DCM mixture as eluent. Then the deprotectionof the PO(NME_2)$_2$ group was carried out by an overnight reaction with 10 mL TFA and 1 mL of water. The TFA and water was then removed by evaporation *in vacuo*. The excess TFA was removed by dissolving the solid in toluene followed by evaporation as azeotropic mixture. The resulting solid was characterized by HPLC and LC-MS. ESI MS +ve $[M+H]^+$ m/z 569 and $[M-H]^-$ m/z 567. Mass spectroscopy and HPLC were used to identify the correct mass and the purity of the peptides. NMR was attempted for further confirmation that the correct peptides had been made however there were solubility issues when preparing the sample of analysis. It is thought that this is down to spontaneous micelle forming characteristics of the peptides at the high concentrations required to obtain an NMR spectrum. A sepctrum could not be obtained.

8.4.3 Fmoc-Tyr$(PO_4)^{3-}$-Ala -NH_2

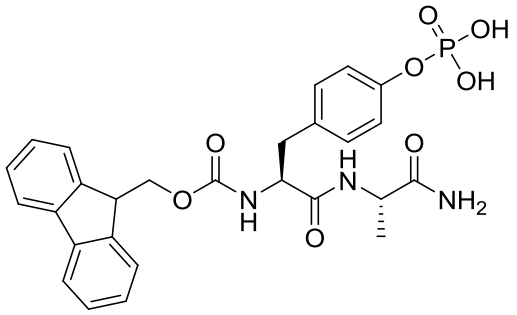

Fmoc-Tyr($PO(NME_2)_2$)-OH (0.5 g, 0.93 mmol), H-Ala-NH_2 (0.137 g, 1.11 mmol), HBTU (0.423 g, 1.11 mmol) and DIPEA (420 μL, 2.3 mmol) were dissolved in anhydrous DMF (10 mL) and left to stir over night. The DMF was removed by evaporation *in vacuo*. The resulting mixture was dissolved in ethyl acetate (50 mL) and washed with equal volumes of saturated sodium bicarbonate, brine and hydrochloric acid (1 M) and brine. The organic layer was dried with magnesium sulfate. The ethyl acetate was then removed by evaporation *in vacuo*. The resulting solid was purified by column chromatography using 1:20 methanol/DCM mixture as eluent. Then the deprotection of the $PO(NME_2)_2$ group was carried out by an overnight reaction with 10 mL TFA and 1 mL of water. The TFA and water was then removed by evaporation *in vacuo*. The excess TFA was removed by dissolving the solid in toluene followed by evaporation as azeotropic mixture. The resulting solid was characterized by HPLC and LC-MS. ESI MS +ve $[M+H]^+$ m/z 554 and $[M-H]^-$ m/z 552. Mass spectroscopy and HPLC were used to identify the correct mass and the purity of the peptides. NMR was attempted for further confirmation that the correct peptides had been made however there were solubility issues when preparing the sample of analysis. It is thought that this is down to spontaneous micelle forming characteristics of the peptides at the high concentrations required to obtain an NMR spectrum. A sepctrum could not be obtained.

8.4.4 Fmoc-Tyr$(PO_4)^{3-}$-Ala-OH/OMe/NH_2 and Fmoc-Phe-Tyr$(PO_4)^{3-}$-OH 20 mM Gel Formation

Gelator (11 mgs) was suspended in 950 μL of pH 8.5 0.6 M PB. This was then sonicated to dissolve the peptide material. 50 μL of alkaline phosphatase was added to the sample and mixed by shaking gently. This was then left to form a gel overnight.

8.4.5 TEM

TEM analysis of Fmoc-Tyr$(PO_4)^{3-}$-Ala-OH and Fmoc-Phe-Tyr$(PO_4)^{3-}$-OH gels was carried out at a concentration of 20 mM peptide. The peptide was mixed in pH 8.5 0.6 M PB and then 50 μL of alkaline phosphatase was added to the sample and mixed by shaking gently. The samples were left at room temperature overnight. Carbon-coated copper grids were glow discharged in air for 30 seconds. 5 μL of sample was applied to the TEM grid and excess removed by filter paper. Samples were then stained (1% aqueous methylamine vanadate obtained from Nanovan, Nanoprobes) before being left to dry. The samples were studied on a TEM FEI TECNAI TEO microscope operating at 200 kV.

8.4.6 Reaction Progress by HPLC

20 mM Fmoc-Tyr$(PO_4)^{3-}$-Ala-OH and Fmoc-Phe-Tyr$(PO_4)^{3-}$-OH gels were prepared and time points taken at different stages throughout the gelation process to monitor conversion of the phosphorylated starting material to the final product. Aliquots of each sample (25 μL) were diluted to 500 μL with 50 % acetonitrile solution in water containing 0.1 % trifluoroacetic acid. 10 μL of sample was injected on a Dionex P680 system operating with a Macherey-Nagel 250 Å, 4.6 × 250 mm, C18 column was used for reversed phase HPLC and water/acetonitrile with 0.1% TFA as the mobile phase ramped from 20 – 80 % ACN over 45 minutes at a flow rate of 1 mL

min^{-1}. Detection of the Fmoc- peptide amphiphiles was carried out using a UVD170U UV-Vis detector at a 300 nm wavelength.

8.4.7 Fluorescence Spectroscopy

20 mM samples of Fmoc-Tyr$(PO_4)^{3-}$-Ala-OH and Fmoc-Phe-Tyr$(PO_4)^{3-}$-OH were monitored by fluorescence spectroscopy. The emission spectrum for each sample was recorded on a Jasco-FP-6500 spectrophotometer. The samples were excited at 295 nm and emission between 300 and 600 nm. An excitation and emission bandwidth of 3 nm was used with a medium sensitivity. Emission was measured orthogonally to the excitation light with a scanning speed of 500 nm min^{-1}.

8.4.8 Rheology

The rheological properties of 20 mM samples of Fmoc-Tyr$(PO_4)^{3-}$-Ala-OH and Fmoc-Phe-Tyr$(PO_4)^{3-}$-OH were measured using a Malvern Kinexus Pro Rheometer with temperature control at 20 °C using a 20 mm parallel plate geometry with a gap of 0.5 mm. Samples were subjected to an oscillatory sweep to determine the strain (%) to apply during the frequency sweep. The strain used throughout the study was 0.1% as it fell within the viscoelastic region for all samples. The frequency sweep was carried out between 0.1 and 100 Hz.

8.4.9 FTIR

FTIR spectra of 20 mM samples of Fmoc-Tyr$(PO_4)^{3-}$-Ala-OH and Fmoc-Phe-Tyr$(PO_4)^{3-}$-OH were acquired using a Bruker Vertex spectrometer with a spectral resolution of 2 cm^{-1}. The spectra were obtained by averaging 32 interferograms for each sample. Measurements were performed in a standard IR cuvette (Harrick Scientific), in which the sample was contained between two CaF_2 windows

(thickness, 2 mm) separated by a 25 μm PTFE spacer. D_2O was used as the solvent for all the infrared spectral measurements.

8.4.10 Phage Display Panning

200 μL of 20 mM Fmoc-Phe-Tyr$(PO_4)^{3-}$-OH and Fmoc-Tyr$(PO_4)^{3-}$-Ala-OH in pH 8.0 600 mM phosphate buffer was added to separate microfuge tubes to allow panning with both substrates. 10 μL of Ph.D 12 10^9 library was added to each gel precursor and this was mixed gently with the pipette tip. The mixture was left to incubate for 3 days. The sample was centrifuged at room temperature, 14,000 rpm for 30 minutes until a phage pellet formed. The supernatant was removed and the pellet was then washed with pH 8.0 600 mM phosphate buffer (PB) before being suspended in 50:50 acetonitrile/water for 30 minutes. The eluted phages were amplified by infection into *E. Coli*, followed by purification by precipitation with 20% w/v polyethylene glycol (PEG) solution. The amplified phages were titrated on Lysogeny Broth (LB) plates containing Xgal (5-bromo-4-chloro-3-indolyl-β-D-galactoside) and IPTG (isopropyl-β-D-thiogalactopyranoside) to obtain individual plaque DNA for sequencing and also to determine the concentration of the sample. The DNA products were amplified by polymerase chain reaction (PCR). This process was then repeated for the second round of panning.

8.4.11 Phosphatase Activity - Dephosphorylation Reaction by HPLC

The precursors Fmoc-Tyr$(PO_4)^{3-}$-Ala-OH and Fmoc-Phe-Tyr$(PO_4)^{3-}$-OH (both 20 mM) were weighed into separate glass vials. Each of these peptide samples weresuspended in 950 μL of pH 8.0 600 mM PB with the addition of 50 μL of the phage solution (10^{11} p.f.u.). The mixture was mixed for 1 minute to ensure dissolution. Samples were incubated at room temperature and samples (25 μL of gel/viscous solution was dissolved in 975 μL of 50:50 acetonitrile water mixture having 0.1 % TFA) were taken after 24, 48, and 72 up to 504 hours for reverse phase

HPLC analysis to determine the percentage conversion. The samples were analyzed be reverse phase HPLC using a Dionex P680 system operating with a Macherey-Nagel 250 Å, 4.6 x 250 mm, C18 column. The mobile phase of water and acetonitrile was ramped from 20-80 % over 46 minutes at a flow rate of 1 mL min^{-1}. Detection of the product peaks was carried out using a UVD170U UV-Vis detector at a 225, 265, 280 and 310 nm wavelengths.

8.4.12 Phosphatase Activity – Dephosphorylation Reaction by UV-Vis

The UV substrate, p-nitrophenol phosphate (*p*NPP), was purchased from Sigma Aldrich. 50 μL of catalytic phage (working concentration variable) in pH 8.5 0.6 M PB was added to 850 μL pH 7.4 PBS. 100 μL of *p*-NPP (working concentration 10 mM) in methanol was added to the sample. Samples were run on a Jasco V-660 spectrophotometer and measured from 300 – 500 nm. The absorbance at 400 nm was recorded every 24 hours for a course of 10 days. The bandwidth was 2.0 nm with a scan speed of 400 nm min^{-1} and medium sensitivity.

8.4.13 Phage Display Panning Optimization

200 μL of 20 mM phosphorylated Fmoc-Phe-Tyr in pH 8.0 100 mM phosphate buffer was added to a microfuge tube. 10 μL of Ph.D 12 10^{11} library was added to the gel precursor and this was mixed gently with the pipette tip. The mixture was left to incubate for 24/48 hours. The sample was centrifuged at room temperature, 14,000 rpm for 15 minutes until a phage pellet formed. The supernatant was removed and the pellet was then washed with 1 mL TBST twice before being suspended in 200 μL of 10 mg/mL chymotrypsin for 30 minutes. The eluted phages were amplified by infection into *E. Coli*, followed by purification by precipitation with polyethylene glycol (PEG) solution. The amplified phages were then used for the next round of panning. In total three rounds of panning were completed. Input and output titrations were carried out throughout the panning process however for the final round; the

amplified phages were titrated on Lysogeny Broth (LB) plates containing Xgal (5-bromo-4-chloro-3-indolyl-β-D-galactoside) and IPTG (isopropyl-β-D-thiogalactopyranoside) to obtain individual plaque DNA for sequencing and also to determine the concentration of the sample. The DNA products were amplified by polymerase chain reaction (PCR).

Titration, amplification and purification as per chapter 8.1.2 and 8.1.3.

9.0 References

9.1 References

1. R. Wolfenden and M. J. Snider, *Acc. Chem. Res.*, 2001, **34**, 938-945.
2. M. O. Guler and S. I. Stupp, *J. Am. Chem. Soc.*, 2007, **129**, 12082-12083.
3. C. M. Rufo, Y. S. Moroz, O. V. Moroz, J. Stohr, T. A. Smith, X. Z. Hu, W. F. DeGrado and I. V. Korendovych, *Nat. Chem.*, 2014, **6**, 303-309.
4. D. Zaramella, P. Scrimin and L. J. Prins, *J. Am. Chem. Soc.*, 2012, **134**, 8396-8399.
5. Z. P. Huang, S. W. Guan, Y. G. Wang, G. N. Shi, L. N. Cao, Y. Z. Gao, Z. Y. Dong, J. Y. Xu, Q. Luo and J. Q. Liu, *J. Mater. Chem. B.*, 2013, **1**, 2297-2304.
6. C. Q. Zhang, X. D. Xue, Q. Luo, Y. W. Li, K. N. Yang, X. X. Zhuang, Y. G. Jiang, J. C. Zhang, J. Q. Liu, G. Z. Zou and X. J. Liang, *Acs Nano*, 2014, **8**, 11715-11723.
7. K. L. Duncan and R. V. Ulijn, *Biocatalysis*, 2015, **1**, 67-81.
8. Y. Maeda, N. Javid, K. Duncan, L. Birchall, K. F. Gibson, D. Cannon, Y. Kanetsuki, C. Knapp, T. Tuttle, R. V. Ulijn and H. Matsui, *J. Am. Chem. Soc.*, 2014, **136**, 15893-15896.
9. S. N. Smith, R. A. Armstrong and M. W. Fowler, *Enzyme. Microb. Technol.*, 1985, **7**, 61-65.
10. G. P. Smith and V. A. Petrenko, *Chem. Rev.*, 1997, **97**, 391-410.
11. M. Hughes, P. W. J. M. Frederix, J. Raeburn, L. S. Birchall, J. Sadownik, F. C. Coomer, I. H. Lin, E. J. Cussen, N. T. Hunt, T. Tuttle, S. J. Webb, D. J. Adams and R. V. Ulijn, *Soft Matter*, 2012, **8**, 5595-5602.
12. J. F. Bazan and R. J. Fletterick, *Proc. Natl. Acad. Sci. U.S.A.*, 1988, **85**, 7872-7876.
13. A. E. Gorbalenya, A. P. Donchenko, V. M. Blinov and E. V. Koonin, *FEBS Lett.*, 1989, **243**, 103-114.
14. J. W. Sadownik, J. Leckie and R. V. Ulijn, *Chem. Commun.*, 2011, **47**, 728-730.
15. N. Singh, M. P. Conte, R. V. Ulijn, J. F. Miravet and B. Escuder, *Chem. Commun.*, 2015, **51**, 13213-13216.
16. Z. Y. Wei, Y. Maeda and H. Matsui, *Angew. Chem. Int. Ed.*, 2011, **50**, 10585-10588.
17. G. P. Smith, *Science.*, 1985, **228**, 1315-1317.
18. T. Palmer, *Understanding enzymes*, Prentice Hall/Ellis Horwood, London ; New York, 4th edn., 1995.
19. L. Stryer, *Biochemistry*, W.H. Freeman Company, New York, 4th edn., 1995.
20. J. Greenwald and R. Riek, *J. Mol. Biol.*, 2012, **421**, 417-426.
21. O. Carny and E. Gazit, *FASEB J.*, 2005, **19**, 1051-1055.
22. H. Neurath and K. A. Walsh, *Proc. Natl. Acad. Sci. U.S.A.*, 1976, **73**, 3825-3832.
23. H. Neurath, *Science.*, 1984, **224**, 350-357.

24. P. Carter and J. A. Wells, *Nature*, 1988, **332**, 564-568.
25. Y. S. Li, Y. F. Zhao, S. Hatfield, R. Wan, Q. Zhu, X. H. Li, M. McMills, Y. Ma, J. Li, K. L. Brown, C. He, F. Liu and X. Z. Chen, *Bioorg. Med. Chem.*, 2000, **8**, 2675-2680.
26. B. G. Miller and R. Wolfenden, *Annu. Rev. Biochem.*, 2002, **71**, 847-885.
27. T. A. Steitz and R. G. Shulman, *Annu. Rev. Biophys. Bio.*, 1982, **11**, 419-444.
28. L. Polgar, *Call. Mol. Life. Sci.*, 2005, **62**, 2161-2172.
29. M. B. Rao, A. M. Tanksale, M. S. Ghatge and V. V. Deshpande, *Microbiol. Mol. Biol. Rev.*, 1998, **62**, 597-635.
30. J. L. T. J. M. Berg, L. Stryer, *Biochemistry. 5th Edition.*, W H Freeman, New York, 5th edn., 2002.
31. M. T. Reetz, C. Torre, A. Eipper, R. Lohmer, M. Hermes, B. Brunner, A. Maichele, M. Bocola, M. Arand, A. Cronin, Y. Genzel, A. Archelas and R. Furstoss, *Org. Lett.*, 2004, **6**, 177-180.
32. L. You and F. H. Arnold, *Protein Eng.*, 1996, **9**, 77-83.
33. F. H. Arnold, *Acc. Chem. Res.*, 1998, **31**, 125-131.
34. D. M. Vriezema, M. C. Aragones, J. A. A. W. Elemans, J. J. L. M. Cornelissen, A. E. Rowan and R. J. M. Nolte, *Chem. Rev.*, 2005, **105**, 1445-1489.
35. L. Pasquato, P. Pengo and P. Scrimin, *J. Mater. Chem.*, 2004, **14**, 3481-3487.
36. M. Gorlero, R. Wieczorek, K. Adamala, A. Giorgi, M. E. Schinina, P. Stano and P. L. Luisi, *FEBS Lett.*, 2009, **583**, 153-156.
37. S. Zhang, T. Holmes, C. Lockshin and A. Rich, *Proc. Natl. Acad. Sci. U.S.A.*, 1993, **90**, 3334-3338.
38. M. Reches and E. Gazit, *Science.*, 2003, **300**, 625-627.
39. J. D. Hartgerink, E. Beniash and S. I. Stupp, *Science.*, 2001, **294**, 1684-1688.
40. M. O. Guler, S. Soukasene, J. F. Hulvat and S. I. Stupp, *Nano Lett.*, 2005, **5**, 249-252.
41. V. Jayawarna, M. Ali, T. A. Jowitt, A. E. Miller, A. Saiani, J. E. Gough and R. V. Ulijn, *Adv. Mater.*, 2006, **18**, 611-614.
42. Z. Yang and B. Xu, *J. Mater. Chem.*, 2007, **17**, 2385-2393.
43. S. Fleming and R. V. Ulijn, *Chem. Soc. Rev.*, 2014, **43**, 8150-8177.
44. A. Mahler, M. Reches, M. Rechter, S. Cohen and E. Gazit, *Adv. Mater.*, 2006, **18**, 1365-1370.
45. A. Aggeli, M. Bell, N. Boden, J. N. Keen, P. F. Knowles, T. C. B. McLeish, M. Pitkeathly and S. E. Radford, *Nature*, 1997, **386**, 259-262.

46. J. H. Collier and P. B. Messersmith, *Bioconjugate Chem.*, 2003, **14**, 748-755.
47. J. P. Jung, A. K. Nagaraj, E. K. Fox, J. S. Rudra, J. M. Devgun and J. H. Collier, *Biomaterials*, 2009, **30**, 2400-2410.
48. Y. N. Wei and M. H. Hecht, *Protein Eng. Des. Sel.*, 2004, **17**, 67-75.
49. S. C. Patel, L. H. Bradley, S. P. Jinadasa and M. H. Hecht, *Protein Sci.*, 2009, **18**, 1388-1400.
50. L. Baltzer, K. S. Broo, H. Nilsson and J. Nilsson, *Bioorg. Med. Chem.*, 1999, **7**, 83-91.
51. K. S. Broo, L. Brive, P. Ahlberg and L. Baltzer, *J. Am. Chem. Soc.*, 1997, **119**, 11362-11372.
52. H. B. Albada and R. A. J. Liskamp, *J. Comb. Chem.*, 2008, **10**, 814-824.
53. F. Rodriguez-Llansola, B. Escuder and J. F. Miravet, *J. Am. Chem. Soc.*, 2009, **131**, 11478-11484.
54. F. Rodriguez-Llansola, J. F. Miravet and B. Escuder, *Chem. Commun.*, 2009, 7303-7305.
55. L. Pasquato, F. Rancan, P. Scrimin, F. Mancin and C. Frigeri, *Chem. Commun.*, 2000, 2253-2254.
56. D. Zaramella, P. Scrimin and L. J. Prins, *Int. J. Mol. Sci.*, 2013, **14**, 2011-2021.
57. A. Madder, L. Li, H. De Muynck, N. Farcy, D. Van Haver, F. Fant, G. Vanhoenacker, P. Sandra, A. P. Davis and P. J. De Clercq, *J. Comb. Chem.*, 2002, **4**, 552-562.
58. A. Clouet, T. Darbre and J. L. Reymond, *Angew. Chem. Int. Ed.*, 2004, **43**, 4612-4615.
59. J. P. Casey, R. J. Barbero, N. Heldman and A. M. Belcher, *J. Am. Chem. Soc.*, 2014, **136**, 16508-16514.
60. G. Gulseren, I. C. Yasa, O. Ustahuseyin, E. D. Tekin, A. B. Tekinay and M. O. Guler, *Biomacromolecules*, 2015, **16**, 2198-2208.
61. R. B. Stockbridge, C. A. Lewis, Y. Yuan and R. Wolfenden, *Proc. Natl. Acad. Sci. U.S.A.*, 2010, **107**, 22102-22105.
62. V. Nanda and R. L. Koder, *Nat. Chem.*, 2010, **2**, 15-24.
63. S. J. Pollack, J. W. Jacobs and P. G. Schultz, *Science.*, 1986, **234**, 1570-1573.
64. P. Forrer, S. Jung and A. Pluckthun, *Curr. Opin. Struc. Biol.*, 1999, **9**, 514-520.
65. R. W. J. Chen, H. Lui, C. Cheng, Y. Zhao, *Lett. Pept. Sci.*, 2001, **7**, 325-329.
66. P. Krattiger, C. McCarthy, A. Pfaltz and H. Wennemers, *Angew. Chem. Int. Ed.*, 2003, **42**, 1722-1724.

67. L. A. Estroff and A. D. Hamilton, *Chem. Rev.*, 2004, **104**, 1201-1217.
68. A. R. Hirst, B. Escuder, J. F. Miravet and D. K. Smith, *Angew. Chem. Int. Ed.*, 2008, **47**, 8002-8018.
69. S. Winkler, D. Wilson and D. L. Kaplan, *Biochemistry*, 2000, **39**, 14002.
70. R. J. Williams, A. M. Smith, R. Collins, N. Hodson, A. K. Das and R. V. Ulijn, *Nat. Nanotechnol.*, 2009, **4**, 19-24.
71. S. Toledano, R. J. Williams, V. Jayawarna and R. V. Ulijn, *J. Am. Chem. Soc.*, 2006, **128**, 1070-1071.
72. A. K. Das, R. Collins and R. V. Ulijn, *Small*, 2008, **4**, 279-287.
73. C. J. Gray, C. J. S. J. Dsilva, J. Boukouvalas and S. A. Barker, *Enzyme. Microb. Technol.*, 1983, **5**, 137-142.
74. I. Cherny, M. Korolev, A. N. Koehler and M. H. Hecht, *ACS Synth. Biol.*, 2012, **1**, 130-138.
75. J. A. Hartsuck and J. Tang, *J. Biol. Chem.*, 1972, **247**, 2575-2580.
76. A. H. Gradman and R. Kad, *J. Am. Coll. Cardiol.*, 2008, **51**, 519-528.
77. J. Rahuel, V. Rasetti, J. Maibaum, H. Rueger, R. Goschke, N. C. Cohen, S. Stutz, F. Cumin, W. Fuhrer, J. M. Wood and M. G. Grutter, *Chem. Biol.*, 2000, **7**, 493-504.
78. C. E. McVey, M. A. Walsh, G. G. Dodson, K. S. Wilson and J. A. Brannigan, *J. Mol. Biol.*, 2001, **313**, 139-150.
79. T. Vernet, D. C. Tessier, J. Chatellier, C. Plouffe, T. S. Lee, D. Y. Thomas, A. C. Storer and R. Menard, *J. Biol. Chem.*, 1995, **270**, 16645-16652.
80. R. V. Ulijn, B. D. Moore, A. E. M. Janssen and P. J. Halling, *J. Chem. Soc. Perk. T. 2*, 2002, 1024-1028.
81. S. K. Verma and K. K. Ghosh, *Indian J. Chem. A.*, 2010, **49**, 1041-1046.
82. G. Host, L. G. Martensson and B. H. Jonsson, *BBA Proteins Proteom.*, 2006, **1764**, 1601-1606.
83. X. Zhao, F. Pan, H. Xu, M. Yaseen, H. Shan, C. A. E. Hauser, S. Zhang and J. R. Lu, *Chem. Soc. Rev.*, 2010, **39**, 3480-3498.
84. M. Zelzer and R. V. Ulijn, *Chem. Soc. Rev.*, 2010, **39**, 3351-3357.
85. A. Mata, L. Hsu, R. Capito, C. Aparicio, K. Henrikson and S. I. Stupp, *Soft Matter*, 2009, **5**, 1228-1236.
86. N. Wiradharma, M. Khan, Y. W. Tong, S. Wang and Y. Y. Yang, *Adv. Funct. Mater.*, 2008, **18**, 943-951.
87. C. H. Gorbitz, *Chem-Eur. J.*, 2001, **7**, 5153-5159.

88. N. S. de Groot, T. Parella, F. X. Aviles, J. Vendrell and S. Ventura, *Biophys. J.*, 2007, **92**, 1732-1741.
89. P. Tamamis, L. Adler-Abramovich, M. Reches, K. Marshall, P. Sikorski, L. Serpell, E. Gazit and G. Archontis, *Biophys. J.*, 2009, **96**, 5020-5029.
90. J. Greenwald and R. Riek, *Structure*, 2010, **18**, 1244-1260.
91. M. J. Krysmann, V. Castelletto, A. Kelarakis, I. W. Hamley, R. A. Hule and D. J. Pochan, *Biochemistry*, 2008, **47**, 4597-4605.
92. S. Marchesan, C. D. Easton, F. Kushkaki, L. Waddington and P. G. Hartley, *Chem. Commun.*, 2012, **48**, 2195-2197.
93. S. Marchesan, L. Waddington, C. D. Easton, D. A. Winkler, L. Goodall, J. Forsythe and P. G. Hartley, *Nanoscale*, 2012, **4**, 6752-6760.
94. P. W. J. M. Frederix, R. V. Ulijn, N. T. Hunt and T. Tuttle, *J. Phys. Chem. Lett.*, 2011, **2**, 2380-2384.
95. M. R. Ghadiri, J. R. Granja, R. A. Milligan, D. E. McRee and N. Khazanovich, *Nature*, 1993, **366**, 324-327.
96. P. W. J. M. Frederix, G. G. Scott, Y. M. Abul-Haija, D. Kalafatovic, C. G. Pappas, N. Javid, N. T. Hunt, R. V. Ulijn and T. Tuttle, *Nat. Chem.*, 2015, **7**, 30-37.
97. L. Monticelli, S. K. Kandasamy, X. Periole, R. G. Larson, D. P. Tieleman and S. J. Marrink, *J. Chem. Theory. Comput.*, 2008, **4**, 819-834.
98. D. H. de Jong, G. Singh, W. F. D. Bennett, C. Arnarez, T. A. Wassenaar, L. V. Schafer, X. Periole, D. P. Tieleman and S. J. Marrink, *J. Chem. Theory. Comput.*, 2013, **9**, 687-697.
99. G. G. Scott, P. J. McKnight, T. Tuttle and R. V. Ulijn, *Adv. Mater.*, 2016, **28**, 1381-1386.
100. J. R. Lakowicz, *Principles of Fluorescence Spectroscopy - Third Edition*, Springer, New York, 2006.
101. R. E. Gillard, F. M. Raymo and J. F. Stoddart, *Chem-Eur. J.*, 1997, **3**, 1933-1940.
102. T. Ban, D. Hamada, K. Hasegawa, H. Naiki and Y. Goto, *J. Biol. Chem.*, 2003, **278**, 16462-16465.
103. M. Tena-Solsona, J. F. Miravet and B. Escuder, *Chem-Eur. J.*, 2014, **20**, 1023-1031.
104. L. Chen, K. Morris, A. Laybourn, D. Elias, M. R. Hicks, A. Rodger, L. Serpell and D. J. Adams, *Langmuir*, 2010, **26**, 5232-5242.
105. J. Raeburn, L. Chen, S. Awhida, R. C. Deller, M. Vatish, M. I. Gibson and D. J. Adams, *Soft Matter*, 2015, **11**, 3706-3713.

106. T. P. Soares da Costa, A. C. Muscroft-Taylor, R. C. J. Dobson, S. R. A. Devenish, G. B. Jameson and J. A. Gerrard, *Biochimie*, 2010, **92**, 837-845.
107. M. Paetzel and R. E. Dalbey, *Trends Biochem. Sci.*, 1997, **22**, 28-31.
108. G. Dodson and A. Wlodawer, *Trends Biochem. Sci.*, 1998, **23**, 347-352.
109. J. Tao and R. J. Kazlauskas, *Biocatalysis for Green Chemistry and Chemical Process Development*, Wiley, Hoboken, New Jersey, 2011.
110. C. Damblon, X. Raquet, L. Y. Lian, J. LamotteBrasseur, E. Fonze, P. Charlier, G. C. K. Roberts and J. M. Frere, *Proc. Natl. Acad. Sci. U.S.A.*, 1996, **93**, 1747-1752.
111. N. S. A. Xavier, *J. Appl. Chem.*, 2014, **7**, 6-15.
112. S. Gorinstein, I. Goshev, S. Moncheva, M. Zemser, M. Weisz, A. Caspi, I. Libman, H. T. Lerner, S. Trakhtenberg and O. Martin-Belloso, *J. Protein. Chem.*, 2000, **19**, 637-642.
113. I. Aoki, T. Sakaki and S. Shinkai, *J. Chem. Soc. Chem. Comm.*, 1992, 730-732.
114. R. Livingston and C. L. Ke, *J. Am. Chem. Soc.*, 1950, **72**, 909-915.
115. G. Papageorgiou, M. Tsimillimichael and J. Isaakidou, *Biophys. J.*, 1975, **15**, 83-93.
116. M. Takezaki and T. Tominaga, *J. Photoch. Photobio. A*, 2005, **174**, 113-118.
117. W. P. J. Arnold C. Satterthwait, *J. Am. Chem. Soc.*, 1974, **96**, 7018-7031.
118. A. Sami, A. S. Shawali and S. S. Biechler, *J. Am. Chem. Soc.*, 1967, **89**, 3020-&.
119. I. Alfonso and V. Gotor, *Chem. Soc. Rev.*, 2004, **33**, 201-209.
120. S. Bandyopadhyay, W. J. Zhou and R. Breslow, *Org. Lett.*, 2007, **9**, 1009-1012.
121. C. Schmuck and J. Dudaczek, *Org. Lett.*, 2007, **9**, 5389-5392.
122. E. N. Efremenko and V. S. Sergeeva, *Russ. Chem. B+*, 2001, **50**, 1826-1832.
123. C. M. H. Cho, A. Mulchandani and W. Chen, *Protein Eng. Des. Sel.*, 2006, **19**, 99-105.
124. R. H. Eaton and D. W. Moss, *Biochem. J.*, 1967, **104**, 65.
125. D. W. Moss and A. K. Walli, *Biochim. Biophys. Acta.*, 1969, **191**, 476-477.
126. M. Wass and Butterwo.Pj, *Biochem. J.*, 1971, **124**, 891-896.
127. K. Thornton, A. M. Smith, C. L. R. Merry and R. V. Ulijn, *Biochem. Soc. Trans.*, 2009, **37**, 660-664.
128. J. Gao, H. M. Wang, L. Wang, J. Y. Wang, D. L. Kong and Z. M. Yang, *J. Am. Chem. Soc.*, 2009, **131**, 11286-11287.
129. X. Cao, *Nat Med*, 2011, **17**, 1344-1346.
130. S. Boonrungsiman, E. Gentleman, R. Carzaniga, N. D. Evans, D. W. McComb, A. E. Porter and M. M. Stevens, *Proc. Natl. Acad. Sci. U.S.A.*, 2012, **109**, 14170-14175.
131. P. A. Price, D. Toroian and W. S. Chan, *J. Biol. Chem.*, 2009, **284**, 4594-4604.

132. Z. M. Yang, H. W. Gu, D. G. Fu, P. Gao, J. K. Lam and B. Xu, *Adv. Mater.*, 2004, **16**, 1440-1444.
133. W. P. Wang and Y. Chau, *Soft Matter*, 2009, **5**, 4893-4898.
134. C. Tang, R. V. Ulijn and A. Saiani, *Eur. Phys. J. E.*, 2013, **36**.
135. C. Tang, A. M. Smith, R. F. Collins, R. V. Ulijn and A. Saiani, *Langmuir*, 2009, **25**, 9447-9453.
136. A. K. Das, R. Collins and R. V. Ulijn, *Small*, 2008, **4**, 279-287.
137. T. G. Mezger, *The Rheology Handbook: For Users of Rotational and Oscillatory Rheometers*, Vincentz Network, Hannover, 2006.
138. K. Thornton, PhD, University of Manchester, 2010.
139. V. Jayawarna, S. M. Richardson, A. R. Hirst, N. W. Hodson, A. Saiani, J. E. Gough and R. V. Ulijn, *Acta Biomater.*, 2009, **5**, 934-943.
140. A. M. Smith, R. J. Williams, C. Tang, P. Coppo, R. F. Collins, M. L. Turner, A. Saiani and R. V. Ulijn, *Adv. Mater.*, 2008, **20**, 37-41.
141. S. Fleming, P. W. J. M. Frederix, I. Ramos Sasselli, N. T. Hunt, R. V. Ulijn and T. Tuttle, *Langmuir*, 2013, **29**, 9510-9515.
142. C. F. Barbas, *Phage Display: A Laboratory Manual*, Cold Spring Harbor Laboratory Press, Cold Spring Harbor, New York, 2001.
143. R. Derda, S. K. Y. Tang and G. M. Whitesides, *Angew. Chem. Int. Ed.*, 2010, **49**, 5301-5304.
144. H. Anni, O. Nikolaeva and Y. Israel, *Alcohol*, 2001, **25**, 201-209.
145. Z. Y. Zhang, D. Maclean, A. M. Thiemesefler, R. W. Roeske and J. E. Dixon, *Anal. Biochem.*, 1993, **211**, 7-15.
146. C. J. Pallen and J. H. Wang, *J. Biol. Chem.*, 1983, **258**, 8550-8553.
147. U. Lorenz, in *Curr. Protoc. Immunol.*, John Wiley & Sons, Inc., 2001.
148. P. W. Snyder, J. Mecinović, D. T. Moustakas, S. W. Thomas, M. Harder, E. T. Mack, M. R. Lockett, A. Héroux, W. Sherman and G. M. Whitesides, *Proc. Natl. Acad. Sci. U.S.A.*, 2011, **108**, 17889-17894.
149. R. J. Chen, S. Bangsaruntip, K. A. Drouvalakis, N. Wong Shi Kam, M. Shim, Y. Li, W. Kim, P. J. Utz and H. Dai, *Proc. Natl. Acad. Sci. U.S.A.*, 2003, **100**, 4984-4989.
150. C. A. Hunter, *Philos. T. R. Soc. A*, 1993, **345**, 77-85.
151. N. B. Adey, A. H. Mataragnon, J. E. Rider, J. M. Carter and B. K. Kay, *Gene*, 1995, **156**, 27-31.